Department of Precision and Microsystems Engineering

Thermomechanical modelling of a hydrostatic machine tool spindle

Bart de Wolf

Report no : MSD 2016.035
Professor : dr.ir.R.A.J. van Ostayen
Specialisation : Mechatronic System Design
Type of report : MSc Thesis
Date : 02-08-2016

TU Delft

Challenge the future

Delft University of Technology

Thermomechanical modelling of a hydrostatic machine tool spindle

ME2490: MSc Thesis

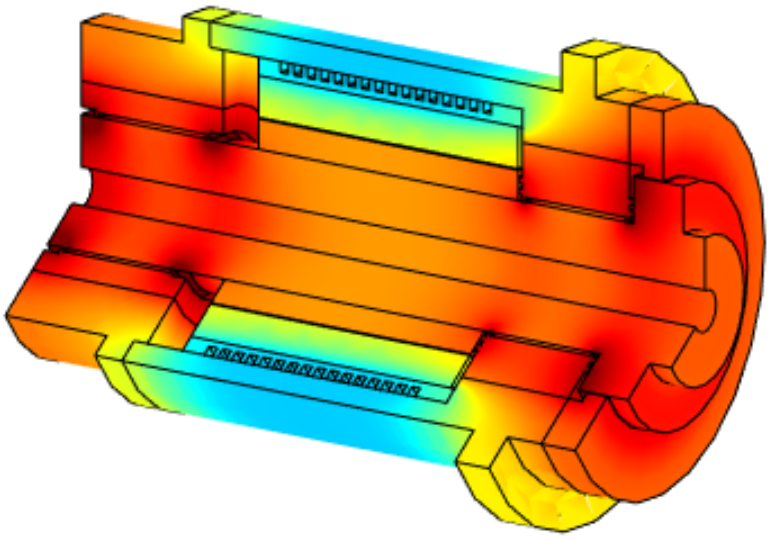

Author:
B.P. de Wolf
MSc PME Student
Student no. 1519050

Supervisor:
dr.ir. R.A.J. van Ostayen
Mechanical Engineering
Associate Professor

August 2, 2016

Contents

List of Figures

Summary

Development of high precision machine tools enables engineers to continuously tighten tolerances and surface finish quality demands. Controlling the thermal state of the machine and process has become the dominant challenge for machine tool manufacturers. Defining models that predict the thermally induced deformations is an important aspect of this development.

This research project focussed on development of a thermomechanical model of a hydrostatic machine tool spindle. Analytical calculations are performed to describe the viscous dissipation in the bearing fluid, losses in the integrated electric motor, the motor coolant circuit and ambient conditions. The resulting parameters and equations are supplied to a finite element model of the spindle assembly. An important characteristic of the model is a fully parametric set-up to enable easy investigation of design variations.

A new modelling method is proposed to address the demand for a parametric finite element model of this complexity. This involves a generalised definitions structure that allows the user to rebuild a model with a single function call. The approach helps eliminate artefacts and provides a platform to store corresponding definitions and simulation results.

Validation of the theoretical model is performed with two series of thermal error measurements on industrial machine tool spindles. The design of the spindles is modified to incorporate internal temperature sensors which provide important insight in the thermal state of the spindle assembly. Comparison of the simulated and experimental results shows that the model is a promising tool for evaluation of the transient thermal behaviour.

Chapter 1

Introduction

The efforts to tighten design tolerances and improve the predictability of precision components can be seen throughout industry. For example, combustion engines have to meet higher efficiency demands while running at increased rotational speeds. Reducing friction, wear and unbalance to achieve these goals all relate to high dimensional accuracy and surface quality. In general, parts for consumer products and the machines that enable their production have to meet ever tightening tolerances. It is the continuing development of machine tools that drives the manufacturing of such precision components. These machines have to enable continuous production of parts within these tight tolerances, which translates to both stable and predictable behaviour of the process (Figure 1.1, [32]).

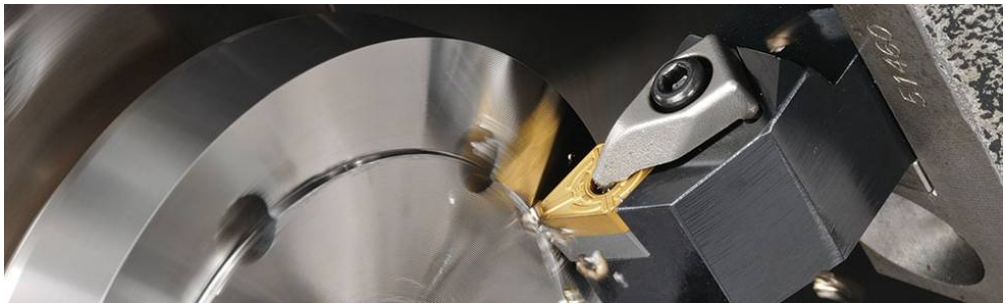

Figure 1.1: High precision turning operation

Thermal control is one of the main challenges in current machine tool design and manufacturing. Especially spindles of lathes and machining centres are susceptible to effects such as thermal expansion since rotating shafts experience high tangential velocities. Heat is generated in the bearing that support the shaft, a problem that increases significantly with higher rotational speeds. The electric motor that drives the spindle adds another disturbing heat input. During intermittent loading and varying load cycles the resulting thermal error can appear to be a random phenomenon.

However, the physics that underlie the error motion encountered by the operator have been known and taught for centuries. Applying these principles to systems that have to repeat their motion to within micrometer tolerance bands is a challenge, but is still essentially deterministic. One of the groups that focus on exploring the field of thermal issues is the Special Interest Group of the European Society for Precision Engineering (Euspen) on this matter. Paul Shore closes his keynote presentation at the 2014 conference with a fitting remark [30].

> "A determinist believes all these sources of error are systematic and therefore can be considered, measured, understood and described"

1.1 Precision manufacturing

Producing high accuracy parts is only possible when the entire machining process is well controlled. Tool manufacturers continually work on improving the actual cutting conditions. State-of-the-art chillers for fluid temperature control can operate at milli-Kelvin levels. The electric motors that drive the spindles have evolved from external asynchronous to built-in synchronous motors. Machine tool builders have to incorporate these advances in their machines and integrate them such that product tolerances in the micrometer level are sustainable in round-the-clock operation.

Thermal effects characterisation

The development of machine tools has long revolved around achieving sufficient positioning accuracy and controlling the motion of the axes. With geometric errors being reduced to sub-micrometer levels and the introduction of CNC control the bottleneck in improving the final accuracy has shifted to thermal control. Variation in temperature of the process fluids, heat input from motors and bearings, and changing environmental conditions all contribute to the final performance. The much referenced categorisation of thermal errors published by Bryan is still an important foothold for thermal error reduction (Figure 1.2, [6]).

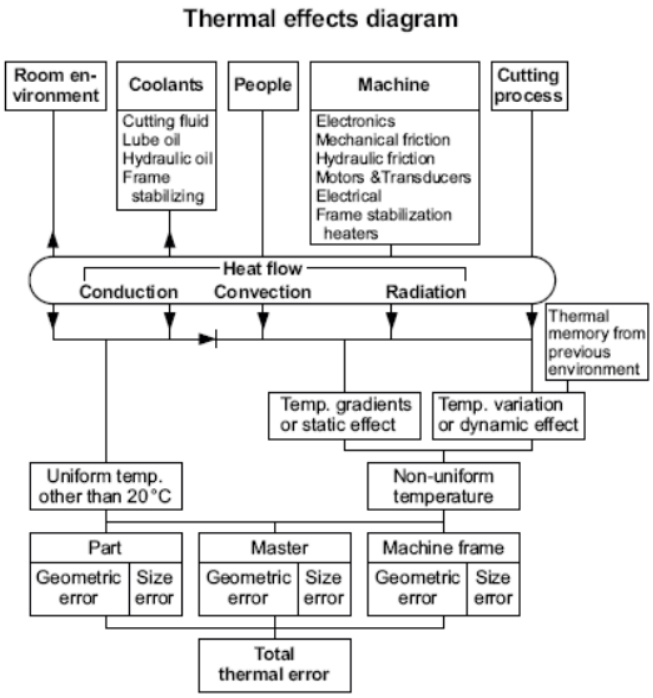

Figure 1.2: Thermal effects diagram by Bryan

Disturbances from the environment and the machine operator are effects that can influence performance significantly, but are poorly defined in advance. It is more efficient to design such that these sources have minimum impact on the final performance and possibly use condition monitoring to compensate for any residual effect. The other three sources are inherent to the actual machining process. In a turning operation, most of the heat generated by the cutting is removed with the metal chips. This leaves only the machine heat sources and process fluids to consider in a thermal model.

The heat sources interact with the machine by three modes of heat flow, which are conduction, convection and radiation. Depending on the characteristics of the heat transfer this

generally leads to non-uniform heating of the geometry. When the heat load is applied or varied this contributes to the dynamic effect noted in Figure 1.2. A complicating factor is the thermal memory of the system, which is a summarising term for the thermal state as a product of previous load cycles. It is easy to imagine how a point load influences a previously uniform temperature field. However, it is much more difficult to predict the outcome when the initial conditions are not uniform, but defined by previous heat input. This poses a considerable challenge for thermal error prediction in actual machines instead of simulated or laboratory conditions.

Industrial research

A large part of research in industry has been aimed at finding prediction and compensation strategies. The quickest path to a more accurate machining process is finding a suitable strategy for correcting the error motion in the CNC control. This requires only little analysis of the system and relies strongly on relating temperatures or measurable deformations to the actual thermal error. Techniques such as regression analysis and neural networks have often been used to set up compensation algorithms. A rather promising approach is the recent development to assess the behaviour in terms of thermal modes.

On the other hand, taking the theoretical approach and validating this with thermal error measurements can be a strategy that leads to more insight in the longer term. A thorough understanding of the dynamics of thermomechanics gives engineers more tools to prevent a larger part of error motions. Additionally, this information can be used to propose the most effective compensation strategy and possibly feed the related algorithm. Reduction methods are often required to reduce the computational load of a model such that it can be used for real-time compensation.

Recent studies have been aimed at a wide variety of approaches. Some researchers advocate the use of simple analytical geometries or networks with many analysis options, whereas others use finite element analysis (FEM) to account for the complexity of the actual deformation. An advantage of the former is the relative ease of performing frequency domain analyses, which sometimes offers more insight than a time domain study. Frequency domain analysis is often more difficult in a FEM model, especially for coupled thermomechanical models. Hybrid approaches are also used to combine limited complexity with sufficient spatial accuracy. However, it is questionable if the additional accounting and coupling is worth the reduction in calculation time that is claimed by this approach.

Developing a model that gives a valid approximation of the actual machine performance is a complex task. Selecting the required components is already a delicate balance of incorporating interacting elements without expanding the model too far. In any case it is important to have clear boundaries and expectations for a model. The final accuracy is most often dominated by the description of the interaction with the environment. Finding suitable parameter values for heat transfer modes, for example, has a large impact on the validity of the model.

It has become clear that motorised spindles in particular exhibit a dynamic and highly non-linear behaviour, which requires adequate modelling. In order for industry to meet the challenge of continuously tightening tolerances this behaviour has to be well understood and controlled. Especially the production of small parts with short cycle times and large series with high process stability requirements can benefit from increased insight in thermal effects. Efficient, flexible and most of all valid tools are required to support the development of a new generation of machine tools.

1.2 Research objectives

Engineers at machine tool manufacturers have a very practical need of a thermomechanical model of their design to evaluate the performance before it is finalised. An important aspect of such a model is a parametric set-up to enable easy variations of designs. This complicates the initial definitions, but results in a much more reliable and insightful framework.

The goal of this masters project is to develop and validate a thermomechanical model for the design of a hydrostatic machine tool spindle. This model is designed to evaluate stationary and transient performance. In accordance with the current industrial standard the spindle is equipped with an integrated motor and cooling circuits. A series of validation experiments is performed to check the validity of the numerical model.

Develop and validate a thermomechanical model of a hydrostatic machine tool spindle

Objectives

- Investigate state of thermal error research
- Define the thermomechanical system
- Develop a model with parametric structure
- Perform experiments on a customised spindle
- Compare simulated and experimental results

A set of objectives is defined to structure the research. The first step is to investigate the current status of thermal error research. The highlights of industrial and academic research are discussed in Chapter 2. Next, the focus is increased to a hydrostatic spindle, the object of this research. A description of the system and modelled components is given in Chapter 4. This is followed by the derivation of the governing equations in Chapter 5. The implementation in a numerical model and the parametric structure are also discussed in this chapter.

A series of experiments have been performed for validation. A state-of-the-art industrial spindle is equipped with additional sensors for transient thermal measurements. The spindle design and measurement set-up are discussed in Chapter 6. Finally, the results of the simulations are analysed and compared to the experiments in Chapter 7.

Chapter 2

Thermal error in machine tools

Thermal effects and the resulting errors have proven to be a formidable challenge in machine tool design. With increasing levels of accuracy and tightening tolerance bands this has become the dominant challenge for many manufacturers. The progress of thermal error research is well captured by several keynote papers from international manufacturing technology conferences.

In this chapter the proceedings of industry and academia in the field of thermal issues in precision machines will be discussed. First, an overview of the field is presented based on a number of keynote papers. The focus lies on the current state-of-the-art in hydrostatic spindle modelling. Since there are various techniques to model such a system specific approaches are given in Section 2.2. In particular, papers on motorised spindles are used as examples and a starting point for further research. The subsequent validation requires measurements of the system in operation. Strategies and techniques for this stage are discussed in Section 2.3. Finally, a summary of the state-of-the-art is presented in Section 2.4.

2.1 Historical perspective

The keynote paper by Bryan in 1990 brought the topic of thermal error in machine tools into worldwide focus. In the period leading up to the publication thermal effects proved to be "the largest single source of dimensional errors and apparent non-repeatability of equipment"[6]. The classification of thermal problems is still one of the best known results from this paper, especially the distinction between deviation from the 20 °C reference and a non-uniform temperature.

Since then, many efforts have been made to tackle what has become the single largest source of error in precision engineering. The general consensus is that the cause of thermal error should be minimised by insulating, shifting or cooling internal heat sources to minimise the effect on machine performance [35]. Precise temperature control of cooling circuits is an important tool to achieve high precision. The remaining error can subsequently be compensated in the machine software by either a direct or indirect strategy. Weck et al. [35] notes that the relation between thermal load and the associated drift is complex. Limited accuracy of the boundary conditions and heat sources make the prediction of drift very difficult.

Ramesh, Mannan, and Poo take this assessment a step further in stating that "it has been found that it is most cost effective to compensate for these thermal errors"[26], as opposed to designing to eliminate these errors completely. The proposed methodology is to measure the temperature at critical points and the induced error in order to derive a compensation model. An analysis of the heat sources can be used to find the appropriate measurement points, although an extensive search can be time-consuming and costly. The complexity can

be reduced by creating individual models for the major subsystems of a machine tool.

Despite the practical desire to compensate thermal errors in order to achieve the required accuracy there has also been a growing demand for sufficiently accurate modelling methods, as mentioned by Abele, Altintas, and Brecher [1]. They discuss the historical development of spindle design and main trends to improve performance with permanent magnet synchronous motors, metallic motor sleeves and condition monitoring. Finally, Abele, Altintas, and Brecher note that these developments have advanced the state-of-the-art, especially in modelling dynamic behaviour. However, the prediction of thermal expansion of spindles has "yet to be solved with sufficient accuracy".

The increased awareness of thermal effects and its complexity is illustrated by the initiation of a special interest group by Euspen. Ruijl highlights some of the main considerations on improvement of machine design, model development, control and validation techniques [29]. With respect to the modelling it is argued that frequency domain analysis of the thermoelastic system is a very effective tool. Although FEM analysis is common, it remains difficult to perform studies in the frequency domain. Switching to a system level description with lumped masses reduces complexity and allows for easy computation of thermal mode shapes. Accurate validation of any model is equally important, both in terms of final performance as insight in behaviour of the sub-systems. Reduction techniques such as proper orthogonal decomposition (POD) of the temperature data appears to be a promising method to analyse these results.

In 2012 Mayr et al. [24] present an update of the research activities on thermal error in machine tools since previous keynote papers [6, 35]. The authors note that machine tool manufacturers are taking "responsibility for the control of thermally induced displacements". This extensive paper describes the complete process of spindle design, performance considerations, sensor integration and control options.

2.2 Modelling techniques

From the previous section it becomes clear that modelling the transient thermal behaviour of a machine tool (sub-assembly) is a complex task. Nevertheless, it is the ambition of many designers to predict this phenomenon through simulation [24]. Identifying the relevant components and selecting the appropriate modelling methods is essential if a reliable result is to be expected. Limiting the complexity and constructing the model around parameters that can be measured also aids in keeping the model manageable.

Heat sources and transfer mechanisms

Thermal modelling revolves around conversion, storage and transfer of energy. The first step in any modelling effort is the identification of heat sources, which are essentially conversion mechanisms such as from electrical to internal (thermal) energy. This holds important considerations of the system boundary. Sources can be viewed as part of the system, integrating the dynamics, or as external disturbances with fixed or tabular values. The latter option simplifies the system, although it might overlook the more intricate dynamics. Bearing friction and dissipation in the spindle motor are generally identified as the main heat sources.

Analytical calculations are often used to define the inputs of the thermal model. Heat dissipation in the electric motor can be derived from winding losses [4], related to the motor efficiency or even neglected due to the system configuration [18]. For hydrostatic bearings the friction and power input can be derived from Couette and Poiseuille flow calculations [8]. When the friction is difficult to model sufficiently accurate it might also be derived

from experiments [4]. The resulting parameters can then be used as model inputs, thereby shifting the boundary of the modelled system.

The energy generated by these sources is either stored in the thermal capacitance of the system or removed by heat sinks, mostly coolant flows and convection to ambient air. The thermal capacitance or heat capacity is the amount of energy stored per unit temperature increase. This is directly related to the geometry and material properties, density and *specific* heat capacity. Having a large capacitance keeps the temperature increase limited for a given energy input. However, it is more useful to assess the thermal diffusivity, the ratio of conductivity over density times heat capacity. This parameter defines the speed at which the temperature field transitions to uniform [28].

Conduction is one of the three modes by which energy is transferred from the heat sources to the sinks. In finite element models this is captured in the geometry and material properties. Having a high thermal conductivity reduces the sensitivity to heat inputs, as energy is easily transferred, and therefore lowers temperature gradients. It also reduces the ratio of thermal expansion over conductivity, an indicator of the amount of bending deformation on one-sided heating. Depending on the choice of system boundary, conduction is generally an internal transfer mode.

Transfer of energy to the environment is dominated by convection, a smaller role is played by radiation if temperature differences are sufficiently large. Process fluids, such as lubricating oil and coolants, as well as the surrounding air, interact with the system through convection. The boundary conditions are relatively simple, linking the rate of transfer to the temperature difference and a convection coefficient. The difficulty lies in determining the appropriate value of these coefficients.

Chen et al. cover an extensive description of the convection to ambient air [8], as does Li et al. in an error estimation model [20]. The use of motor coolant is not always incorporated in assembly models, although Chien and Jang present a comprehensive paper on modelling a motor cooling channel [11]. Generally, convection coefficient estimates are based on experimental correlation functions. These have been determined for a variety of conditions. Textbooks such as by Mills [25] and Wong [36] provide an extensive description of the generally accepted correlations and their applicability. Nevertheless, it is wise to evaluate the sensitivity of the final performance to these parameters.

An additional element is the thermal contact resistance at material interfaces. At any interface, only the asperities of the *rough* surfaces are in physical contact. This limitation of the contact area has a significant influence on thermal conduction [2, 3]. A comparison of FEM based solutions to this phenomenon is presented by Driesen, Belmans, and Hameyer [15]. These include adding a thin layer with lower conductivity, scaling the size of the contacting components or adjusting the conductivity. However, the most promising approach is numerically detaching the nodes at the interface and reconnecting them with weak form PDE's that model the contact resistance.

For all of the mentioned physical descriptions it is true that there is a large number of coefficients and assumptions involved. In order to achieve a reliable result it is important to have suitable estimates and conduct validation experiments of the sub-systems. Performing a sensitivity analysis can help identify the critical coefficients and assess if the estimates are sufficiently accurate.

Modelling spindle assemblies

After defining the relevant physics of the components a choice has to be made with respect to the modelling method of the assembly. Ruijl argues that a lumped mass approach is useful for reduced complexity and more analysis options [29]. On the other hand, FEM models

allow more accurate depiction of the geometry and automatic discretisation [24].

In thermal lumped mass models the system is modelled as a group of capacitances that are linked by the respective heat transfer mechanisms [21]. These can be viewed as resistances in a network model [10, 21]. The result is essentially a first order state-space description. This allows for great flexibility in defining the interactions, performing transformations from time to frequency domain and model reduction techniques [5].

Another interesting approach is given by Bossmanns and Tu who derived a power flow model for a high speed spindle with ball bearings [4]. This is also effectively a network analysis which can be used to define a lumped mass or finite difference model. FDM models typically have a moderate number of rectangular elements. The advantage of this approach is the high level of control over the sectioning and definitions, since the system of equations is defined manually.

Thermally induced deformations that include bending or other non-uniform expansion are often modelled using finite elements. Sometimes a hybrid approach is chosen, with a thermal FDM model and a coupled FEM description of the deformations [18, 23]. This uses the speed of a FDM model, for instance to compute a transient response, with the added information of the deformation state at discrete time points. For the cylindrical sub-assembly of a spindle a 2D axisymmetric model may apply, which reduces the model size significantly [16]. In other cases partial or full 3D models have been developed to assess the performance of the coupled thermomechanical system [8, 20].

Software implementation

Solving transient multi-physics analysis with finite elements has become increasingly fast and flexible over the past decades. Although FEM based models typically generate very attractive visualisations, they don't necessarily result in more accurate results. The dominant influence on accuracy is often the estimation of parameter values and matching these to real world conditions. The additional lack of modal and frequency domain study options in thermal finite element models is cause to carefully consider the benefits of both lumped mass and FEM based approaches.

Both methods require some kind of software to implement the model. Lumped mass and analytical models can be set up by hand in a self-coded environment such as Python or Matlab. The latter is a much used and well known platform used in both academia and industry. It offers many toolboxes for simulation and visualisation, but this comes with a price tag. Although Python is not commonplace in high level analyses its data type flexibility, object oriented structure and free availability make it a very interesting alternative.

When the model is implemented as a finite element approximation the leading option is provided by ANSYS. With its history dating back to 1970, the early days of numerical computing, it is accepted as a standard in FEM analysis. This package offers solutions for many physical domains, which can be linked by the Workbench environment, and provides the user with a high level control over the models and solvers.

There are many alternative software packages available for finite element modelling. One that is particularly interesting is Comsol Multiphysics. It has a slightly different approach, most importantly in the sense that its structure allows full coupling of physical domains and differential equations. Practically, this means it is possible to solve a temperature and displacement field simultaneously, rather than iteratively in separate solvers.

2.3 Thermal error measurement

Measurement of the thermal behaviour of a machine tool is an important aspect for both system identification and validation purposes. Stationary tests [8] only give limited insight, step responses provide much more information about the system [4, 20]. Parameters can also be varied to broaden the validity of the model [11]. Simulating the actual working conditions and the effect of periodic loading can be achieved by performing cycle tests [9].

Equipment

The selection of the measurement equipment has a large impact on the quality and reliability of the results. In thermal error measurements a combination of temperature and displacement sensors have to be used. Depending on the specifications of the system additional sensors, such as flow rate or pressure sensors might be used.

Industrial temperature measurements are often based on Pt100 elements. These are platinum based resistors with a positive temperature coefficient (PTC). The name refers to the resistance at 0 °C, which is 100 Ω. Linearity is one of the main advantages, but they have a low absolute resistance and sensitivity. Thermocouples and thermistors (negative temperature coefficient resistances, NTC) are alternatives to the PTC standard. Ruijl argues that the latter is most suitable for high accuracy measurement due to the high sensitivity and high electrical resistance [28], among other attributes.

A high quality in displacement measurement can be achieved with capacitive or inductive probes. These non-contact sensors allow a rotating target with accuracy in the tens of nanometres. A typical industrial example of such a system is the spindle analyser made by IBS Precision Engineering (Figure 2.1 [17]).

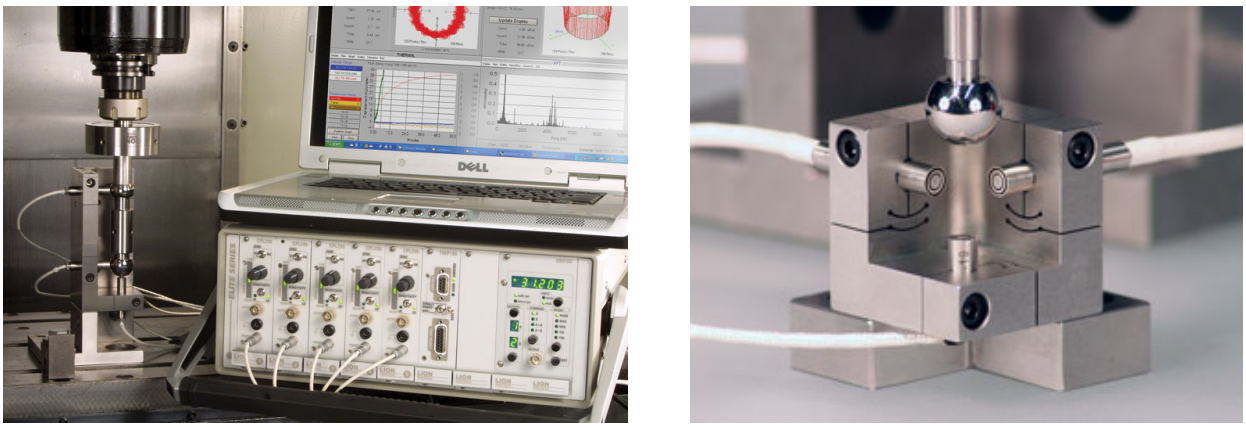

(a) Spindle analyser set-up

(b) Probe nest

Figure 2.1: Spindle analyser with capacitive probes

Measurement strategies

Choosing the appropriate measurement methods is equally important as good equipment. Step response tests are often used to characterise the transient response. In such measurements it is important to allow the test to run long enough to capture the longer time constants that are often found in large scale thermal systems.

When working with a complex assembly it is useful to identify small sub-systems that can be validated individually. The work of Chien and Jang provides a nice indication of

the numerical analysis and validation of a helical cooling channel [11]. It also serves as an example of how a combined numerical and experimental research can be conducted.

Selecting the appropriate placement of the sensors is also important. When a large number of temperature probes is used the results can be analysed in terms of a thermal modal response [19]. Koevoets et al. demonstrates that the use of modal information results in a much better approximation of thermal deformation than simply using the temperature probes directly. This method is applicable when the system, with its capacity and conduction properties, is well known, but the heat loads are not. When there is information about the latter it is also possible to use proper orthogonal decomposition (POD) to reduce the temperature data. With this method the full vector space of temperature distributions can be found and subsequently analysed, a technique that is advocated by Ruijl [29] as a validation technique. A nice introduction of the method is presented by Chatterjee [7].

Generally, error measurements are also used as input to define compensation strategies. A distinction can be made between a direct method, using displacement sensors, or indirect using temperature or other variables. The clear advantage of the former is that there is no conversion between physical quantities. This translates to a higher robustness and possibly improved accuracy [9]. However, finding a suitable measurement set-up is more difficult and costly than with temperature probes. An interesting combination might be found in regression analysis with temperature and displacement information, which merges the types.

2.4 Current state-of-the-art

From the progress at the most recent meeting of the Euspen group on thermal issues (Prague, March 2016, [31]) it becomes clear that the field is very active in all aspects of this kind of error. Thermomechanical models of spindles and entire machine tools, optionally with fluid domain coupling, have been developed for transient analysis. Some researchers have also made the effort to reduce these models for lower computation times or additional frequency domain studies. Additionally, new measurement techniques are being developed to assess 3D deformation at the tool tip. Correction methods use increasingly large numbers of temperature probes or direct local displacement measurements to compute the deformation state of the system.

Chapter 3

Machine tool spindles

Spindles in machine tools share a number of features that can be found in all designs. The general system layout and components are described in the first section. Some of the more specific design choices for this thesis are worked out next. A short introduction to hydrostatic bearings is presented along with a number of definitions with respect to geometry and heat generation in Section 3.2. The motor and associated coolant in Section 3.3 conclude this chapter on the spindle configuration.

3.1 System description

The purpose of a spindle in a machine tool is to provide a stable support for a rotating workpiece or tool. Depending on the application the speed can range from hundreds to well over 25000 rpm. In Chapter 1 the scope was limited to motorised spindles with hydrostatic bearings. Additionally, a choice is made to specifically investigate spindles of lathes with rotational speeds up to 4000 rpm.

An example of a motorised spindle is shown in Figure 3.1. This spindle assembly is used in the second measurement series. The large block is the base of the assembly. Part of the spindle can be seen as a composition of blackened and bare metal parts.

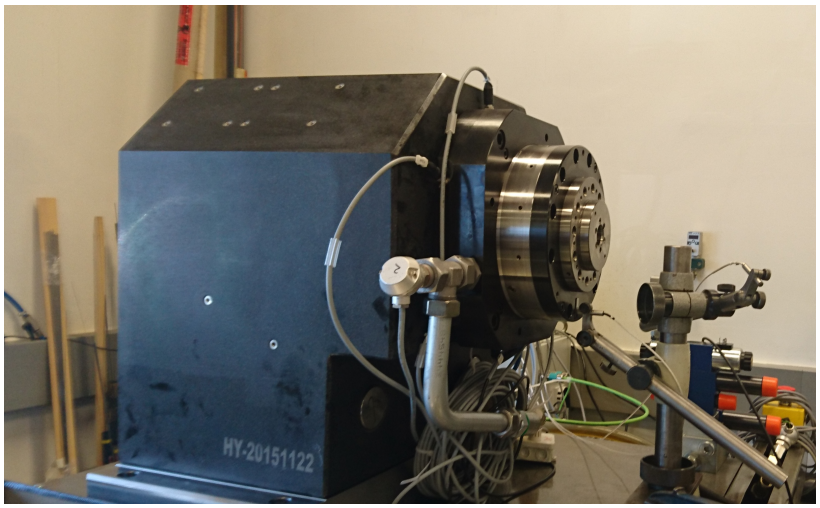

Figure 3.1: Industrial motorised spindle

Model boundary

One of the most defining choices in any model is the location of the boundary that separates the internal dynamics from external interaction. Before working out the physics that underlie the performance an assessment of the system boundary is required. The objective of the research is to develop a model of a spindle assembly that describes the thermomechanical behaviour. The critical performance parameter is the thermal drift of the spindle nose (right side in Figure 3.2), the mounting surface for a product clamping device.

This displacement is measured with respect to a mechanical reference, which is chosen to be the mounting surface of the spindle housing. A large machine base with a high thermal capacity supports the spindle at this interface. It is assumed that the base has limited influence on the short term thermal error[1]. Choosing this boundary also reduces the system to components that are essentially axisymmetric, a feature that can be used to limit the model complexity.

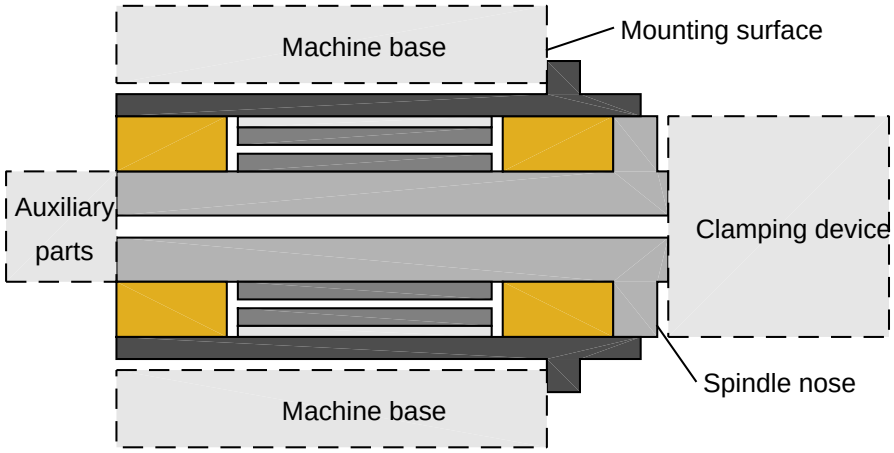

Figure 3.2: System boundary and surroundings

The clamping device attached to the spindle nose is left out of the model, since this is very process specific and distracts focus from the dynamics that cause the thermal error. For the same reason any auxiliary parts on the rear of the spindle are omitted.

A selection of the relevant components of the spindle assembly is made next. In principle, only the areas that contribute to the thermal expansion of the spindle nose have to be included. Given the layout from Figure 3.1 this could exclude the entire geometry behind the front bearing from the model. However, the stator and cooling jacket could well influence the thermal state of the housing and bearing. Moreover, the demand for a parametric set-up keeps the position of the housing flange with respect to the internal components flexible. For these reasons a broader selection of components is considered.

There is also a desire to assess the thermal characteristics of both front and rear bearing for design evaluation. Since the physics for analysing hydrostatic lubrication have to be worked out for the front bearing it is a small effort to include the rear one as well.

There are three fluids (oil, coolant and air) that interact with the solid spindle assembly and have to be incorporated in the model. Bearing oil is supplied at a constant pressure and temperature and drained by a free outflow. Motor coolant is supplied at a constant flow rate and regulated inlet temperature. Finally, the ambient air provides convective cooling at the housing wall and spindle nose.

[1]Figure 3.2 only displays a small part of the base. Generally, this is a large cast or welded frame that also holds the linear axes. The influence on thermal error occurs in the time range of hours to multiple days, whereas the spindle responds more in the range of seconds to minutes.

Component overview

Based on the considerations of the system boundary the choice is made to include all major components within the housing in the modelling. This includes both front and rear bearings, and the electric motor group with cooling channel. An overview of the components is given in Figure 3.3.

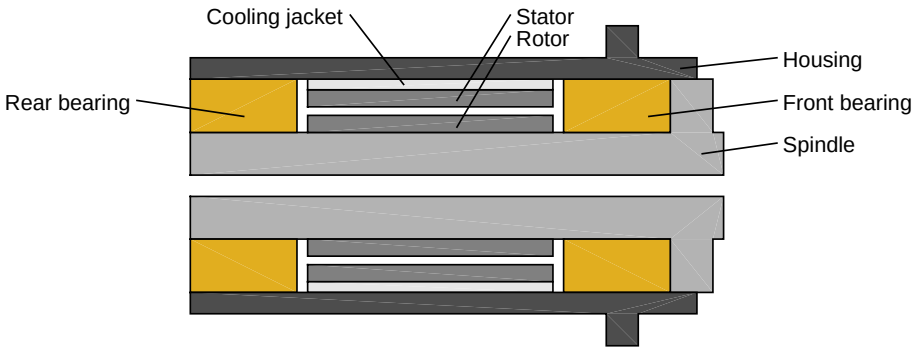

Figure 3.3: Spindle internal components

The housing provides a basis to assemble the other stationary components, which are the bearings and stator side of the electric motor. The other half of the motor is mounted on the spindle. These two components are suspended in the hydrostatic bearings. Usually, the front bearing offers combined axial and radial support, whereas the rear one is only radially supporting. This prevents over-constraint of the spindle, keeps the axial reference in the front and thereby eliminates most of the influence of thermal disturbances on the rear side of the axial bearing.

Several materials are used in the system. The spindle and housing are made of steel, the most common choice for structural machine components. For the bearings a bronze alloy is used, a popular choice in machine engineering [34]. The cooling jacket is aluminium and the motor parts are mostly composed of copper windings, magnets and a steel housing.

Selecting the appropriate materials is a balance of cost and performance. A housing and spindle made of invar would significantly reduce the thermal expansion. The material and manufacturing cost, however, would make the spindle much more expensive. Selection of materials for the model is based on the actual properties of the spindle used for validation.

3.2 Hydrostatic bearings

As mentioned, the research is focussed on spindles with fully hydrostatic bearings. This bearing type is characterised by the use of an externally pressurised lubricant, such as oil or water, to separate the shaft from the bearing. As opposed to hydrodynamic bearings, there is always a fluid film separating the rotating from the stationary part, irrespective of the speed.

Hydrostatic bearings have many qualities that are desirable in a precision machine. Since the shaft floats on an oil film, there is never mechanical contact between the rotating and stationary part. This results in very low friction, zero wear and small eccentricity (radial run-out) [27]. Oil bearings in particular can be designed to very high film stiffness, with values of up to 10^9 N/m, which make them very interesting for precision machining.

Hydrostatic bearing principle

The basic principle of a hydrostatic bearing is to inject a fluid between two surfaces at a controlled pressure to generate a thin lubricating film. Figure 3.4 shows a simplified cross-section of a hydrostatic bearing. In terms of Ohm's Analogon each bearing is a simple network with two resistances. The oil enters the system with a supply pressure p_s. A fixed[2] flow resistance R_c reduces the pressure to approximately half of the supply pressure p_r. Next, the oil passes the outflow wall (with variable resistance R_o) and exits at ambient pressure p_a. Due to the large difference between the outflow gap height and recess depth it can be assumed that the pressure p_r in the pocket is uniform.

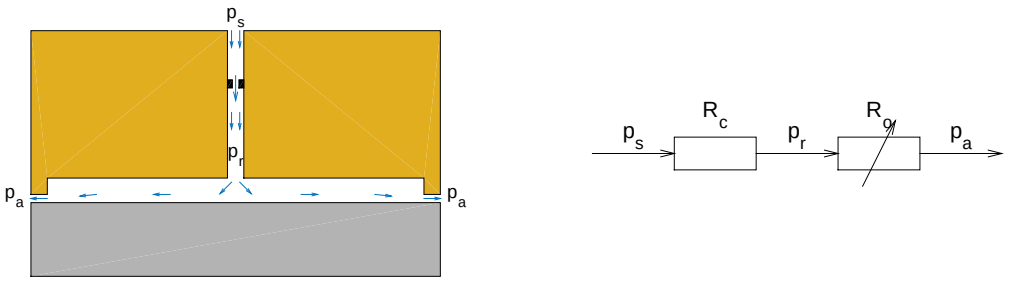

(a) Bearing cross-section

(b) Single recess flow network

Figure 3.4: Hydrostatic bearing principle

Oil conditioning equipment is required in order for the spindle to function properly. A high pressure pump circulates the oil through the closed system at a supply pressure in the order of 10^6 Pa. The temperature of the oil increases by viscous dissipation as flows through the bearings, an effect that is amplified by high rotational speeds. Before the oil is recirculated it is actively cooled to the required supply temperature. The need for oil conditioning equipment and the relatively high engineering cost of the custom design are some of the drawbacks of such bearings [34].

Bearing geometry

There are several different types of bearing geometry, relating both to the shape and configuration of the pads. Journal bearings confine a shaft in the radial direction, a planar type can be used to offer axial support. Either type can be recessed or plain, although using a recess is common in hydrostatic bearings. Since oil based bearings can only produce positive pressure opposing pads are used to confine the shaft. For a journal bearing a configuration of 4 or 6 recesses is generally chosen for a uniform radial stiffness. More background information on bearing geometry can be found in the books of Rowe [27] and Van Beek [34].

The spindle assembly has two journal bearings for radial support. Each of these is a recessed type with 6 pockets and viscous flow restriction. Axial support is given by a pair of planar bearings with a single annular recess. As opposed to a multi-recess planar bearing, this type does not give any tilt stiffness. Each side is fed by a dedicated channel, also with a viscous restrictor. The geometry of the bearing is defined by the diameter, length, land widths and gap height. Figure 3.5 shows the geometry of a combined axial and radial bearing. The gap height, which is distance between bearing lands and shaft, is amplified for visualisation purposes.

[2]There are examples of variable flow resistances, which can be used to increase the stiffness of the bearing. For thermal analysis and the scope of this research such methods are not considered.

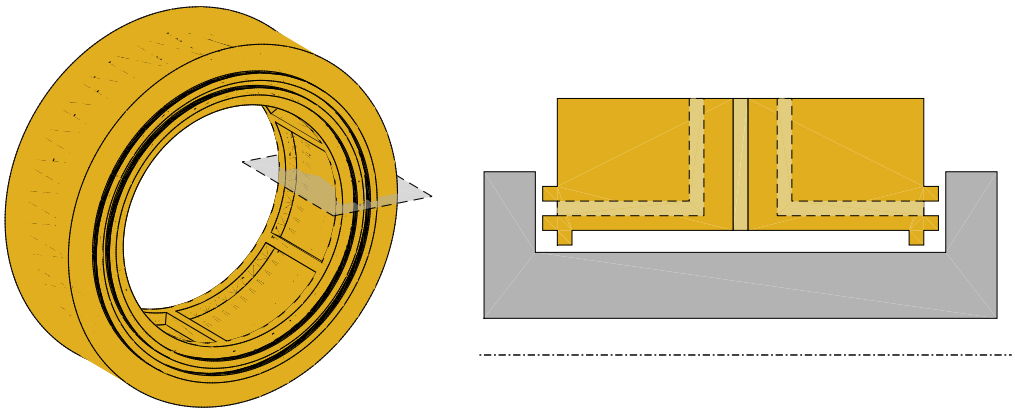

(a) Total bearing geometry (b) Bearing cross-section

Figure 3.5: Combined axial and radial bearing

At the bearing lands there is only a thin film of oil separating the spindle from the bearing surface. The size of these lands influences the flow rate and stiffness, but also the amount of viscous dissipation. A recessed journal bearing has two kinds of walls. Those in between the recesses will be referred to as tangential walls. The two outflow walls along the circumference are the axial walls. For the axial bearing the terminology is simply inner and outer wall.

A hydrostatic bearing is externally pressurised, which requires feed channels from the pressure pump to the recesses. Each of the 6 radial and both axial recesses have dedicated channels with a viscous flow restrictor. This results in eight parallel branches such as described in Figure 3.4b. These channels are distributed along the circumference of the bearing body, the channel geometry in Figure 3.5b is only indicative.

Flow profiles

The hydrostatic bearings are one of the most important sources of heat. Oil is forced through the bearing gap due to the difference between recess and ambient pressure. Typically, the gap height is very small compared to the land width, a ratio of 1:100 is quite common. Therefore, it is reasonable to neglect the entrance and exit effects and consider the flow to be fully developed along the majority of the gap length. Moreover, the gap is much like a thin film on the relatively large diameter of the spindle. This makes it analytically equivalent to an infinitely wide flat duct. These analogies are used in the analytical calculations.

Imposing a pressure difference Δp over the bearing wall results in a Poiseuille duct flow, well known in fluid mechanics, with a parabolic velocity profile (Figure 3.6). Additionally, the rotation of the spindle imposes a moving wall on the fluid. The situation with two parallel plates, with one stationary and the other moving, is captured in the Couette flow model.

From the theoretical fluid profiles it is clear that there is a velocity gradient in the oil, causing viscous shear. At this point it is important to note that the relative dimensions are such that it is essentially a 2.5D problem. Variation of pressure and temperature across the film height is limited. This also allows one to derive the relation between the velocity profile and viscous dissipation from the Reynolds equation, instead of the full Navier-Stokes description. A more elaborate discussion of the assumptions is given in Section 7.2.

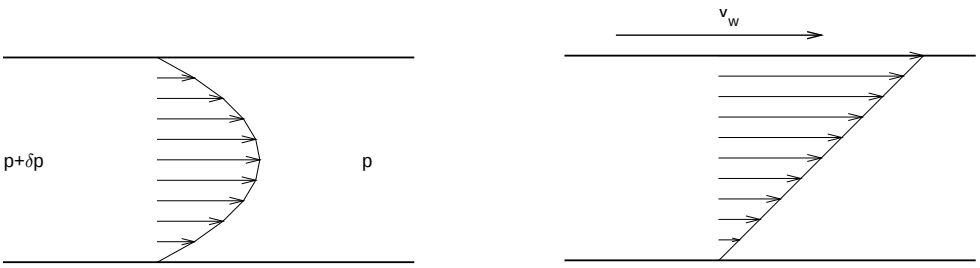

(a) Poiseuille flow (b) Couette flow

Figure 3.6: Theoretical flow profiles

3.3 Integrated motor

Positioning the electric motor in between the bearings has a number of benefits. One of the main advantages is the elimination of mechanical disturbances from the motor coupling and shaft alignment. It also allows a more compact design for a given bearing geometry. However, the key challenge is handling the thermal load in such an important location.

A configuration with integrated motor obligates the use of a cooling channel to keep the motor temperature low. This can be either a separate cooling jacket or a built-in channel designed by the motor manufacturer.

Electric motor losses

Currently, the industrial standard is the use of permanent magnet synchronous motors (PMSM). This motor type has the magnets on the rotor side and windings in the stator, thereby eliminating the need for rotating contacts. A PMSM type electric motor suffers from three types of electrical losses and mechanical friction. The current flowing through the windings in the stator causes internal heating of the copper P_c. Additionally there are losses in the iron core P_i and from magnetic field stray P_s. Figure 3.7 gives a visualisation of the power flow for a PMSM type motor [33], which also includes the mechanical losses from the bearings P_f. The efficiency is defined as the ratio of mechanical output power P_m over electrical input power P_e.

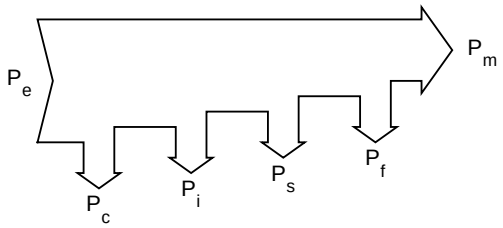

Figure 3.7: PMSM Motor power flow and losses

All of the losses describe paths by which the electrical power input is converted to heat. Most of the energy is converted by the copper losses in the stator windings. It is not the aim of this research to perform an in-depth analysis to relate the three phase current to each of the losses and compute the associated heat load. Instead it is noted that the generation of heat is located almost exclusively in the stator. The sum of the losses is attributed to the stator as an external heat load.

Motor cooling circuit

An integrated electric motor requires some kind of cooling system to extract the dissipated energy. This is generally done with a helical channel between the housing and stator. In a permanent magnet type motor the majority of the energy is dissipated in the stator. Figure 3.8 shows a cooling jacket with helical channel.

Various geometries of the channel can be found in industry. Chien and Jang describe a case with a double helix in which the fluid flows forward and back through parallel parts of the channel [11]. Alternatively, a single channel can be used. In that case, an additional straight channel might be required to feed and drain the coolant from one side. The channel in this research has a single helix with a narrow rectangular cross-section, leading to a high flow velocity. This is beneficial for the heat transfer, as it keeps the flow turbulent.

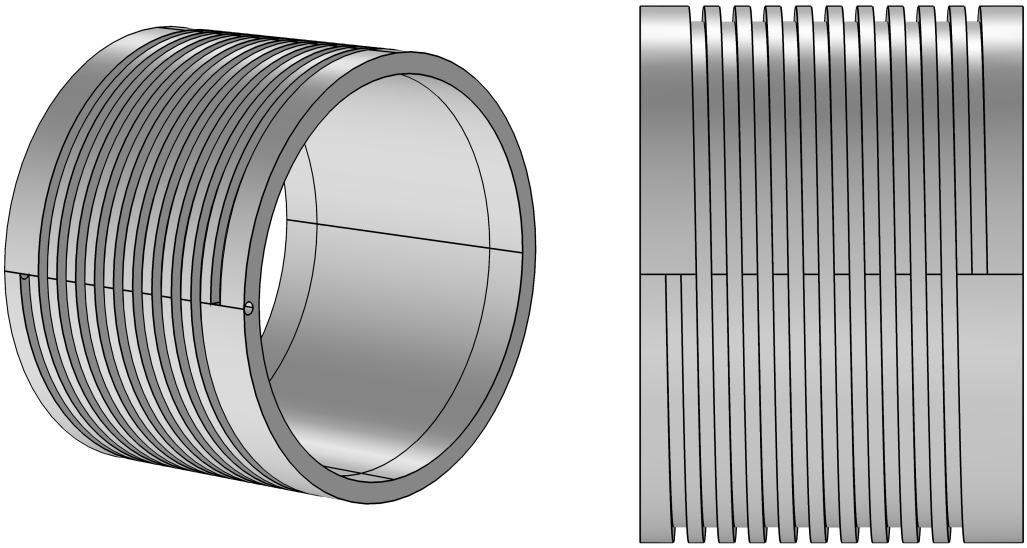

(a) Perspective view (b) Orthographic side view

Figure 3.8: Cooling channel geometry

The coolant that flows through the helical channel is supplied at a constant temperature and flow rate. This fixes the temperature at one side of the channel. At the other end the temperature will vary as a result of the heated wall. Placing the inlet at the side of the front bearing ensures that the desired temperature is passively enforced where it influences the thermal error most.

Chapter 4

Thermomechanical model

A model of the thermomechanical behaviour is derived in this chapter. In order to perform simulations that are valid for new designs the model has to be based on physical principles rather than experimental data. An attempt is made to identify all relevant physics and give a suitable analytical description. This theoretical background is the foundation for the implementation in a numerical model.

First, a general description of the heat transfer mechanisms is presented in Section 4.1. The choice of modelling strategy and the corresponding governing equations are discussed next in Section 4.2. A description of the model geometry follows in Section 4.3. This is the basis for defining physics and the associated equations, which are discussed per component group. The bearing flow and dissipation relations are discussed in Section 4.5. Stator heat losses and the accompanying cooling channel follow in Section 4.6. The final thermal aspect is the heat transfer to the ambient air, which is analysed in Section 4.7. Mechanical aspects of the model are discussed in Section 4.8.

4.1 Heat transfer mechanisms

The three modes of heat transfer have been discussed briefly in Chapter 2. In this section the mechanisms are discussed in more detail. A basis is provided for numerical evaluation of the related quantities. This is used in subsequent sections where the specific components and analytical values are discussed.

Conduction and thermal contact

Transfer of heat within solid components is described by Fourier's law of heat conduction. The relation between the heat flux and temperature gradient is well known and easily understood in 1 dimension. The most interesting approach to conduction, and heat transfer in general, is the analogy with an electrical circuit. In 2 or 3-dimensional models discretisation techniques are required to assess the temperature field, which is described in Section 4.2.

The model consists of an assembly of components resulting in a number of interior boundaries. It is often assumed that the contacting walls have the same temperature, which provides a numerical basis to link the components. However, as mentioned in Section 2.2, there can be a thermal contact resistance at interior boundaries. This leads to an apparent discontinuity of the temperature field across the contact.

In practice, there is no discontinuity, but rather a steep gradient across the contacting surface asperities. Figure 4.1 shows a graphic representation from Attia and Kops of the heat flux through contacting surface asperities [3]. It shows the constriction of the conductive heat flux. Additionally, there is some conduction and radiation through the interstitial medium.

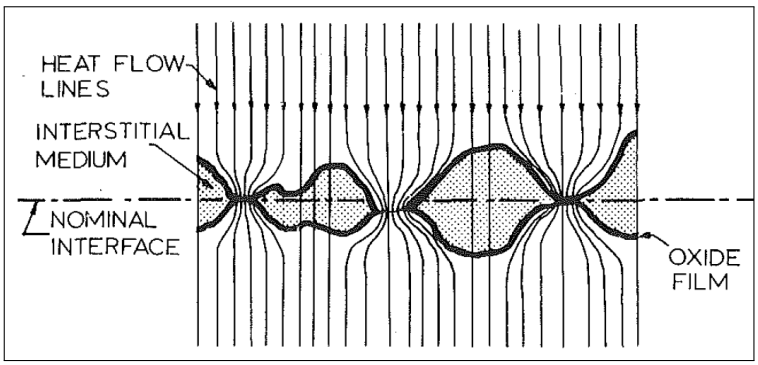

Figure 4.1: Heat flux across contacting surface asperities

A description of the heat flow across the interface can be expressed in terms of a contact resistance or interfacial conductance [25]. The mathematical relation is identical to the convective heat flow at a boundary. Equation 4.1 shows the heat flux across the contact q_{tc} as a function of the interface heat transfer coefficient h_{i} and the temperature of the walls just below the interface, before the heat flow lines start to constrict.

$$q_{\mathrm{tc}} = h_{\mathrm{i}} \left(T_1 - T_2 \right) \tag{4.1}$$

Convection

Energy transfer between the fluids and solid components is described by convection. This applies to the heat transfer between the spindle and ambient air, and also to the coolant and oil. Convective heat transfer is described by Newton's Law of Cooling, which is actually a definition of the convective heat transfer coefficient h_{c} [25]. The heat flux q_{c} is proportional to this coefficient and difference between fluid (bulk) and wall temperature, respectively T_{f} and T_{w}.

$$q_{\mathrm{c}} = h_{\mathrm{c}} \left(T_{\mathrm{f}} - T_{\mathrm{w}} \right) \tag{4.2}$$

Although Equation 4.2 appears to be quite simple, the difficulty lies in finding correct coefficient values. These are not given in explicit tables, such as material properties, but have to be derived from experimental data. The amount of convective heat transfer is determined by the fluid flow that is caused by a combination of the temperature gradients (and the related buoyancy forces) and possibly external forces. Dimensionless quantities such as the Reynolds and Grashof number are used to define the flow regime. These quantities are used in correlation functions for the Nusselt number, which can be seen as a dimensionless heat transfer coefficient [25]. The final step to the actual convective heat transfer coefficient follows from Equation 4.3, in which k is the thermal conductivity of the fluid and L the characteristic length.

$$h_{\mathrm{c}} = \frac{\mathrm{Nu}\, k}{L} \tag{4.3}$$

Internal radiation

Thermal radiation is defined in terms of an incident and outgoing energy flux, respectively named irradiation G and radiosity J. Both are related to the Stefan-Boltzmann law of black body radiation (Equation 4.4 and 4.5). A black body in an enclosed space has a net radiant heat flux given by Equation 4.6 [25].

Real surfaces are generally modelled as a grey surface, of which the emittance ϵ is defined as the fraction of emissive power with respect to a black body. In the special case of an enclosed body the radiative heat flux is given by Equation 4.7. When the temperature difference is small this can be linearised for a quick estimate or reduced computation time (Equation 4.8), where T_m is the mean temperature.

$$J = \sigma T^4 \tag{4.4}$$
$$G = \sigma T_\mathrm{e}^4 \tag{4.5}$$
$$q_\mathrm{r} = J - G = \sigma \left(T^4 - T_\mathrm{e}^4\right) \tag{4.6}$$
$$q_{12} = \epsilon_1 \sigma \left(T_1^4 - T_2^4\right) \tag{4.7}$$
$$q_{12} \approxeq \epsilon_1 \sigma \left(4T_\mathrm{m}^3\right)(T_1 - T_2) \tag{4.8}$$

4.2 Modelling strategy

The implementation of the model is worked out in the next chapter. However, a choice has to be made with respect to the modelling strategy. Both finite element and lumped mass approaches have appealing characteristics. A qualitative assessment is performed to argue which is the suitable choice for this application.

Lumped mass assumption

The underlying assumption in a lumped mass approximation is a uniform temperature field in the mass elements. A quantitative assessment of the expected temperature gradients in a system can be made by computing the Biot number for (part of) the system. The relation is given in equation 4.9 [25], with the average convective heat transfer coefficient h_c, characteristic length L and thermal conductivity of the solid k_s.

This dimensionless group describes the ratio of internal conduction over external convection resistance. When this value is small the external resistance is dominant, allowing the internal temperature field to approach a uniform distribution. Based on a number of simplified geometries it is stated in Mills that $\mathrm{Bi} < 0.1$ ensures that the assumption of uniform temperature is justified.

$$\mathrm{Bi} = \frac{\text{Internal conduction resistance}}{\text{External convection resistance}} = \frac{L/k_\mathrm{s}A}{1/\bar{h}_\mathrm{c}A} = \frac{\bar{h}_\mathrm{c}L}{k_\mathrm{s}} \tag{4.9}$$

The Biot number is evaluated at several locations in the model. Both the bearing and cooling jacket surfaces have high speed laminar and turbulent flows which result in high values of the convective heat transfer coefficient. Convection at the outer wall is also evaluated to assess if there are parts of the geometry where a lumped mass approach might be valid.

Table 4.1 shows the parameters and corresponding Biot number for a selection of important model locations. The values used in this analysis follow from the analytical calculations later in this chapter. At the bearing gap and outflow areas the Biot number is approximately 2, well above the limit for a uniform temperature. For the cooling channel the value is much lower at 0.3, although this still produces significant gradients. Only the housing section, with free convection to the air, has a sufficiently low Biot number.

From the analysis of the Biot number it can be concluded that the assumption of a uniform temperature field is not valid for this model. The gradients that are expected to occur in some of the components (bearings, cooling jacket) are likely to influence the housing sufficiently to assume a non-uniform field in the entire geometry. Therefore it is justified to choose a finite element approximation as the modelling method for the spindle assembly.

Location	$\bar{h}_c$ (W/m^2 K)	L (m)	k_s (W/m K)	Bi (-)
Axial bearing gap	$29 \cdot 10^3$	0.003	51	1.7
Outflow regime	$2 \cdot 10^3$	0.050	51	2.0
Cooling channel	$5 \cdot 10^3$	0.010	180	0.28
Housing wall	15	0.020	14	0.02

Table 4.1: Biot number for various locations

Governing equations

Modelling the thermal error of a machine tool spindle revolves around the heat balance of the assembly and the resulting thermal expansion. Any heat transfer analysis is essentially based on the first law of thermodynamics, conservation of energy (Equation 4.10, p.721 [14]). For a solid assembly there is no internal convection, and viscous work and transport terms can be omitted. This leaves a reduced form that only covers storage, internal conduction and external heat sources (Equation 4.11).

$$\rho C_p \left(\frac{\partial T}{\partial t} + (\mathbf{u} \cdot \nabla) T \right) + \nabla \cdot \mathbf{q} = \tau : \mathbf{S} - \frac{T}{\rho} \left. \frac{\partial \rho}{\partial T} \right|_p \left(\frac{\partial p}{\partial t} + (\mathbf{u} \cdot \nabla) p \right) + \mathcal{Q} \quad (4.10)$$

$$\rho C_p \frac{\partial T}{\partial t} + \nabla(-k \nabla T) = Q \quad (4.11)$$

The external sources captured in the term $\mathcal{Q}$ are convection from fluids, heat generation in the motor and possibly radiation. The only boundary that could be subjected to conductive heat transfer is the mounting surface of the spindle housing. For this research the boundary is assumed to be insulated. All other boundaries are connected to air, bearing oil or motor coolant. The dominant form of heat transfer to the environment is therefore convection. Low power radiation takes place internally due to the difference between motor temperature and housing. It is assumed that there are no external radiation sources with sufficient power to significantly influence the system.

The description of the mechanical system is relatively straightforward. In general, it is based on a balance of the internal stresses and external loads, both at the boundary and distributed over the body. Equation 4.12 shows the stationary balance equation, where S denotes the second Piola-Kirchhoff stress tensor and F_v the loads. In an instationary situation the time dependent term is added (Equation 4.13). However, given the relatively slow response to thermal loads on this length scale the mechanical system will behave as quasi-static.

In a thermomechanical model the most important aspect is the thermal expansion. This is incorporated in the term ϵ_{th} in Equation 4.14. The link to the governing equation is made through the internal stresses. In a system with only thermal expansion the stress state is determined by the double contraction of the elasticity tensor and the strain state minus the current thermally induced strain.

$$0 = \nabla S + F_V \quad (4.12)$$

$$\rho \frac{\partial^2 u}{\partial t^2} = \nabla S + F_V \quad (4.13)$$

$$\epsilon_{th} = \alpha \left(T - T_{ref} \right) \quad (4.14)$$

$$S = \mathbf{C} : (\epsilon - \epsilon_{th}) \quad (4.15)$$

4.3 Component geometry

The development of the numerical model is based on an industrial spindle that is also used for the validation process. Figure 4.2 shows the worked out geometry of the spindle. There are 9 components in the final assembly, indicated by three letter tags. The geometry is simplified as much as possible while keeping the component perimeter close to the actual design[1]. One of the important simplifications is the reduction to an axisymmetric geometry, which only requires the modelling of one half of the cross-section.

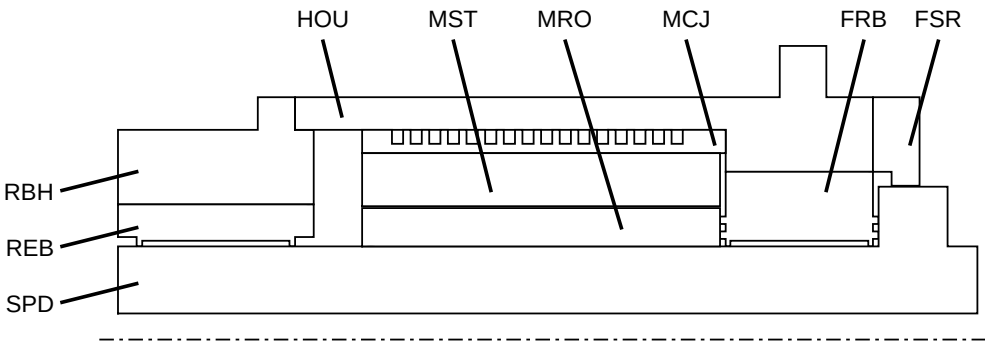

Figure 4.2: Model geometry and component definition

The housing (hou) is the central component in which all other components are mounted. It holds the front bearing (frb) and the front seal ring (fsr). A separate rear bearing housing (rbh) connects the rear bearing (reb) to the housing. This separation is made to match the design and create an opportunity to exclude the rear bearing section from the model. Defining separate components is not only a matter of geometry. It provides a basis to assign different materials to geometric domains. The boundaries created by the segmentation also serve as entities to assign additional physical conditions.

In the middle of the assembly the stator (mst) and rotor (mro) are found. The cooling jacket (mcj) attaches the stator to the housing. There is a small air gap between the stator and rotor, although this is not distinguishable in figure. This is also true for the bearing gaps, which have even smaller relative dimensions. The rotor and spindle shaft (spd) are geometrically disconnected from the other components.

4.4 Thermal contact

The assembly of components results in mechanical interfaces that have a limited thermal conductance. This leads to temperature gradients over a short interface length that may have an important influence on the transient thermal behaviour. The general equation presented in Section 4.1 already showed a definition of the heat transfer at the interface. Reference values range from 1700 to 3700 $\mathrm{W/(m^2\,K)}$ for steel-steel contact and 3000 to 4500 $\mathrm{W/(m^2\,K)}$ for steel-aluminium contact [25].

Detailed information about the physical behaviour of thermal contact interfaces is scarce and the accuracy is difficult to assess. However, the Comsol heat transfer interface does offer the possibility of a thermal contact description based on the material properties at the interface. The constriction conductance is based on the Cooper-Mikic-Yovanovich correlation[12], which uses the surface roughness, asperity slope, contact pressure and hardness. This results in a heat transfer coefficient that is imposed on the interface.

[1] A more detailed definition of the spindle design can be found in Appendix A.

4.5 Bearing flow and dissipation

The bearing domains of the spindle assembly are highlighted in Figure 4.3. As discussed in Section 3.1, the front bearing is a combined axial and radial bearing. The rear bearing only serves for radial support. The geometry defines the fluid flow from which the mechanical and thermal properties can be derived.

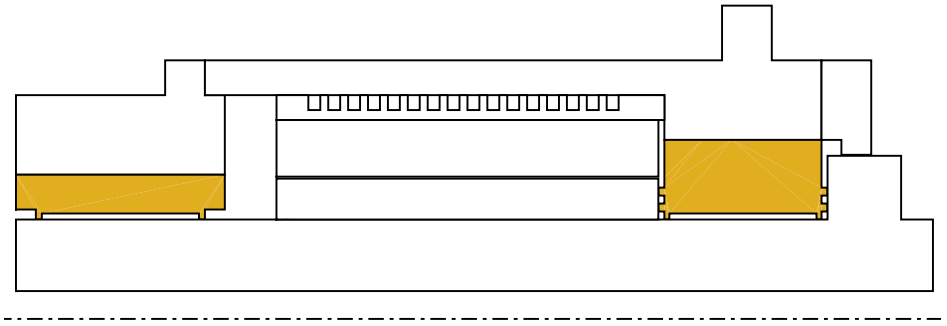

Figure 4.3: Hydrostatic bearing body

Fluid flow

The bearing fluid domain is modelled by bulk elements. In order to determine the viscous dissipation it is necessary to set-up an analytical model of the fluid flow. A network analysis is the foundation of the derivation of the flow characteristics, dissipation and heat transfer coefficients. From this analysis the parameters of the global equations are derived.

Figure 4.4 shows the front bearing with a description of the flow. The gap height is amplified to show the bulk element that represents the bearing gap. Black arrows indicate the direction of flow. At the lower left and right corner there is an intermediate outflow domain for the radial bearing and lower axial bearing wall. Bypass channels at the front and rear of the bearing feed the oil to the total outflow domains (top left and right).

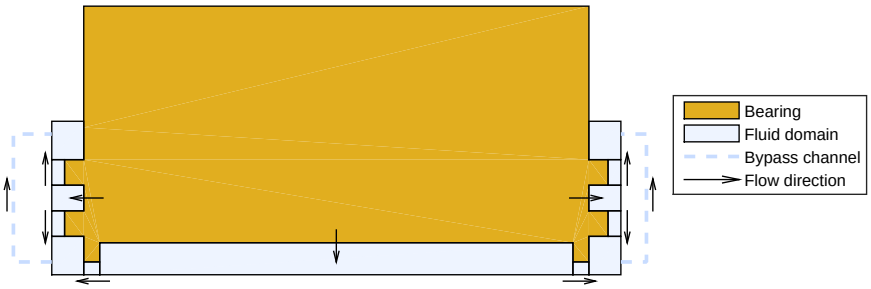

Figure 4.4: Front bearing fluid flow

The flow can be analysed as a network of resistances. A constant supply pressure is imposed on a network with a number of parallel paths. Each path represents one of the bearings. These consist of a fixed flow restrictor, recess volume and variable outflow resistance. It is assumed that the oil supply channel and recess have a negligible resistance compared to the restrictor and bearing gap.

The flow restrictors are set such that there is a nominal pressure ratio between recess and supply of 0.5. This means that the nominal value of the outflow and resistor resistance

are equal. Since all bearing paths are parallel, the calculations are done separately and subsequently summarised for the total flow[2].

Bearing geometry

The thermal performance of the bearing is mostly determined by the geometry of the lands. Figure 4.5 shows the most important dimensions. The axial and radial gap height, h_{ga} and h_{gr} respectively, are defined by the difference of bearing and spindle dimensions. In general, all diameters are denoted with a capital D and lengths with L.

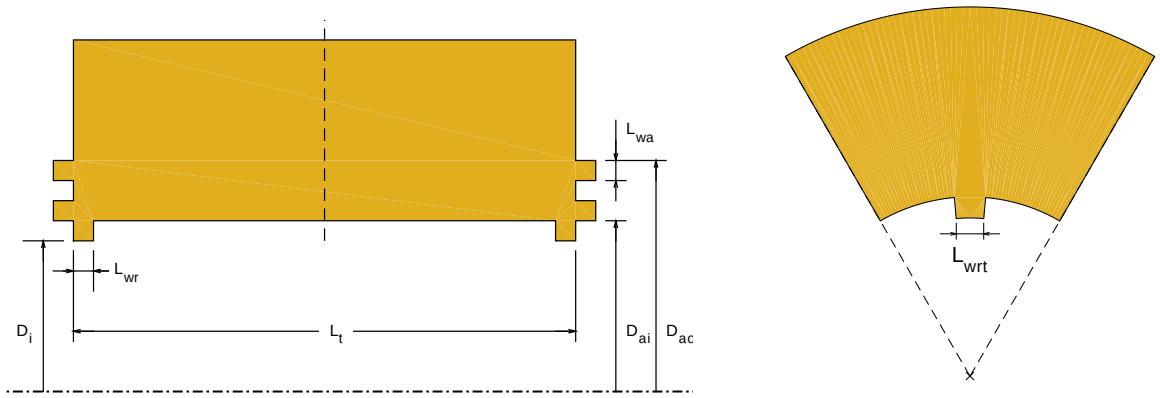

(a) (b)

Figure 4.5: Bearing geometry definitions

One of the difficulties of modelling an assembly with similar components is that the dimensions have to be named. All parts in this assembly have a length, and inner and outer diameters. Distinguishing between the dimensions can result in elaborate names and lengthy subscripts. A structured approach to this challenge is presented in the next chapter.

For each bearing the land and recess area is derived from the geometry. Figure 4.5 shows the geometry of the combined radial and axial bearing with the corresponding dimensions. The area of the axial wall (aw), tangential wall (tw) and recess (r) is then given by equations 4.16-4.18.

$$A_{\mathrm{aw}} = 2\left(\pi D_{\mathrm{i}} L_{\mathrm{wr}}\right) \tag{4.16}$$

$$A_{\mathrm{tw}} = 6L_{\mathrm{wrt}}(L_{\mathrm{t}} - 2L_{\mathrm{wr}}) \tag{4.17}$$

$$A_{\mathrm{r}} = (\pi D_{\mathrm{i}} - 6L_{\mathrm{wrt}})(L_{\mathrm{t}} - 2L_{\mathrm{wr}}) \tag{4.18}$$

The flow in the thin film across the land is well described by the Poiseuille flow model for laminar flow between parallel plates. For this well known model[3] the volumetric flow rate follows from Equation 4.19. The fluid speed is then obtained by dividing by the cross-sectional area. Finally, the Reynolds number follows from Equation 4.21. In this case the gap is thin annulus or slot, so the hydraulic diameter D_{h} is equal to twice the gap height

[2]The calculations are based on the relations from Rowe, Chapter 5 [27]. The pressure ratio of 0.5 is a common starting point in the design of hydrostatic bearings. It provides a good balance between load capacity and film stiffness.

[3]See also 2.8 in [27].

(see Rowe, p. 483 [27]).

$$Q_\mathrm{r} = \frac{L_\mathrm{o} h^3}{12\mu}\frac{dp}{dx} = 2\frac{\pi D_\mathrm{i}\beta p_\mathrm{s} h_\mathrm{gr}^3}{12\mu L_\mathrm{wr}} \tag{4.19}$$

$$U_\mathrm{r} = \frac{Q_\mathrm{r}}{2\pi D_\mathrm{i} h_\mathrm{gr}} \tag{4.20}$$

$$\mathrm{Re}_\mathrm{r} = \frac{\rho U D_\mathrm{h}}{\mu} = \frac{2\rho U h_\mathrm{gr}}{\mu} \tag{4.21}$$

Viscous dissipation

The friction power is a function of the tangential speed, area and gap height (Equation 4.22). It is quadratically related to the tangential speed. Additionally there is the dissipation from the pressure drop, which is described in Equation 4.23. Combined with the flow rate, density and heat capacity the adiabatic temperature increase (upper limit) can be calculated for each stationary speed. In the model, however, the power is used to compute the transient behaviour and account for heat transfer to the solid domains.

$$P_\mathrm{fr} = \mu\left(\frac{\omega D_\mathrm{i}}{2}\right)^2\left[\frac{A_\mathrm{aw}+A_\mathrm{tw}}{h_\mathrm{gr}} + \frac{4A_\mathrm{r}}{h_\mathrm{rr}}\right] \tag{4.22}$$

$$P_\mathrm{p} = Q_\mathrm{r} p_\mathrm{s} \tag{4.23}$$

Next, the fluid elements are determined. This is based on the physical size and configuration of the fluid domains[4]. Each element is assigned a label, volume, flow rate and heat transfer coefficient. Figure 4.6 shows a flow diagram with all the corresponding labels. The layout is chosen to match the geometry. The three and four letter abbreviations are tags of the elements. For instance, RRF stands for "radial recess front".

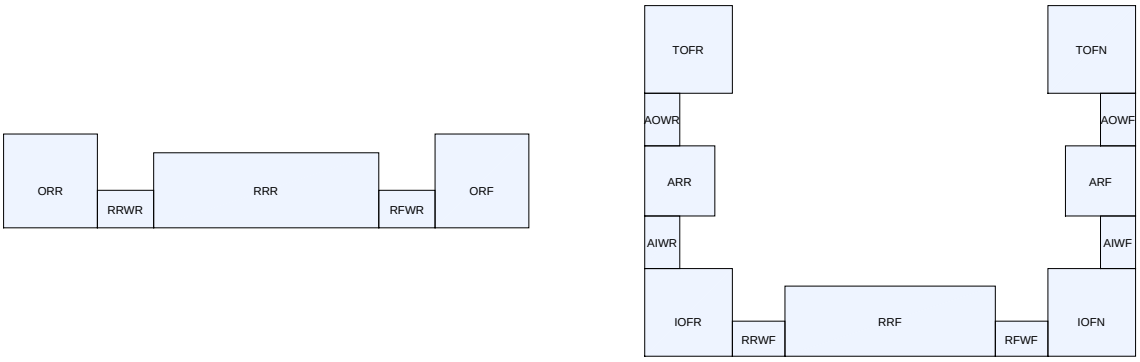

(a) Rear bearing (b) Front bearing

Figure 4.6: Bulk element naming

The flow rate follows from the analytical bearing calculation discussed above. For the radial bearings, the flow across each wall is half the total flow. However, for the axial bearings the flow is based on the corresponding wall dimensions, as the inner wall differs from the outer one. The element volumes are computed analytically using the variable dimensions and summation of simple ring volumes. It is assumed that all elements are completely filled with oil, although this is not exactly defined for the outflow domains.

[4] A detailed cross-section of these domains can be found in Appendix A.

In each element there is a heat input from viscous shear of the fluid. The power input is calculated above, as P_{fr} and P_{p}, for the recesses and gap domains[5]. The spindle speed is accounted for in a speed parameter λ (Equation 4.24), which is the ratio of actual over maximum speed. Since the friction power is proportional to the speed squared the actual power can be derived from the product of the maximum value $P_{\mathrm{fr,max}}$ and speed parameter squared (Equation 4.25).

Additionally, there is convective heat transfer between the fluid and the wall. This is evaluated in Comsol by a line integral over the fluid-solid boundaries of the total heat flux (Equation 4.26). The inner product of the heat flux vector $\mathbf{q}$ and boundary normal $\mathbf{n}$ is used so only the heat transfer across the boundary is integrated.

$$\lambda = \frac{n_{\mathrm{act}}}{n_{\mathrm{max}}} \tag{4.24}$$

$$q_{\mathrm{s}} = \lambda^2 P_{\mathrm{fr,max}} + P_{\mathrm{p}} \tag{4.25}$$

$$q_{\mathrm{t}} = \oint 2\pi R \left(\mathbf{q} \cdot \mathbf{N}\right) \mathrm{dL} \tag{4.26}$$

Each element represents a control volume for which a thermal balance can be created. The viscosity and density of the fluid are assumed to be independent of temperature. A constant volumetric flow therefore equals a constant mass flow. As the fluid is considered incompressible, there is no change in the mass of the control volume. The rotation of the spindle only adds a tangential speed to part of the fluid, but the flow in the R-z plane is maintained.

The energy balance is written in terms of storage, transport, shear heat input and convective heat transfer. The rate of change of the internal energy equals the sum of transport, shear $\mathcal{Q}_{\mathrm{s},i}$ and convection $\mathcal{Q}_{\mathrm{c},i}$. The transport term is defined as the difference between the bulk temperature and inlet temperature. For element with multiple inlets (mutual outflow domains), the inlet term is sum of all inlet flow rate and temperature pairs. The fluid is assumed to exit the control volume at bulk temperature. Equation 4.27 shows the basic form. This is implemented in null form and solved for the bulk temperature.

$$\frac{d\left(\rho c_{\mathrm{p}} V_i T_i\right)}{dt} = \rho c_{\mathrm{p}} Q_i (T_{i-1} - T_i) + \mathcal{Q}_{\mathrm{c},i} + \mathcal{Q}_{\mathrm{s},i} \tag{4.27}$$

Solving the energy balance results in the fluid temperature of the bulk elements. These are used to set up the convective boundary conditions at the walls of each element. The heat transfer coefficients for the gap domains are computed next to complete the boundary condition. Due to the high aspect ratio it can be assumed that the flow is laminar and fully developed (Equation 4.28). The average Nusselt number for flow between isothermal parallel plates is given by Equation 4.29 (p. 274 [25]).

$$\mathrm{Re} = \frac{2\rho U h_{\mathrm{g}}}{\mu} \tag{4.28}$$

$$\overline{\mathrm{Nu}}_{\mathrm{D_h}} = 7.54 + \frac{0.03\left(D_{\mathrm{h}}/L\right)\mathrm{RePr}}{1 + 0.016\left[\left(D_{\mathrm{h}}/L\right) D_{\mathrm{h}}\mathrm{Pr}\right]^{2/3}} \tag{4.29}$$

$$\overline{h}_{\mathrm{c}} = \left(\frac{k}{D_{\mathrm{h}}}\right) \overline{\mathrm{Nu}}_{\mathrm{D_h}} \tag{4.30}$$

The assumption of isothermal walls will have to be checked after a simulation, otherwise a constant wall heat flux might be more appropriate. The stationary solution at 4000 rpm

[5]For the outflow domains the viscous shear is set to zero.

Element	Re $(-)$	$\overline{\mathrm{Nu}}$ $(-)$	$\bar{\mathrm{h}}_\mathrm{c}$ $(kW/(m^2\,K))$
Front radial bearing wall	11.9	9.15	22.9
Axial inner wall	2.2	7.69	28.8
Axial outer wall	2.5	7.71	28.9
Rear radial bearing wall	9.9	8.71	21.8

Table 4.2: Heat transfer coefficients for bulk fluid gap elements

shows the largest temperature at the outer axial bearing wall. The increase along the wall is less than 1 °C for an average temperature around 45 °C. Note that the correct heat transfer coefficients are not yet implemented in this analysis.

It is a little more complicated to find suitable heat transfer coefficients for the recess and outflow elements. In an idle state the speed in these areas is relatively low since the cross-section is much larger. However, as the spindle speed increases the outflow area becomes a turbulent region and the actual heat transfer is poorly defined. The performance of the model is evaluated for several values of the heat transfer coefficient to assess the influence of this parameter.

4.6 Electric motor losses and cooling

Stator dissipation

The spindle is driven by an internal electric motor (Figure 4.7), which is the second source of heat. As described in the previous chapter, most of the thermal dissipation is located in the stator. Internal heating of the magnets in the rotor is neglected.

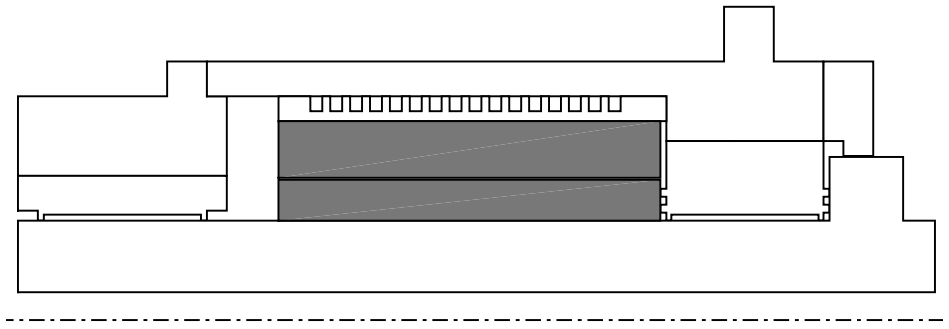

Figure 4.7: Electric motor components

The efficiency of the motor depends on both the load and speed at a certain time. This relation is determined in collaboration with the motor manufacturer. Figure 4.8 shows a graphic representation of this relation. The red line represents the efficiency at a given speed with only the stationary bearing friction. Other friction sources, such as in the air gap with the rotor or in the seals, are neglected.

When the efficiency of a state is determined, the dissipated power can also be calculated. Equation 4.31 shows the generic relation between dissipated power P_d, mechanical power P_m and electrical power P_e for a given efficiency η. The dissipated power at stationary conditions is presented in more detail in Appendix C.

$$P_\mathrm{d} = P_\mathrm{e}(1-\eta) = P_\mathrm{m}\frac{1-\eta}{\eta} \tag{4.31}$$

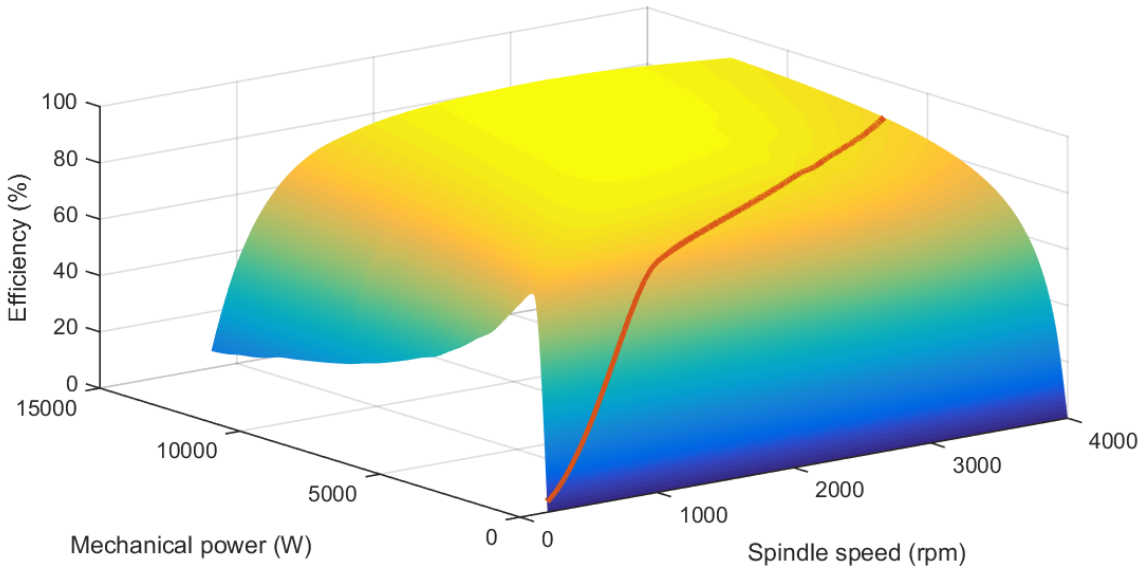

Figure 4.8: Electric motor efficiency

Stator radiation

Earlier in this chapter it is stated that external radiation sources are assumed to be negligible. However, radiation can still be relevant in the free space around the electric motor. If the stator temperature becomes sufficiently high, a net radiative heat transfer can take place between stator, rotor and other surrounding components.

An estimate of the potential radiative heat transfer can be made based on the observation that the stator temperature is limited to 100 °C, above this value the controller will force a spindle halt. Assuming a 20 °C temperature of the spindle the maximum heat transfer can be calculated. The Stefan Boltzmann constant σ is $5.67 \cdot 10^{-}8\,\mathrm{W/(m^2\,K^4)}$ and the emissivity of the steel housing ε is approximately 0.30.

The surface area of the stator is evaluated from the Comsol model at 0.232 $\mathrm{m^2}$. The estimated maximum heat transfer evaluates to 47 W (Equation 4.32), only 0.5% of the dissipated power at maximum speed. If a coating would make the surface more emissive, the heat flux would still be limited to 158 W.

$$\dot{Q}_{\max} = 0.30 \cdot 0.232 \cdot 5.67 \cdot 10^{-8} \left(373^4 - 293^4\right) = 47\,\mathrm{W} \tag{4.32}$$

From the estimate it appears that radiative heat transfer can be neglected in the preliminary check of the model. Figure 4.9 shows the heat flux for a stator temperature from 20 to 100 °C. The dotted line gives the maximum flux if the stator were a black body. The spindle temperature and stator surface are equal to the approximation above.

Cooling channel

The cooling jacket connects the stator to the spindle housing (Figure 4.10). A spiral groove is machined in the outer wall through which a water and ethylene-glycol solution flows to cool the stator. The inlet is at the spindle nose side to ensure minimal thermal influence of the stator on the housing between the mounting surface and spindle nose. As mentioned, the inlet temperature is set at a constant temperature.

The simplified axisymmetric geometry has repetitive grooves, representing the helical channel. Figure 4.11 shows the geometry and dimension definitions. Both the outer and

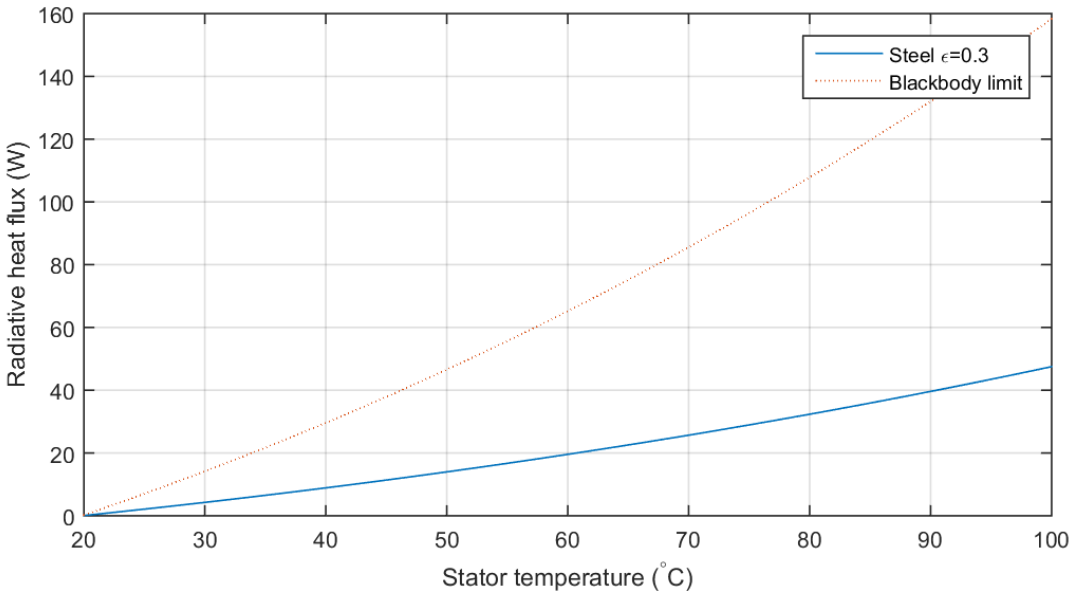

Figure 4.9: Theoretical stator radiative heat flux

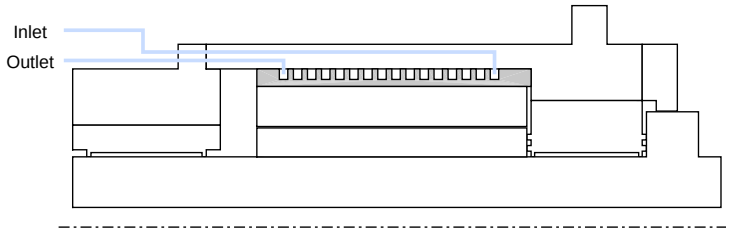

Figure 4.10: Cooling jacket component

channel dimensions are fully parametric. The cross-section is defined by the length L_c and height h_c, the pitch follows from the sum of channel and wall length. Definition of the number of turns follows from the total length, pitch and end length L_e.

To compute the heat transfer between the aluminium jacket and coolant the flow is analysed. The channel has a 6 by 7.5 mm cross-section through which coolant flows at 6 L/min. The hydraulic diameter then follows from Equation 4.33. For these parameters, the Reynolds number is approximately 10^4 (Equation 4.34) which is sufficient to assume fully established turbulence[6]. With the 90° angle at the entrance it is likely that the flow is turbulent in the entire channel.

$$D_h = \frac{4A_c}{\mathcal{P}} = \frac{4L_c h_c}{2L_c + 2h_c} = 6.7\,\text{mm} \tag{4.33}$$

$$\text{Re} = \frac{\rho U D_h}{\mu} = \frac{\rho (Q/A_c) D_h}{\mu} = 1.03 \cdot 10^4 \tag{4.34}$$

If a thermally fully developed flow is assumed the power law formula from Equation 4.36 can be used to compute the Nusselt number (see Mills, equation 4.44, p.270, [25]). This formula is valid for a smooth tube with $\text{Pr} > 0.5$ and $\text{Re}_D > 10^4$. With a Prandtl number of 22.4 and a finished turned spiral both assumptions are valid, although the Reynolds number is close to the lower validity boundary.

[6] A value of approximately 2300 is generally assumed as the transition to turbulence. However, turbulence only becomes fully established for $\text{Re}_D > 10^4$ (see Mills, p.269, [25]). Below this value the turbulence can be intermittent.

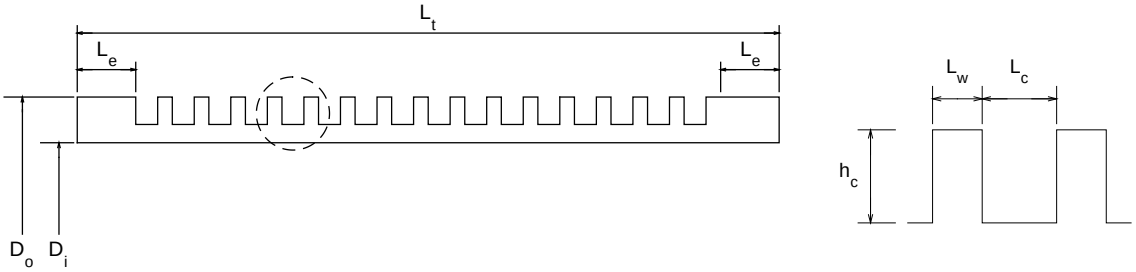

(a) Overall geometry (b) Channel dimensions

Figure 4.11: Cooling jacket geometry definitions

Alternatively, Gnielinski's formula in Equation 4.38 can be used, which is more accurate ($\leq$ 20% experimental error) and valid for a wider range of Reynolds numbers (see Mills, p.270, Equation 4.45). This formula requires the friction factor, which for smooth walls follow's from Petukhov's formula (Mills, Equation 4.42) in Equation 4.37. For the first analysis the power law formula from Equation 4.36 will be used. Finally, the convective heat transfer coefficient evaluates to $5\,\mathrm{kW/(m^2K)}$. Compared to the estimated range in Mills this value can be expected for forced convection in water.

$$\mathrm{Pr} = \frac{c_\mathrm{p}\mu}{k} = 22.4 \tag{4.35}$$

$$\mathrm{Nu_D} = 0.023\mathrm{Re_D}^{0.8}\mathrm{Pr}^{0.4}; \qquad \mathrm{Re_D} > 10^4 \tag{4.36}$$

$$f = (0.790\ln(\mathrm{Re_D}) - 1.64)^{-2}; \qquad 10^4 < \mathrm{Re_D} < 5\cdot 10^6 \tag{4.37}$$

$$\mathrm{Nu_D} = \frac{(f/8)(\mathrm{Re_D} - 1000)\mathrm{Pr}}{1 + 12.7(f/8)^{1/2}(\mathrm{Pr}^{2/3} - 1)}; \qquad 3000 < \mathrm{Re_D} < 10^6 \tag{4.38}$$

$$h_\mathrm{c} = \frac{k}{D_\mathrm{h}}\mathrm{Nu_D} = 5\cdot 10^3\ \mathrm{W/(m^2\,K)} \tag{4.39}$$

In the model a convective heat flux is defined with the computed heat transfer coefficient and a constant temperature equal to the inlet temperature. The latter assumption is principally incorrect. For a 1 kW total heat transfer and the defined material properties, the temperature increase will be approximately 2.5 °C. It is assumed that the viscosity is sufficiently low to neglect the viscous dissipation in the coolant.

4.7 Outer wall convection

At the outer wall the spindle unit is exposed to air, which is considered to be an infinite volume at ambient conditions. The housing wall and spindle nose are analysed separately to account for the rotation of the spindle. Figure 4.12 shows the distinction in the model geometry.

Heat transfer at the housing wall can be analysed as flow on a heated horizontal cylinder. This type of natural convection results in laminar flow for Grashof numbers smaller than 10^9 [25]. Equation 4.40 shows the relation, with the volumetric expansion coefficient β_air, temperature difference ΔT, gravitational acceleration g, diameter D and kinematic viscosity ν.

The Rayleigh number $\mathrm{Ra_D}$ (Equation 4.41) is computed as intermediate variable, it is the product of the Grashof and Prandtl numbers. This variable is used for the correlation functions in Equations 4.42 and 4.43. Considering the thermal properties of air at 20 °C and

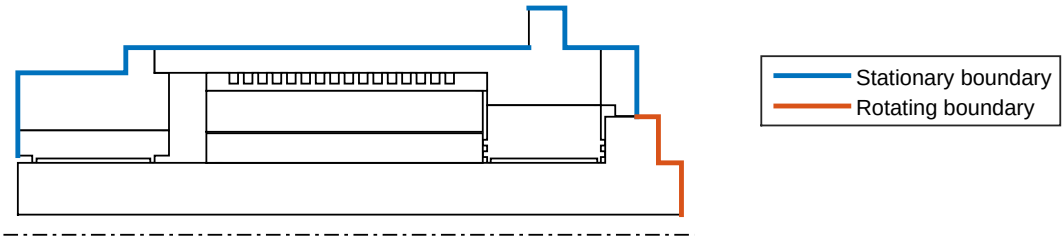

Figure 4.12: Outer wall convection

an average diameter of 165 mm the Grashof number evaluates to $6.6 \cdot 10^5$ per degree Celsius. With this observation it can be concluded that the convection stays in the laminar regime. Since the heat transfer depends on the actual temperature difference the relations have to be incorporated in the numerical model, rather than setting a fixed coefficient.

$$\mathrm{Gr_D} = \frac{\beta_{\mathrm{air}} \Delta T g D^3}{\nu^2} \tag{4.40}$$

$$\mathrm{Ra_D} = \mathrm{Gr_D Pr} \tag{4.41}$$

$$\overline{\mathrm{Nu_D}} = 0.36 + \frac{0.518 \mathrm{Ra_D}^{1/4}}{\left[1 + (0.559/\mathrm{Pr})^{9/16}\right]^{4/9}}; \qquad 10^{-6} < \mathrm{Ra_D} \lessapprox 10^9 \tag{4.42}$$

$$\overline{\mathrm{Nu_D}} = \left(0.60 + 0.387 \left[\frac{\mathrm{Ra_D}}{\left(1 + [0.559/\mathrm{Pr}]^{9/16}\right)^{16/9}} \right]^{1/6} \right)^2; \qquad \mathrm{Ra_D} \gtrapprox 10^9 \tag{4.43}$$

The rotating spindle nose consists of a cylindrical and planar surface. For both surfaces the Reynolds number has to be evaluated, which is a function of the angular velocity ω, radius R and again the kinematic viscosity. A modified version of the Grashof number is also required (Equation 4.45), which is based on the radius R. Equation 4.46 gives the average Nusselt number for convection at the axial surface [36].

$$\mathrm{Re} = \frac{\omega R^2}{\nu} \tag{4.44}$$

$$\mathrm{Gr} = \frac{\beta_{\mathrm{air}} \Delta T R^3 \pi^{3/2}}{\nu^2} \tag{4.45}$$

$$\overline{\mathrm{Nu}}_{\mathrm{ax}} = 0.4 \left(\mathrm{Re}^2 + \mathrm{Gr}\right)^{0.25} \tag{4.46}$$

For the radial surface three regimes of the Reynolds number can be distinguished (Equations 4.47-4.49, [36]). The first relation describes free convection, which is only valid below 17 rpm. A mixed free and forced convection regime exists until a Reynolds number of $5 \cdot 10^4$. At higher Reynolds numbers fully forced convection sets in. In terms of spindle speed this transition occurs between approximately 1000 and 2100 rpm. The correlation for the forced regime requires an additional coefficient $\mathrm{C_D}$, which is defined as an implicit function of the Reynolds number. Figure 4.13 shows the three regimes and the transition region for a

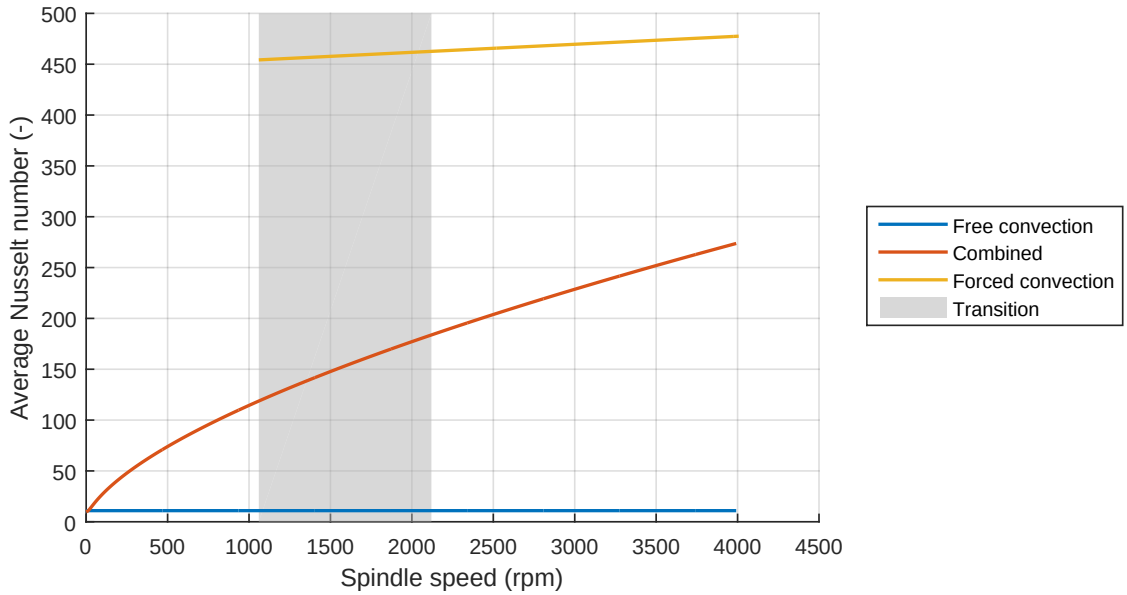

Figure 4.13: Average Nusselt number for radial spindle nose wall

temperature difference of 1 °C and ambient air conditions at 20 °C.

$$\overline{\mathrm{Nu}}_{\mathrm{rad}} = 0.456\,(\mathrm{Gr}\cdot\mathrm{Pr})^{0.25}; \qquad \mathrm{Re} < \sqrt{\mathrm{Gr}/\mathrm{Pr}} \tag{4.47}$$

$$\overline{\mathrm{Nu}}_{\mathrm{rad}} = 0.18\left[\left(0.5\mathrm{Re}^2 + \mathrm{Gr}\right)\mathrm{Pr}\right]^{0.315}; \qquad \mathrm{Re} < 5\cdot 10^4 \tag{4.48}$$

$$\overline{\mathrm{Nu}}_{\mathrm{rad}} = \frac{\mathrm{RePr}\sqrt{\mathrm{C_D}/2}}{5\mathrm{Pr} + 5\ln\left(3\mathrm{Pr}+1\right)} + \sqrt{2/\mathrm{C_D}} - 12; \qquad 10^5 < \mathrm{Re} \tag{4.49}$$

$$B = \mathrm{Re}\sqrt{\mathrm{C_D}} \tag{4.50}$$

$$\frac{\mathrm{Re}}{B} = -1.828 + 1.77\ln(B); \qquad 950 > B \tag{4.51}$$

$$\frac{\mathrm{Re}}{B} = -3.68 + 2.04\ln(B); \qquad B < 950 \tag{4.52}$$

4.8 Spindle suspension

The components are defined such that the bearing gaps are actually included in the geometry. This gives the mechanical model freedom to expand non-uniformly into the gap. If the spindle is linked by its nodes to the bearing surface the thermal deformation mimics the situation of a seized bearing.

Separating the spindle from the other components also severs the relationship to the mounting surface that acts as a mechanical reference. Since the model is defined in an axisymmetric frame the radial direction is inherently constrained. However, the spindle geometry has to be linked to the front bearing to properly constrain the model. Figure 4.15 shows a schematic of the axial constraint, a numerical spring between the bearing and spindle.

Implementing the springs is achieved by evaluating the displacement of the bearing and spindle surfaces. For each side, the difference between the displacement of the two parts is calculated. This value, multiplied by a constant k_{ax}, is applied as an external force to

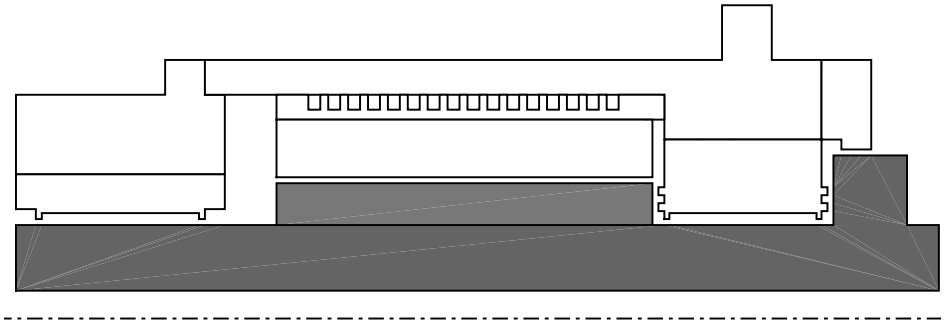

Figure 4.14: Spindle assembly with amplified gap height

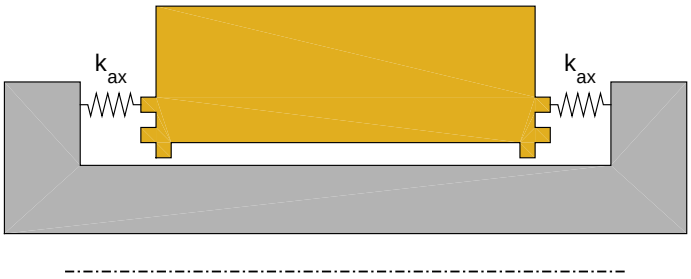

Figure 4.15: Schematic of the axial spindle constraint

the spindle surface (Equation 4.53)[7], a factor 2 is included to account for the two springs in parallel. The constant is numerically equivalent to the bearing film stiffness (Equation 4.54, derived from [27]). This linearisation is valid at the nominal gap height h_{ga}. The static bearing pressure is omitted, as it's influence is eliminated by using the initial deformation state as a reference. It is not the purpose to evaluate the effect of static forces on the geometry, only to apply a constraint force that centres the spindle in the axial bearing.

$$F_{\mathrm{ax}} = 2k_{\mathrm{ax}}\left(\bar{w}_{\mathrm{frb}} - \bar{w}_{\mathrm{spd}}\right) \tag{4.53}$$

$$k_{\mathrm{ax}} = 3\beta\left(1-\beta\right)p_{\mathrm{s}}\frac{\pi\left(r_{\mathrm{om}}^2 - r_{\mathrm{im}}^2\right)}{h_{\mathrm{ga}}} \tag{4.54}$$

[7]Note the use of the variable w for the axial displacement. In a finite element model the variables (x, y, z) generally denote the nodal coordinates, whereas the set (u, v, w) gives the displacements per material point.

Chapter 5

Numerical implementation

The equations that describe the thermomechanics are implemented in a numerical model to evaluate the system behaviour. First, the implementation in the modelling software is described in Section 5.1. The demand for a parametric model requires the development of a new structure to generate the model. An overview of the required methods is also given in this section. The parametric structure of the model itself is worked out in Section 5.2. A description of the contents of the model itself follows in Section 5.3. Methods for reviewing and analysing the results are presented in Section 5.4.

5.1 Modelling software

The review of modelling methods for thermal error resulted in two possible approaches, lumped mass and finite element. At the start of the research there was limited insight in the internal temperature field and influence of the various boundary conditions. The assessment of the Biot number in Section 4.2 had not been performed yet at that stage. However, there was a clear indication that there would be significant temperature gradients in the components, especially in the front bearing. Considering the complicated deformation of a non-uniformly heated structure the choice is made to proceed with a finite element model.

Modelling is performed in the finite element program Comsol Multiphysics. This software package was mentioned in Section 2.2 for its inherent multi-physics approach that allows fully coupled analyses. It also has an interface for Matlab to enable a scripting perspective of the modelling process. The module, called LiveLink^{TM} *for* Matlab, sets up a server-client interaction between the two programs.

All functionality of the software is contained in the LiveLink, including the full API, only the desktop interface is not started. A user can use the Matlab command window or scripts to perform operations on the model. Comsol considers a model to be an object with a structured set of properties, values and settings. Accessing and modifying a model object can be done with Java based commands. The basics on the LiveLink interface are described nicely in the *LiveLink for Matlab User's Guide* [22]. More detailed information on the commands are worked out in the *Comsol Programming Reference Manual* [13].

Comsol model structure

A model object in Comsol is similar to a custom class in Matlab. It is built on a Java based structure and contains both the model information and methods (internal functions) to modify the model object. Figure 5.1 shows the standard structure of a model, which can be recognised from the model tree in the Comsol desktop. The model object is the root, containing global definitions, one or multiple components, study nodes and results. This architecture is reflected in the object structure.

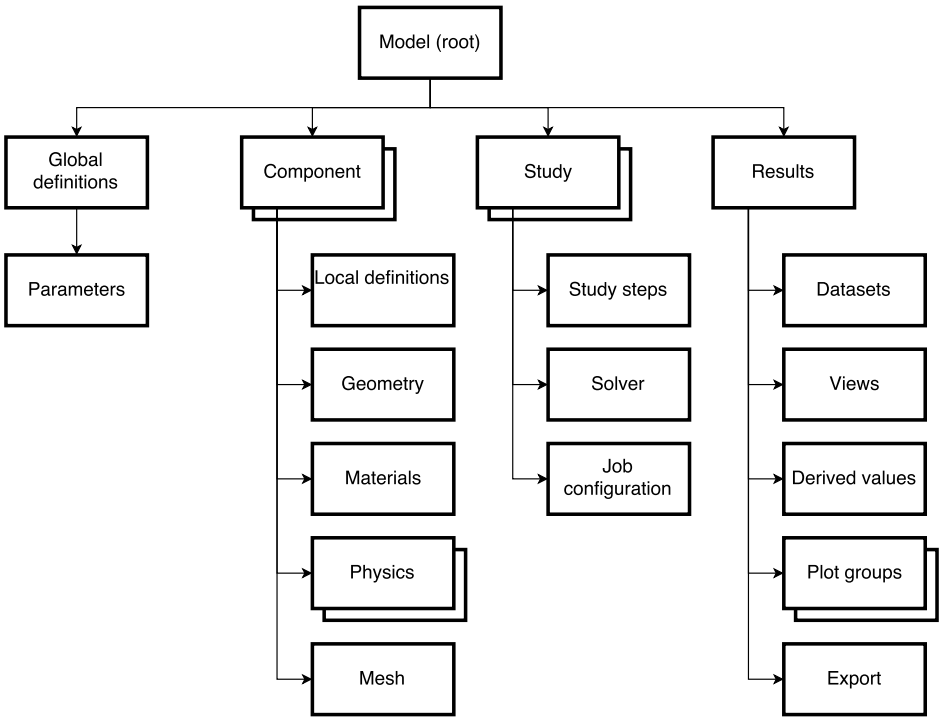

Figure 5.1: Comsol model structure

Example 5.1 shows the commands required to start a new model. First, the methods and utilities have to be imported to the workspace (line 1-2). A model object can then be created (line 5) and any number of top level properties can be set (line 6). The global definitions node is the only one present by default. Adding a component has to be done manually by calling the *create* method in line 7.

```
1   import com.comsol.model.*                    % Import model prototype
2   import com.comsol.model.util.*               % Import utility methods
3
4   % Create default model
5   Model = ModelUtil.create('Model');           % Create Model object
6   Model.hist.disable;                          % Disable history
7   Model.modelNode.create('comp1');             % Create component
```

Example 5.1: Creating a new model object

The code excerpt gives an indication of the syntax style. It is important to note that all calls to methods are performed using this dot-notation. The structure is somewhat similar to the Matlab data type *structure*, in which fields are separated from the parent variable by dots. A key difference is the fact that the model instance is an object, containing both data

and functions, whereas Matlab variables only contain data[1].

Definition of the model features is performed next. Most of the features have to be created first, some are present by default, and can subsequently be configured. Example 5.2 gives two typical sets of commands for a new feature. The first definition is a selection feature, which allows the user to select a geometric entity from a feature name, instead of from it's number[2]. The sequence consists of a *create* call, followed by definition of a *label* and any number of *set* operations to define the properties.

Features can also be nested, which is demonstrated in the second part of Example 5.2. This snippet of code shows the definition of a study node `'std1'` (level 1) and a nested study step `'stat'` (level 2). One of the properties of the latter feature is modified in the last line using a *set* operation.

```
1      % Create selection and set properties
2      Model.selection.create('coolingChannel','Box');
3      Model.selection('coolingChannel').label('Cooling channel');
4      Model.selection('coolingChannel').set('entitydim',1);
5
6      % Create study and study step
7      Model.study.create('std1');
8      Model.study('std1').create('stat', 'Stationary');
9      Model.study('std1').feature('stat').set('initstudyhide', 'on');
```

Example 5.2: Creating and configuring features

For some modelling purposes it is possible to define a model in the Comsol Desktop and only apply modifications from Matlab. Working from the desktop environment is easier to learn and provides more assistance in defining the features. Unfortunately, partially predefined models can not be used in this case since the basis of the model, the geometry, is flexible in nature. This forces all other features to be Matlab based as well.

Working strictly from the Matlab environment implies that all features have to be defined in code. Selecting boundaries or domains for specific conditions is therefore programmatic, not visual. Every entity selection for a feature must be defined based on geometry. This also makes model more robust for changes in geometry.

Standardised framework

The code syntax examples demonstrate a high level of code repetition, especially when nested features are created and modified. This makes the script much less readable and is generally considered bad practice among programmers. A partial solution to the code repetition is given in Example 5.3. The Comsol model instance in the Matlab workspace is a pointer to the actual object running on the Comsol server. Additional pointers can be created to link to (nested) features, which is demonstrated in the code example. This eliminates much of the repeating parts of the commands.

Although the use of additional pointers reduces the code to some extent, there are still many uses of the same types of calls. Moreover, this method of programming has little or no separation of the model feature definitions (data) and the methods that are used to create

[1]The only way to combine data and functions in a Matlab variable is to define a custom class.

[2]Each node, boundary and domain of a finite element model is numbered by the underlying software. The difficulty of script based definitions is that these numbers depend on the exact geometry. A better approach is to create geometry based selections with text identifiers and use these to apply the selection to a feature.

them. Defining and creating a model is completely intertwined, leaving no possibility to save the definitions separately. In the course of the research several structures have been tried to separate the data from the methods. First of all, the numeric data that is required for the model can be stored in Matlab variables (Example 5.3). This takes care of the separation of dimensions and coefficients from the implementation. However, the choice of features and the corresponding settings are still hard-coded.

```
% Create study and study step (simplified)
Study = Model.study.create('std1');
Step  = Study.create('stat', 'Stationary');
Step.set('initstudyhide', 'on');

% Create selection and set properties (simplified, parametric)
x   = 12;
Sel = Model.selection.create('coolingChannel','Box');
Sel.set('xmin',x);
```

Example 5.3: Simplified feature definition

A generalised approach is developed to completely separate the definition of features from the methods that create them. This allows easy rebuilding to eliminate artefacts, provides a structured approach to larger models and enables saving of the definitions in a Matlab environment. Reviewing the commands used to create all features, from global parameters to output, resulted in a select number of recurring calls. All features are created with (variations of) the methods shown in Example 5.4.

The type and amount of methods required to configure a feature depends on where it is located in the Comsol model tree from Figure 5.1. Most features have a tag (unique identifier), type and simple *set* properties. Materials and physics features are also attributed to an entity by means of a selection.

The calls from Example 5.4 are wrapped in a function that automatically runs all methods for a given feature. A variable that contains all feature information is required as an input variable, as is a pointer to the current state of the model. Methods for which no input data is provided are skipped. There is also some additional coding to account for variations in the structure programmed by Comsol developers. The function outputs a pointer to the augmented model. A comprehensive description of the function is provided in Appendix D.

```
Feat = Parent.create(<tag>,<type>,<model>)      % Create feature
Feat.label(<label>)                             % Add text label
Feat.geom(<geometry>,<dimension>)               % Attribute to geometry
Feat.selection.named(<selection>)               % Select geom. entity
Feat.set(<name>,<value>)                        % Set properties
Feat.setIndex(<indexTag>,<value>,<row>,<col>)   % Set indexed properties
Feat.(<namedFeat>)(<argument>)                  % Set named properties
```

Example 5.4: Generalised feature methods

5.2 Parametric model definition

After separating the data from the methods a structure for the model definitions can be set up. This part can be customised for every model, only the feature properties have to be formatted to match the generalised structure. All other aspects of the model definition can be defined as required by the analysis. In general, the approach can be re-used in other projects, since it is based on generating a model tree that contains all information to generate a Comsol model and store any number of results.

Figure 5.2 gives an overview of the proposed structure. All information is captured in a single variable of the data type *structure* with fields for the general information, definitions, features and results. This set-up give the user the opportunity to save and load models and use scripting techniques for comparison and modification.

The general information is a collection of model meta data, such as file names, date of creation, path and Comsol version. The parameters that describe properties of the model are stored in the *definitions* field. Next, a strictly formatted set of feature properties can be found in the *features* field. The contents structure corresponds to the generalised approach presented in the previous section. Finally, the *results* field provides a storage location for the model output.

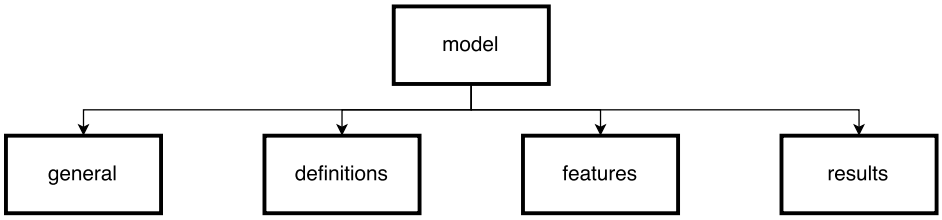

Figure 5.2: Matlab model structure

Definitions

The definitions section contains a further categorisation in system variables, geometry, materials and analytical calculations. Design parameters are defined and stored in the first three fields, these capture all design choices. The values are used to perform analytical calculations. This separation is strict in the sense that the field *analytical* contains all results from these calculations and no design parameters.

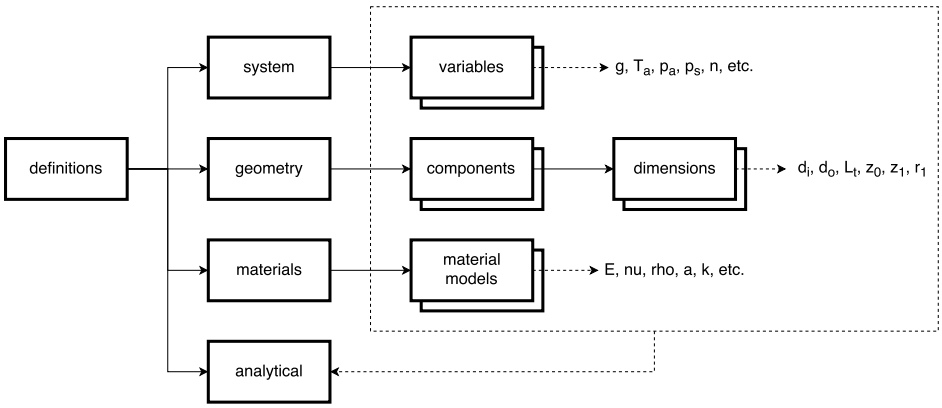

Figure 5.3: Matlab definitions structure

Due to the complexity of the system, which is defined by 104 interrelated dimensions, it is practical to store the geometric information per component. This simplifies the naming,

since the parameter suffix only has to differentiate within the scope of one component. All components contain the variables z_1 and r_1, which are vectors describing the geometry in a cylindrical coordinate system.

A similar approach is taken for the materials, where each material model is stored in a separate field. Therefore, the material properties do not have to carry suffixes to identify the material type.

Features

Definition of the features requires a strict formatting to enable the use of the generalised Comsol methods. Features are defined by a structure with a set of twelve fields. Each field is related to a specific Comsol method. For example, the string in the *label* field is fed to the `Feat.label(<string>)` method. For *set*, *index* and *named* fields it is also possible to define many properties in a compact way. If fields are empty the corresponding methods are skipped.

Field	**Data type**	**Description**
feature	char, cell array	Comsol (nested) parent type
create	boolean	Create (1) or call existing (0)
tag	char	Unique identifier (custom)
type	char	Comsol feature type
label	char	Custom description
model	char	Model or geometry identifier
dimension	numeric	Space dimension
selection	char	Tag of selection feature
value	cell array	List of set properties
index	cell array	Index based properties
named	char, cell array	List of other named properties
enabled	boolean	Incorporate (1) or skip (0)

Table 5.1: Generalised properties for Comsol feature

5.3 Numerical implementation

The system is modelled as an two-dimensional thermomechanical model, axial symmetry is an additional geometry setting within this space dimension. The description of the features in this section will follow the structure of the Comsol model tree from Figure 5.1. A specific order of definitions is required, since there are dependencies between the features. Boundary conditions, for instance, can only be assigned to a defined geometry with a selection feature. In that case the order of creation is geometry, selection, boundary condition.

Global definitions

System level parameters are set in the global definitions scope. For this model these include the spindle speed and the inlet and ambient conditions. Table 5.2 gives a list of the global parameters, which are matched to the actual operating conditions in the validation stage. These are also the properties that are available for parametric sweeps in the study settings.

Parameter	Symbol	Value
Oil inlet temperature	T_{oil}	18 °C
Coolant inlet temperature	T_{gly}	20 °C
System pressure	p_{s}	60 bar
Pressure ratio	β	0.5
Actual spindle speed	n	2000 rpm
Maximum spindle speed	n_{max}	4000 rpm
Glycol flow rate	Q_{gly}	6 L/min

Table 5.2: Operating condition parameters

The fluid domains described in Section 4.5 are included in the model as bulk elements, rather than geometric entities. Each bulk element is assigned a volume, heat transfer coefficient and volumetric flow rate. These are used to implement global equations that describe the heat balance in the simplified fluid system.

Component

The component contains the standard categorisation of geometry, materials, physics and mesh. Additionally, local definitions are used to select features, couple model quantities and compute intermediate variables.

Definition of most features is based on the flexible component geometry, which is defined first. The dimensional vectors that were defined in Section 5.2 are used to create Bézier polygons that represent the components. Each of the nodes is defined and linked by first order (linear) segments to form a solid geometry. Axial symmetry is applied as a boolean setting in the main geometry node. Figure 5.4 shows the Bézier polygon of the housing.

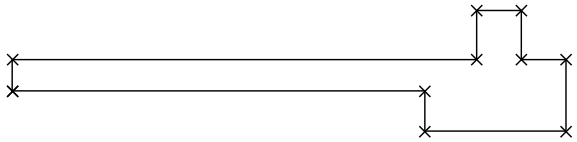

Figure 5.4: Bézier polygon of the housing

Next, a set of local definitions is defined. Named selections, such as described in Section 5.1, are created first to automatically attribute features to geometric entities. In a FEM model nodes, boundaries and domains are automatically numbered by the software. When working in a desktop environment feature entity selections are performed by mouse clicks. From the server side the user can either select directly based on entity number or by tag name of a selection feature (third field in Table 5.1).

The latter option is chosen in this study to allow maximum flexibility. Changing dimensions and optionally omitting components makes entity numbers difficult to predict. This challenge is met by defining selection features, which consist of a selection method, space dimension, range and tag. Figure 5.5 shows a box selection of the mounting surface as an example. The coordinates are coupled to the same dimension parameters as the geometry, which keeps the model consistent as long as the topology is maintained.

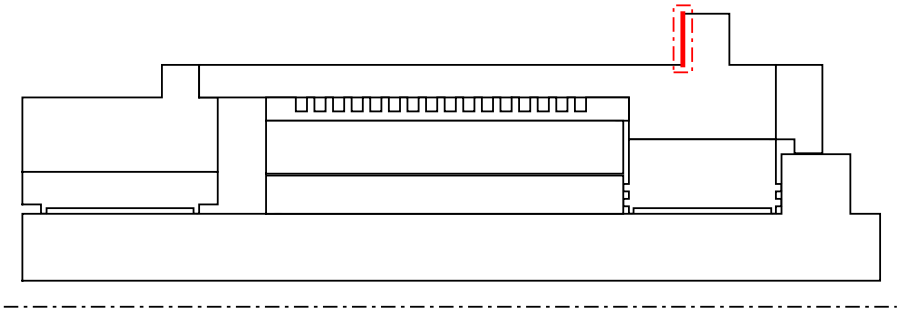

Figure 5.5: Box selection of the mounting surface

Domain selections are made in a similar fashion, which are mostly used to attribute the material types to the geometry. These are defined according to the description in Chapter 4. A list of material properties is included in Appendix B.

The local definitions group is also the parent of the coupling operators, functions and local model variables. Average operations are used to determine the axial bearing displacements. Integration operators over the solid walls of the bulk fluid elements serve to find the total heat transfer $\mathcal{Q}_\mathrm{t}$ at the fluid-solid interface. One integration is performed per bulk element. An example is shown in Figure 5.6 with the integration boundary shown in red. This example relates to the wall of the front axial recess. The operator itself is only the selection and the choice of 4^th order numerical integration (default setting).

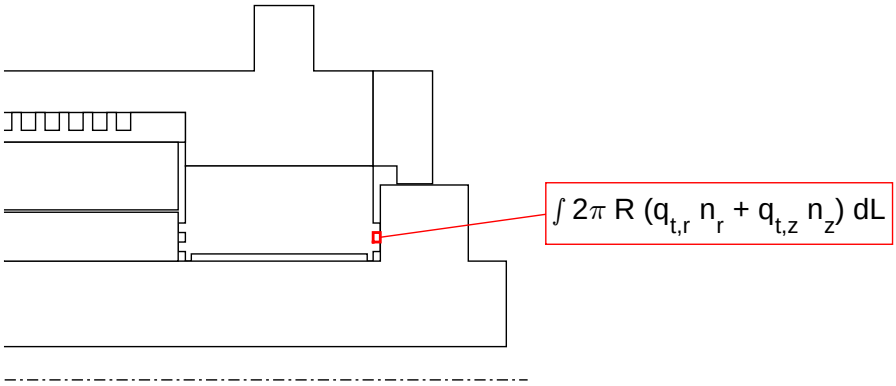

Figure 5.6: Bulk element wall integration

A function is defined to determine the dissipated power P_d in the moter, as described in Section 4.6. It is essentially an interpolated look-up table that evaluates the power at a given speed. The data is corresponds to the stationary motor conditions discussed in Appendix C.

The flexible nature of the model requires a large number of user defined variables. An important difference between variables and parameters is that the former are evaluated at every time point, instead of only at the start of the solution. Three sets are defined to separate variables related to general conditions, bulk elements and heat transfer.

In the first set of variables a number of general conditions are calculated. The recess inlet temperature T_r of the oil is computed here to account for the pressure drop in the restrictor. A speed ratio λ is derived to scale the viscous dissipation.

The second set of variables contains the evaluation of the dissipated and transferred heat for every bulk element. The former, $\mathcal{Q}_{\mathrm{s},i}$ in Equation 5.1, follows from the dissipation at maximum speed $\mathcal{Q}_{\mathrm{d},i,\mathrm{max}}$ (see Section 4.5), the squared speed ratio and pumping power $\mathcal{Q}_{\mathrm{p},i}$ (stationary part). This approach is relatively easy to implement, while keeping the squared

relation between speed and viscous dissipation from the spindle rotation. The transferred heat $\mathcal{Q}_{t,i}$ is derived from the integration of the normal total heat flux at the bulk element boundary. Equation 5.2 shows the relation that also appears in Figure 5.6.

$$\mathcal{Q}_{s,i} = \lambda^2 \mathcal{Q}_{d,i,max} + \mathcal{Q}_{p,i} \tag{5.1}$$

$$\mathcal{Q}_{t,i} = \int 2\pi R \left(\mathbf{q}_t \cdot \mathbf{n}\right) dL \tag{5.2}$$

Finally, a set of variables is defined to describe the heat transfer to the environment at the outer wall of the shaft and spindle unit. This includes computation of the Reynolds, Grashof and Rayleigh numbers to assess the heat transfer regime. From this the relevant Nusselt number and heat transfer coefficients are derived (Section 4.7). The model has to account for the different regimes, which is achieved by using conditional statements in the variable definition. Equation 5.3 gives an example of the average Nusselt number of the spindle nose radial wall, for which three regimes are defined. The model automatically switches between free Nu_{free}, combined Nu_{com} and forced Nu_{for} based on the spindle speed n and Reynolds number.

$$\mathrm{Nu} = \mathrm{Nu}_{free}\left(n < 17\right) + \mathrm{Nu}_{com}\left(n > 17 \& \mathrm{Re} < 10^5\right) + \mathrm{Nu}_{for}\left(\mathrm{Re} > 10^5\right) \tag{5.3}$$

The physical relations described in Chapter 4 are captured in the *Heat Transfer in Solids* and *Solid Mechanics* physics interface. The former is the most elaborate, as many boundaries have individual heat transfer coefficients and external temperature.

Figure 5.7 shows an overview of the boundaries that have a specified condition. The conditions are highlighted and categorised as convective, radiative and thermal contact. It also shows the only domain condition, which is the dissipated power in the stator. The actual list of boundary conditions consists of 25 entries to account for the varying parameters.

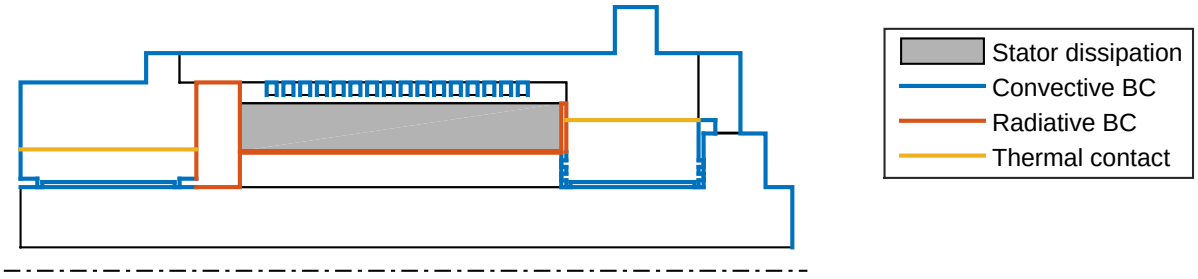

Figure 5.7: Heat transfer boundary condition overview

Defining the mechanical interface is much less intricate. This only describes the thermal expansion, mounting surface constraint and spindle suspension. Figure 5.8 gives an overview of the boundary conditions. There is a unidirectional coupling between the two physics interfaces, from temperature to displacement by thermal expansion. The reverse coupling is omitted in this model to keep the complexity manageable[3].

The mesh is one of the few aspects of the model that is generated without customised settings. A physics based triangular mesh is used, which leads to the distribution shown in Figure 5.9. This consists of a total of 3026 elements with an average quality of 0.91, a quite high value indicating nicely shaped elements. The minimum quality of 0.39 ensures that sliver shaped elements are not present. In the coupled analysis this results in slightly less than 20 thousand degrees of freedom.

[3]Thermal expansion also causes the bearing gaps to change in size, which influences the viscous dissipation. Since this variable is dependent on the gap height cubed the effect can be significant for small changes.

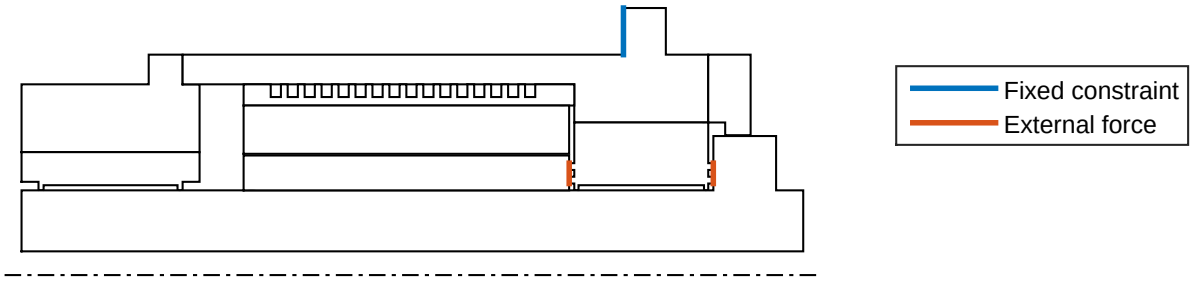

Figure 5.8: Solid mechanics boundary condition overview

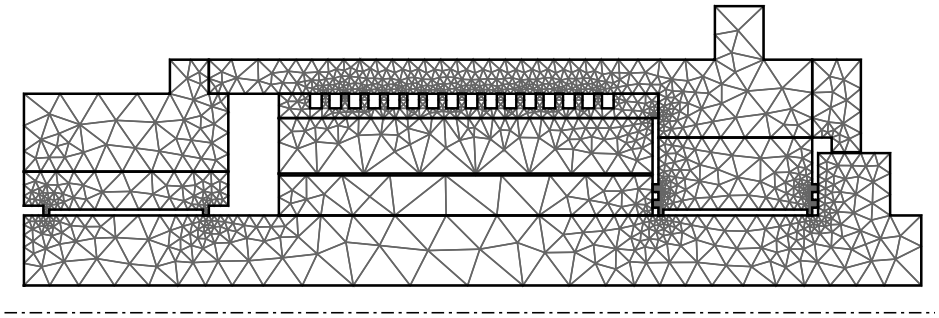

Figure 5.9: Free tetrahedral mesh

Finally, a number of probes are defined. These are evaluation parameters that can also be viewed during solving from the desktop environment. Their names also allows evaluation from the server at all time points after the solution is complete. Several types of probes exist, relating to the space dimension. Point probes are especially interesting since these can be placed anywhere on the geometry, irrespective of the mesh nodes. More information on the specific use of these probes is given at the end of this section.

Study settings and solvers

A study with two steps is set up to investigate the thermal response. For a coupled thermomechanical model there is only a limited number of study types available in the current software. First, a stationary solution is computed for zero spindle speed. This is the reference state for the step responses. Secondly, a transient study is performed with a speed step starting at the first time point.

Both study steps are prepared for a parametric sweep of spindle speeds. The maximum deformation at a given speed is quickly computed with the stationary step, whereas the time constants follow from the transient step. Changes to any of the global parameters can also be investigated with this approach. More fundamental changes, such as to geometry or bearing parameters, have to be driven from Matlab to account for all dependencies. The solvers of both steps are the default versions for the given study types. Trial simulations result in quick and properly converging results.

Results evaluation

Working with multiple solutions, in this case a stationary and transient, requires the explicit definition of datasets that correspond to the solver output. A dataset is linked to a solver by the solver's tag, which in turn is linked to a study step. Defining datasets with specific tags is also important for results evaluation from Matlab.

Results are displayed in the desktop environment in plot groups. A group can be seen as an axes in a Matlab figure, in which multiple plots can be displayed simultaneously. Plot groups relating to the temperature and deformation field are included for evaluation. These can be viewed in Matlab figures or when the model is opened in the desktop environment. The latter option is very useful in the testing stages, when server based changes are continuously checked in the updated desktop model. The options for results extraction are discussed in more detail in the next section.

A number of evaluation variables have been defined to assess the model dynamics. Table 5.3 shows a list of variables used for the evaluation and validation process. Most of these relate to the temperature field, which provides a number of useful intermediate variables. The final performance is related to the actual thermal expansion of the spindle nose.

Name	**Symbol**	**Type**
Oil inlet temperature	T_{in}	Parameter
Front bearing outlet temperature	T_{frb}	Global variable probe
Rear bearing outlet temperature	T_{reb}	Global variable probe
Front bearing core temperature	T_{hfrb}	Point probe
Housing core temperature	T_{hhou}	Point probe
Housing wall temperature	T_{whou}	Boundary probe
Glycol inlet temperature	T_{gin}	Parameter
Glycol outlet temperature	T_{gout}	Global variable probe
Motor temperature	T_{m}	Domain probe
Front seal ring drift	X_{fsr}	Boundary probe
Spindle nose drift	X_{spd}	Boundary probe

Table 5.3: Model evaluation variables

Note that the results are defined in the Comsol server enviroment, they are available in the desktop environment or with server calls. The actual evaluation and extraction of the results requires some additional considerations.

5.4 Extracting results

After running the model the results only exist in the scope of the Comsol server environment. Saving the model at this point stores both model and results in a model file. Evaluating the performance can be done by opening the model in the Comsol user interface, generating plots from the server visualisation tools or extracting results to the Matlab workspace.

Model results can be evaluated in the desktop environment of Comsol. This is the easiest way to define new results visualisations. The drawback of this approach is that saving results requires many manual operations. A lot of care has to be taken to ensure that the visualisations, colour scales and all other options are coherent across may different models.

Generating the Comsol based visualisations from the server environment gives the same results visualisation from a coding perspective. This approach guarantees that the next model variation uses the same evaluation routine and formatting. The visualisation itself can be performed in server graphics (Windows operating system only) or Matlab figures. The former option gives quick results, although all properties (title, labels, etc.) must be set in the plot group data structure. Using Matlab figures allows the user to set these properties with native Matlab commands and augment the graphics with any desired feature. Unfortunately,

there appears to be a limitation on the model size that allows this approach. During the course of the research the number of features exceeded a limit which causes an error on displaying simple plot groups.

The third option is to define a set of result variables and import these to the Matlab workspace. This method requires detailed knowledge about the data structure in Comsol and has the most additional coding. The benefits of the increased effort are complete freedom to perform post-processing operations, self-coded results formatting and comparison across a wide range of models. Comsol provides options to display results of parametric sweeps and model extensions. However, there are no direct methods to compare data from different model files. The Matlab based approach also enables saving of the results in the Matlab model structure.

Method	**Advantages**	**Disadvantages**
Comsol UI	No additional coding effort	High manual effort, limited batch options, only Comsol based analysis
Server graphics	Limited coding, use of plot groups, quick results	Limited model size allowed, no additional analysis
Extract to ws	Post-processing freedom, self-coded formatting, save results with definitions structure	High coding effort

Table 5.4: Comparison of model evaluation strategies

An overview of the model evaluation strategies is given in Table 5.4. The general trade-off is between coding effort and control versus easily defined results. In the course of this research all of the above methods have been used. For the purpose of a flexible model that can be easily compared to experimental data the final choice is made for extracting the results to Matlab.

The chosen approach takes the largest effort to develop, but also yields the most effective results for industrial use. Generating new data for revised designs is a simple task since the structure is pre-defined. Saving the results in a Matlab variable keeps the definitions, model features and results in a single file. This gives additional assurance that the definitions and results are consistent. Moreover, it generates the most compact dataset, which is quite relevant when many models are stored on a server.

Results structure

Solutions of a Comsol study are stored in datasets. All sets are linked to a specific solution in the solver sequence, a list of solutions can be found by requesting the solution information of a model. The dataset itself contains general information on the linked solution. This includes the mesh selection, parametric sweep variables and batch configuration.

The actual data of the solution is separated according to space dimension. Global variables, parameters and probes can be evaluated at all solution points with their corresponding tags. Distributed variables have an additional selection of boundary or domain mesh as a basis for evaluation. Any variable that is defined by the physics interface can be evaluated.

An example of the temperature state of the model in idle state and after 600 seconds at 2000 rpm is shown in Figures 5.10 and 5.11. The thermal response is characterised in terms

of the chosen global variables, which is worked out in more detail in Section 7.1.

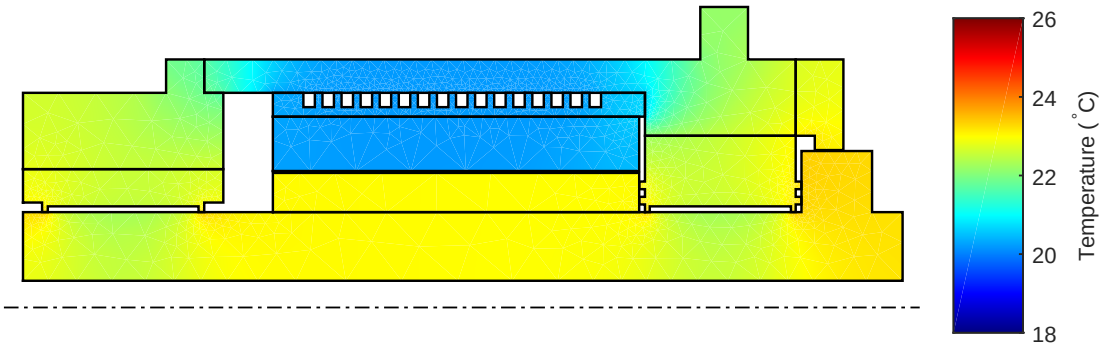

Figure 5.10: Simulated thermal state (idle)

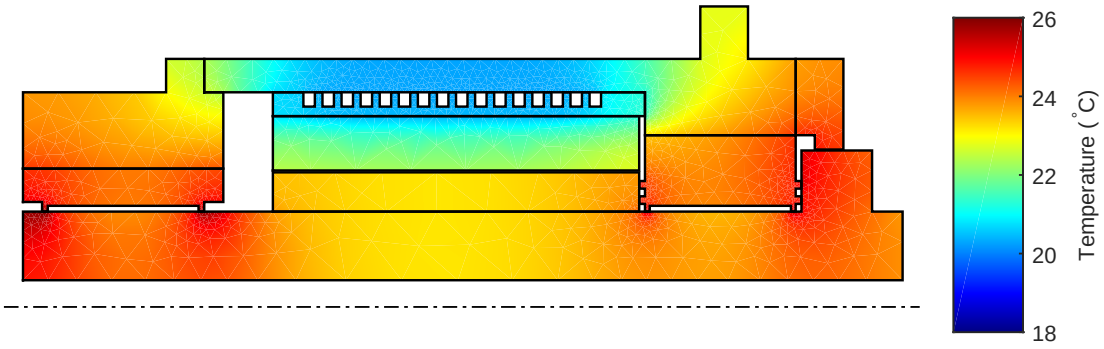

Figure 5.11: Simulated thermal state (2000 rpm, t=600 s)

Chapter 6

Thermal error measurement

Two series of measurements have been performed to analyse the system and validate the model. For both series some modifications were made to the spindle assembly to incorporate additional temperature sensors. The first set of measurements, described in Section 6.1, is performed in a finished machine. A second series is worked out in Section 6.2, which relates to thermal error of the spindle sub-assembly.

6.1 Configuration 1: Finished machine

The first measurement series is performed in a fully assembled machine. A modification is made to the spindle assembly to incorporate temperature sensors in the housing. Figure 6.1 shows the sensor position in a cross-section. The actual temperature probe is a thermistor, a resistance with a negative temperature coefficient (NTC), that is glued in a copper plug[1]. Six sensors are positioned around the circumference at 60° intervals.

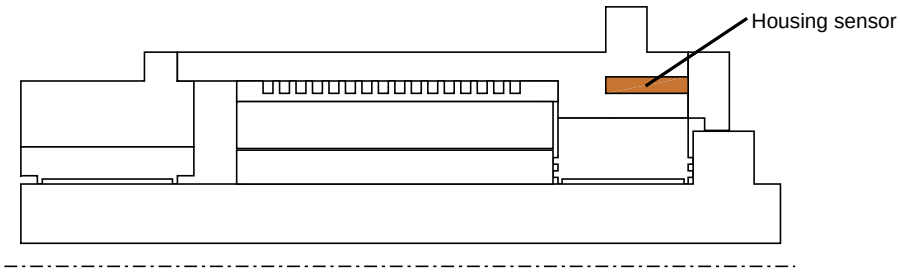

Figure 6.1: Housing sensor placement design sketch (configuration 1)

A number of other sensors are mounted externally to monitor the thermal state and heat input. Temperature sensors are placed on the oil in and outlets, the housing wall and an air temperature sensor is placed near the spindle assembly for ambient conditions. For this machine, the motor coolant is bearing oil instead of an ethylene-glycol solution, which is fed by the same supply line as the bearings. The inlet pressure, flow rate and outlet temperature of the oil cooling are monitored, as well as the actual motor temperature. Finally, two capacitive displacement probes are used to measure the deformation at the front seal ring and spindle nose. A list of all sensors is given in Table 6.1.

Monitoring and storage of the sensor data is Keysight 34972A multiplexer with two 16-channel modules. A sample rate of 2 Hz is used, which is sufficient to capture the thermal

[1]The choice for copper plugs is made in conjunction with a project to determine suitable temperature sensor placement for thermal error compensation. The high conductivity of the copper is expected to have an averaging effect that could be beneficial for the compensation method.

Description	Sensor type	Symbol	Unit
Oil inlet temperature	Pt100, 4 wire	T_{in}	°C
FRB outlet temperature	Pt100, 4 wire	T_{frb}	°C
REB outlet temperature	Pt100, 4 wire	T_{reb}	°C
MCJ outlet temperature	Pt100, 4 wire	T_{mcj}	°C
Housing temperature (6x)	5 kΩ Thermistor	T_{h1}, T_{h2}, ..., T_{h6}	°C
Housing wall temperature	Pt100, 4 wire	T_{w}	°C
Ambient temperature	Pt100, 4 wire	T_{air}	°C
MCJ inlet pressure	Trafag NAT 25	p_{mcj}	bar
MCJ flow rate	Kobold DRG	Q_{mcj}	L/min
Stator temperature	KTY84/130	T_{m1}, T_{m2}	°C
FSR displacement	Capacitive probe	X_{fsr}	μm
SPD displacement	Capacitive probe	X_{spd}	μm

Table 6.1: Sensor list (measurement series 1)

behaviour that takes place at a time scale of minutes to hours. All temperature sensors are referenced with respect to a measurement of the thermal state after two days of inactivity. At this point the machine is assumed to be in an almost uniform temperature state. The reference measurement is performed to eliminate the static offset from the connections and production tolerances.

The displacement sensors are mounted on the machine tool changer (Figure 6.2). This gives the opportunity to perform a check of the sensitivity of the sensors (see Appendix E), which are sensitive to the material of the counter surface. The machine axes are not used shortly before and during the thermal measurements to minimise disturbances.

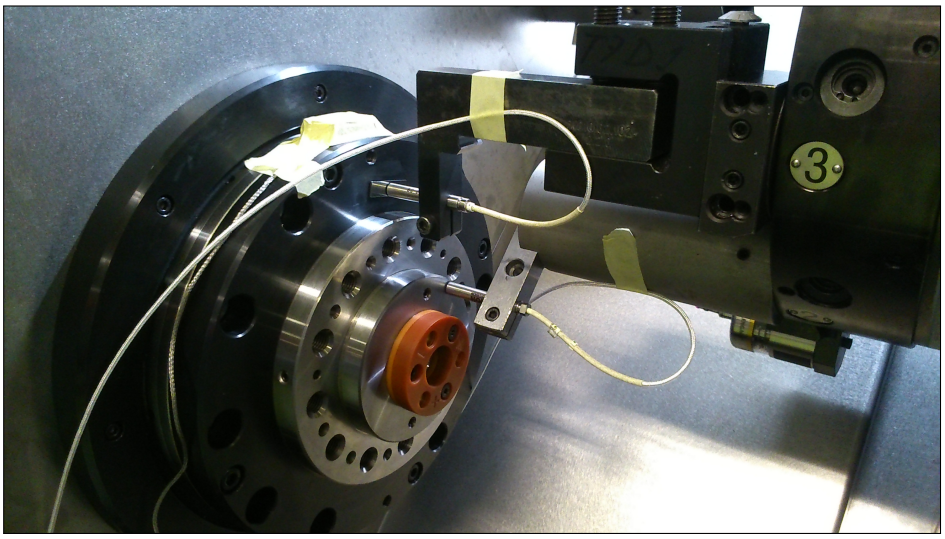

Figure 6.2: Displacement sensors in machine error measurement

Measurement results

The thermal behaviour is best characterised by a step response measurement. A warm-up time of at least one hour has been taken into account to let the machine achieve a steady state after the oil supply is turned on. At the start of a measurement a 5 minute idle time is incorporated to check if the measured variables are indeed stationary. After this time the spindle is set to a speed of 2000 rpm for 30 minutes.

Figure 6.3 shows results of a step response test. The top axes gives the temperature of the oil, housing and housing wall. The values of the six sensors in the housing are averaged ($T_{\mathrm{h1-6}}$). During the test the inlet temperature is relatively constant at a mean value of 17.7 °C. The oscillations are caused by the chiller, which has a switching controller. In the idle state, the temperature rise in the oil is approximately 2.6 °C. At 2000 rpm the front bearing outlet temperature increases to 24.2 °C, a 6.5 °C difference with the inlet. At the end of the measurement all temperature values of the system are within 0.1 °C of their initial value. Only the ambient air has risen by 0.75 °C.

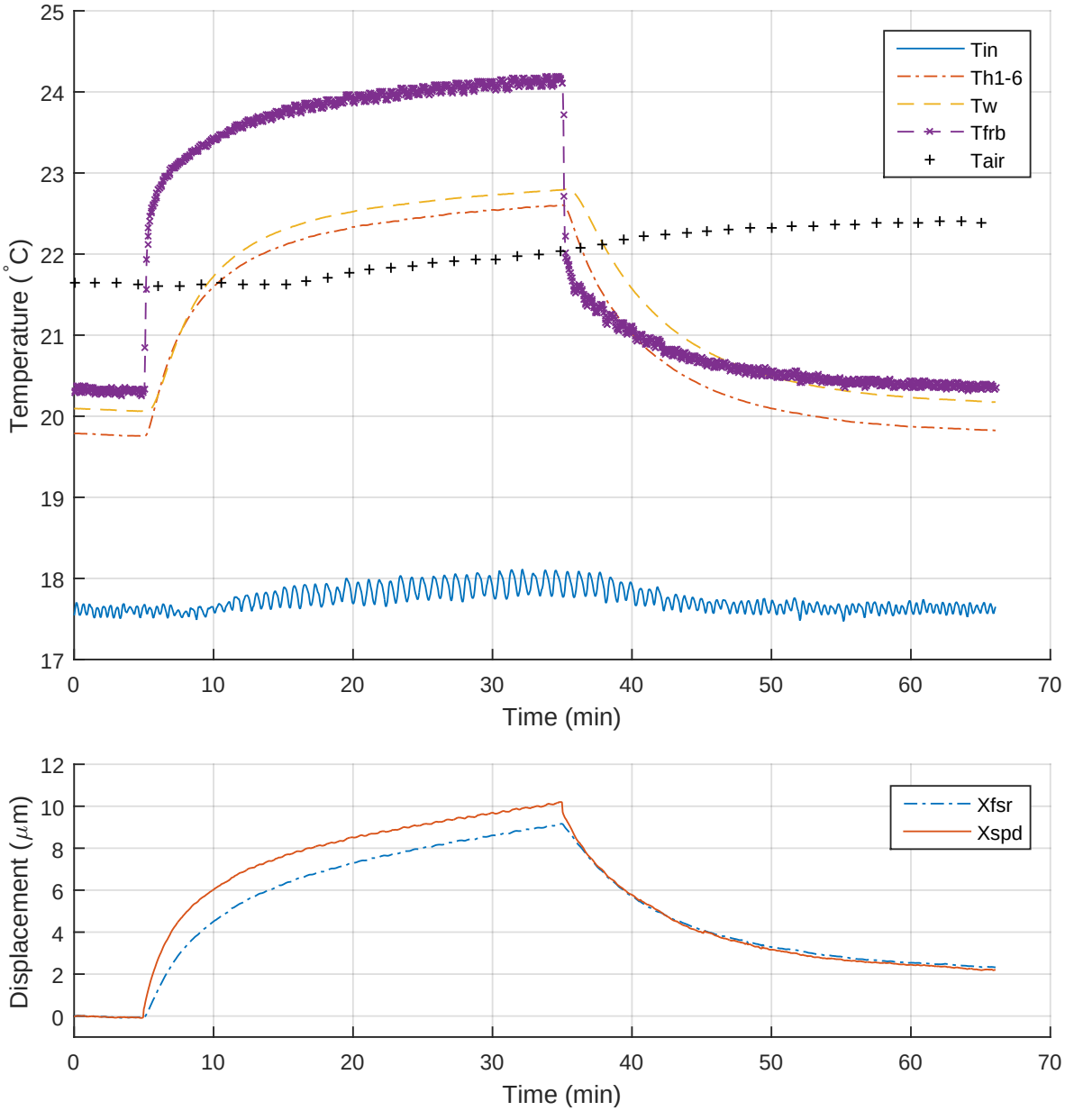

Figure 6.3: Configuration 1: 2000 rpm Step response bearing temperature

In the bottom axes the displacement of the spindle and front seal ring are displayed. The two variables show a similar response that is typical for the first order nature of thermal systems. At the spindle nose the maximum value is 10.2 μm, about 1.1 μm more than the stationary seal ring. The thermal expansion still has to reach a stationary value at the end of the step and is still 2 μm from the idle state at the end.

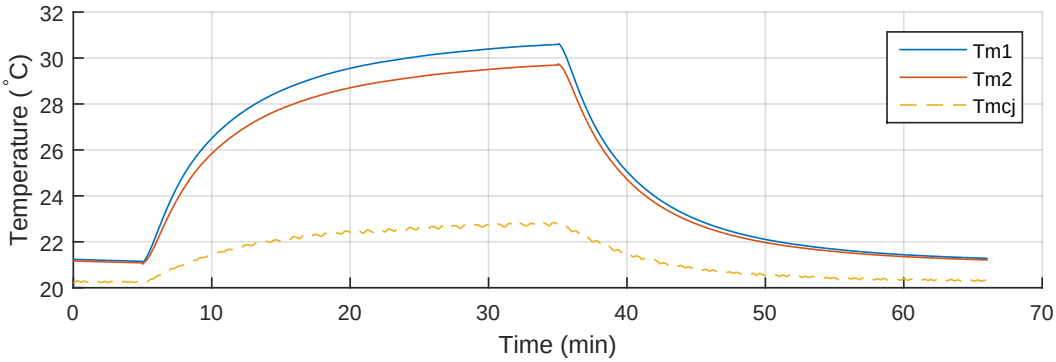

Figure 6.4: Configuration 1: 2000 rpm Step response motor temperature

The motor cooling circuit has a steady flow of 11.5 L/min. Figure 6.4 shows the temperature of the motor and cooling jacket outlet. The stator temperature peaks at 30.6 °C, the oil at 22.8 °C. Similar to the front bearing temperatures the temperature increase has yet to reach a steady state at the end of the test.

6.2 Configuration 2: Spindle sub-assembly

A second measurement series is performed on a separate spindle sub-assembly. The design of the internal sensors is revised to increase the amount of information from the same set of sensors. Figure 6.5 shows a sketch of the modified sensor placement. Three are still located in the housing, the other three are moved to the body of the front bearing. The placement is still every 60° around the circumference, with an alternating pattern of front bearing and housing sensor type.

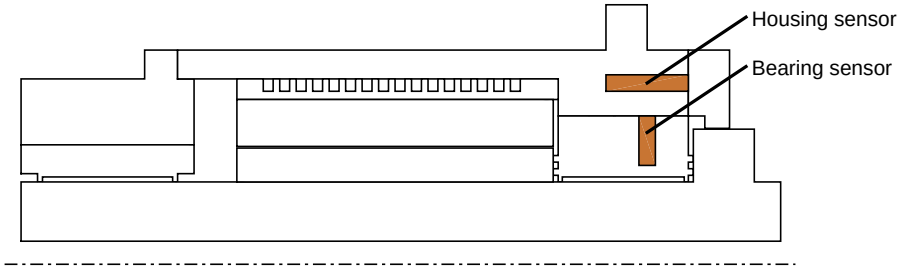

Figure 6.5: Sensor placement design sketch (configuration 2)

There are also some changes to the peripheral sensors. The spindle motor in this configuration is cooled with the ethylene-glycol mixture that was described in Section 4.6. A dedicated chiller is used to regulate the inlet temperature. Sensors at the in- and outlet are used to monitor coolant temperature and flow rate. The Pt100 at the rear bearing outlet is omitted to make room . An updated sensor list is provided in Table 6.2.

In the previous measurement the spindle sub-assembly was mounted to the machine bed. This series, the spindle and it's granite housing are bolted to a steel table. A probe stand is clamped to the table to provide a stable basis for the displacement sensors. The measurement

Description	Sensor type	Symbol	Unit
Oil inlet temperature	Pt100, 4 wire	T_{in}	°C
FRB outlet temperature	Pt100, 4 wire	T_{frb}	°C
FRB temperature (3x)	5 kΩ Thermistor	T_{frb1}, T_{frb2}, T_{frb3}	°C
Housing temperature (3x)	5 kΩ Thermistor	T_{h1}, T_{h2}, T_{h3}	°C
Housing wall temperature	Pt100, 4 wire	T_{w}	°C
Ambient temperature	Pt100, 4 wire	T_{air}	°C
Glycol inlet temperature	Pt100, 4 wire	T_{gin}	°C
Glycol outlet temperature	Pt100, 4 wire	T_{gout}	°C
Glycol flow rate	SMC PF2W720	Q_{mcj}	L/min
Stator temperature	KTY84/130	T_{m}	°C
FSR displacement	Capacitive probe	X_{fsr}	μm
SPD displacement	Capacitive probe	X_{spd}	μm

Table 6.2: Sensor list (measurement series 2)

set-up is shown in Figure 6.6. The current set-up is chosen to improve the accessibility and eliminate machine disturbances.

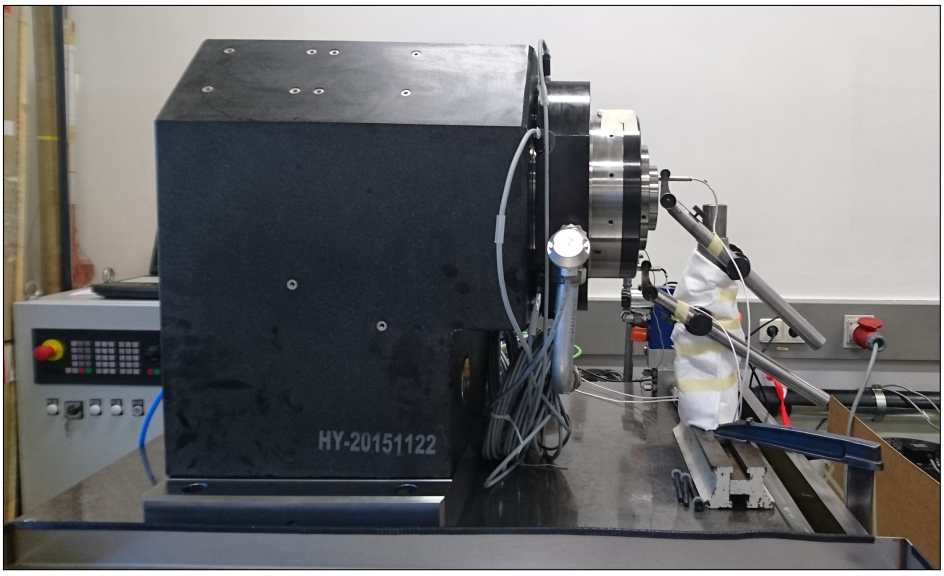

Figure 6.6: Spindle sub-assembly set-up

A series of step responses are performed to assess the time required to achieve a stabilised temperature distribution. For the case of a 2000 rpm spindle speed a step duration of 90 minutes appears to be sufficient. Several placements of the probe stand are tried to find a configuration that minimises the influence of the thermal behaviour of the metrology loop. Insulation material is also added to reduce the influence of external temperature variations.

The most promising results are shown in Figure 6.7. It shows how the temperature of the front bearing is higher than that of the housing. The housing wall is another step lower in temperature. Unfortunately, the inlet temperature increases as a result of the heat load on the chiller. In this set-up, the oil supply is shared with a number of test tables.

Comparing the results with the first configuration it can also be observed that the oil inlet temperature is approximately 2 °C higher. The difference between the oil in- and outlet temperature in the idle state is slightly lower at 2.2 °C. At the end of the step, the difference

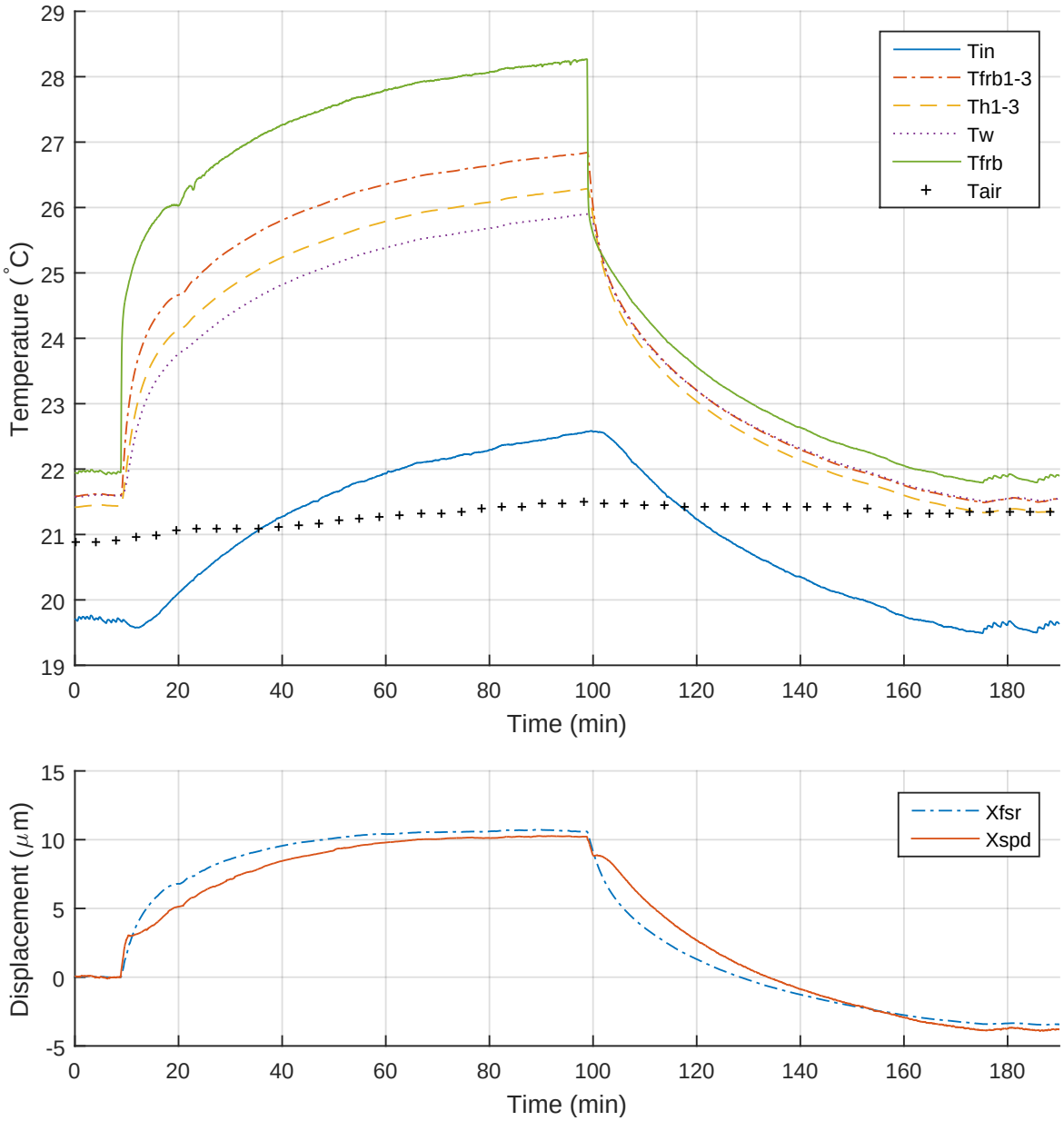

Figure 6.7: Configuration 2: 2000 rpm Step response bearing temperature (1)

is 5.7 °C, also lower than previously. The ambient air temperature is more constant in this environment, with only a 0.5 °C increase over more than three hours.

The thermal error of the seal ring and spindle nose is comparable at 10.7 and 10.3 μm respectively. In this case, the stationary part has the larger deformation. With this observation is has to be noted that the displacement sensor of the seal ring is placed at the bottom in this measurement, whereas it was placed at the top in the first measurement series. In the signal of the spindle nose some disturbances from a smooth first order behaviour can be observed. Despite the disturbance the thermal expansion has reached a steady state at the end of the step.

Figure 6.8 shows the motor and coolant temperatures. In the idle state the stator temperature is 22 °C, the same as the oil outlet temperature of the front bearing. The coolant inlet is very steady at 20.2 °C, which is maintained within 0.1 °C for the duration of the measurement. During spindle operation the motor stabilises at 29.8 °C with a coolant exit temperature of 22.3 °C. The motor temperature increase of 7.8 °C is 14 % lower than in the first series.

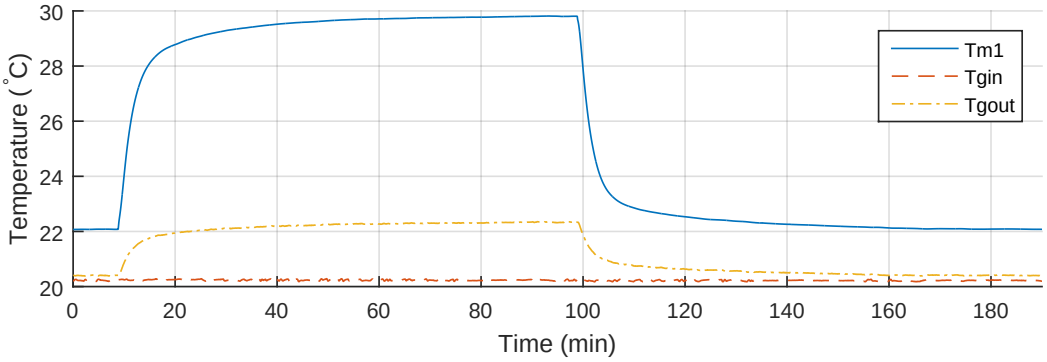

Figure 6.8: Configuration 2: 2000 rpm Step response motor temperature (1)

A second step response measurement, also at 2000 rpm, is shown in Figure 6.9 and 6.10. During this measurement the oil inlet temperature is maintained more accurately, although the variation is still more than 0.4 °C. The ambient air conditions are slightly worse than in the previous run with a drift of 2 °C over the course of two hours.

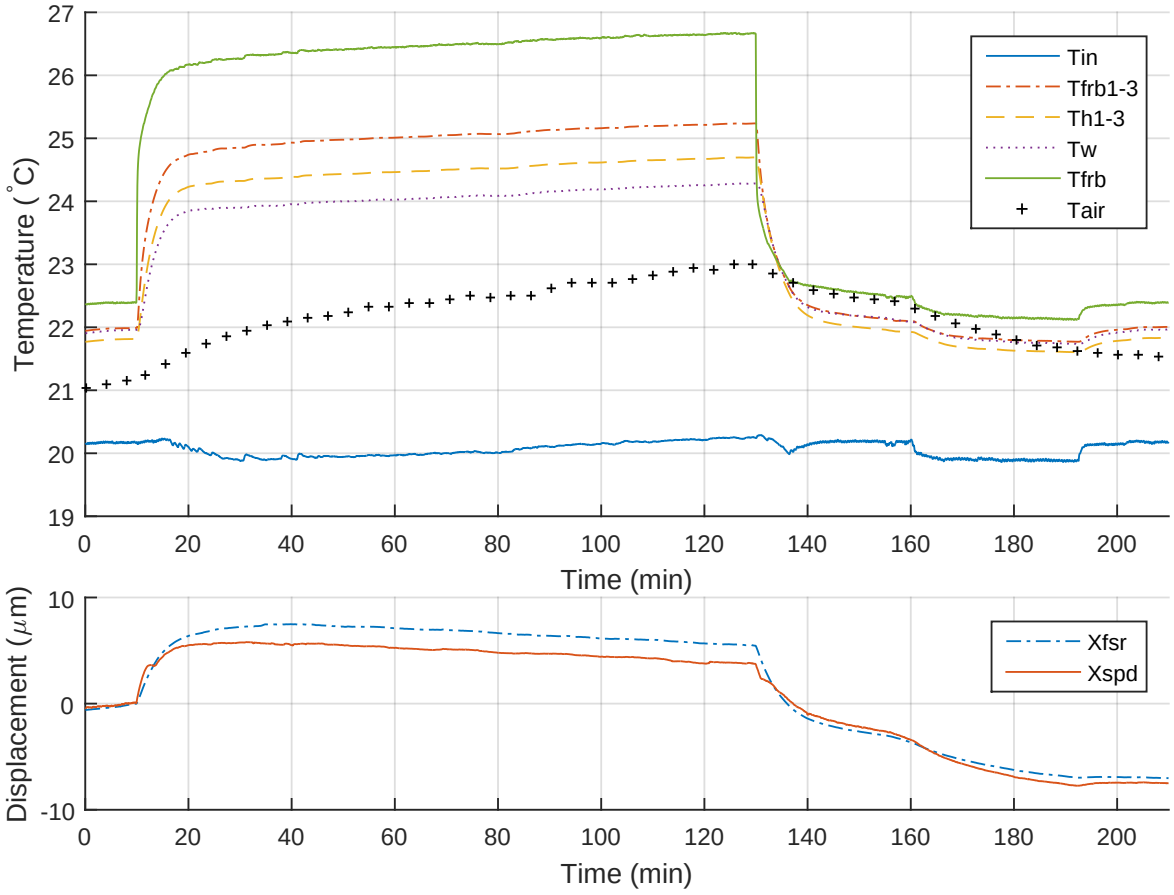

Figure 6.9: Configuration 2: 2000 rpm Step response bearing temperature (2)

The improved stability of the inlet temperature can also be seen in the values of the oil outlet and internal temperature sensors. These variables have a more pronounced step behaviour. The drift in air temperature causes a gradual increase of the temperatures measured in the spindle. This also has a disturbing effect on the displacement measurement. After an initial positive response these parameters show a negative trend. It is likely that

the change in air temperature caused the table and sensor mounting to expand and move away from the spindle assembly.

The results of the motor and coolant temperature are almost indistinguishable from the previous measurement. A very clear step response is measured and the stationary values match closely to the ones found before.

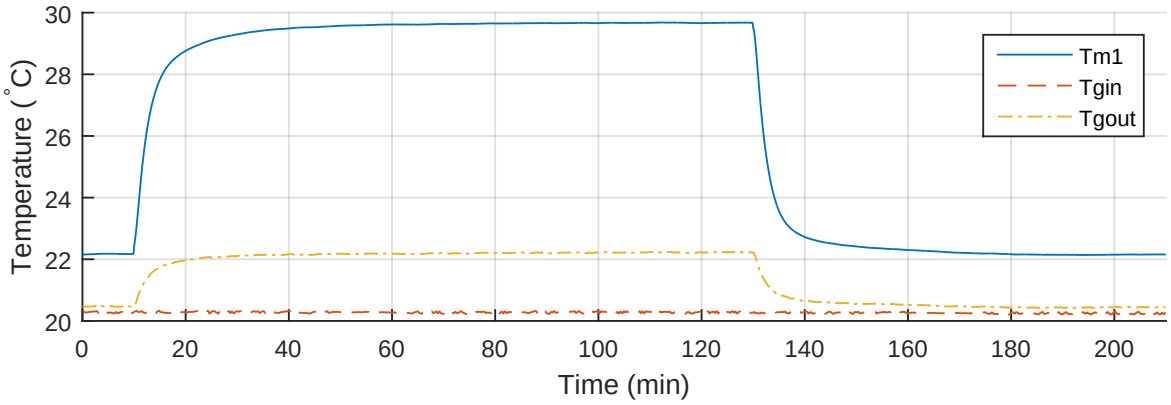

Figure 6.10: Configuration 2: 2000 rpm Step response motor temperature (2)

Chapter 7

Model results and validation

The performance of the numerical model is evaluated with simulated parameter variations and a comparison of the simulated and experimental results. In Section 7.1 a series of experiments is performed to give an estimate of the sensitivity to changes in parameter values. Next, a number of modelling assumptions are checked in Section The model, with its settings as derived in Chapter 4, is then compared to the experimental results in Section 7.3.

7.1 Theoretical thermal response

The importance of good parameter estimates has been discussed at length in the previous chapters. Several important model settings are identified and simulations are performed for a limited range of variations. First, the heat transfer coefficient in the outflow domains is varied. These areas constitute the largest surface area where warm bearing oil transfers energy into the spindle assembly. Next, the convection to ambient air is investigated. Thermal contact between the bearing and housing components follows in the third set of simulations. In the final simulation the radiative heat transfer is omitted to see the influence on the front of the spindle assembly. All model variations are compared to a reference model with the parameters as discussed in the previous chapters. The temperature response[1] of the reference model is shown in Figure 7.1.

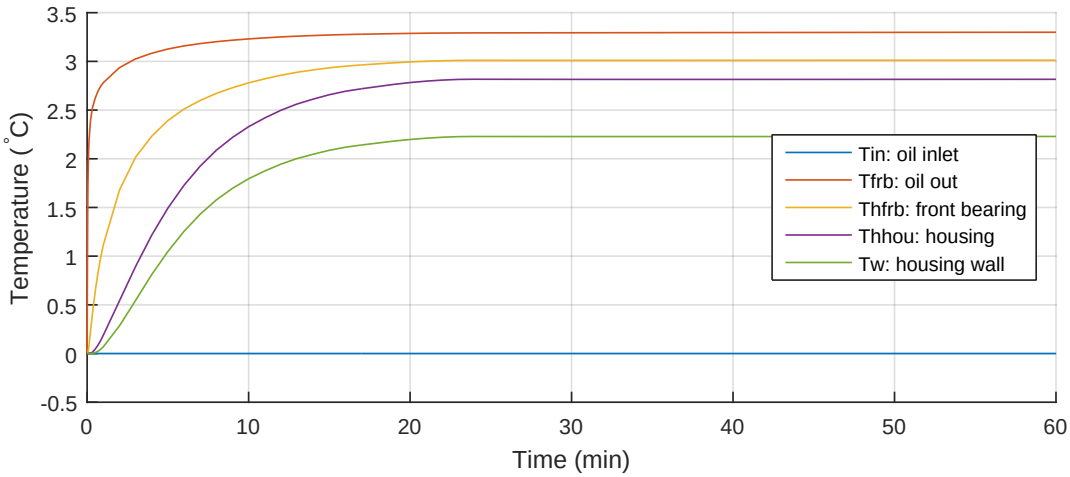

Figure 7.1: Reference model temperature response

[1]The inlet temperature is omitted in the comparison, since this is a constant input parameter value.

Outflow domain heat transfer

The flow regime in the outflow domains can not be defined as accurately as in the gap domains, which makes the heat transfer coefficient difficult to estimate very accurately. A value of 2000 $\mathrm{W/(m^2\,K)}$ is used in the reference model. Two simulations are added with respectively 500 and 20,000 $\mathrm{W/(m^2\,K)}$ as coefficient value of all outflow domains. These represent an expected upper and lower limit, based on the gap coefficients and Mills [25].

Figure 7.2 shows the global parameter evaluations for the three models. The reference model is shown with a solid graph, the variations are shown dashed and dotted for the low and high value of the coefficient. Black arrows also indicate the direction of increasing convective heat transfer coefficient.

The results show a clear difference in component temperature probes, both in terms of the response speed and stationary value. The effect on the bearing oil temperature is quite limited and in the opposite direction. In general, the higher coefficient value results in increased component temperature and quicker response. This also corresponds to the displacement values, since the thermal state directly influences the amount of thermal deformation.

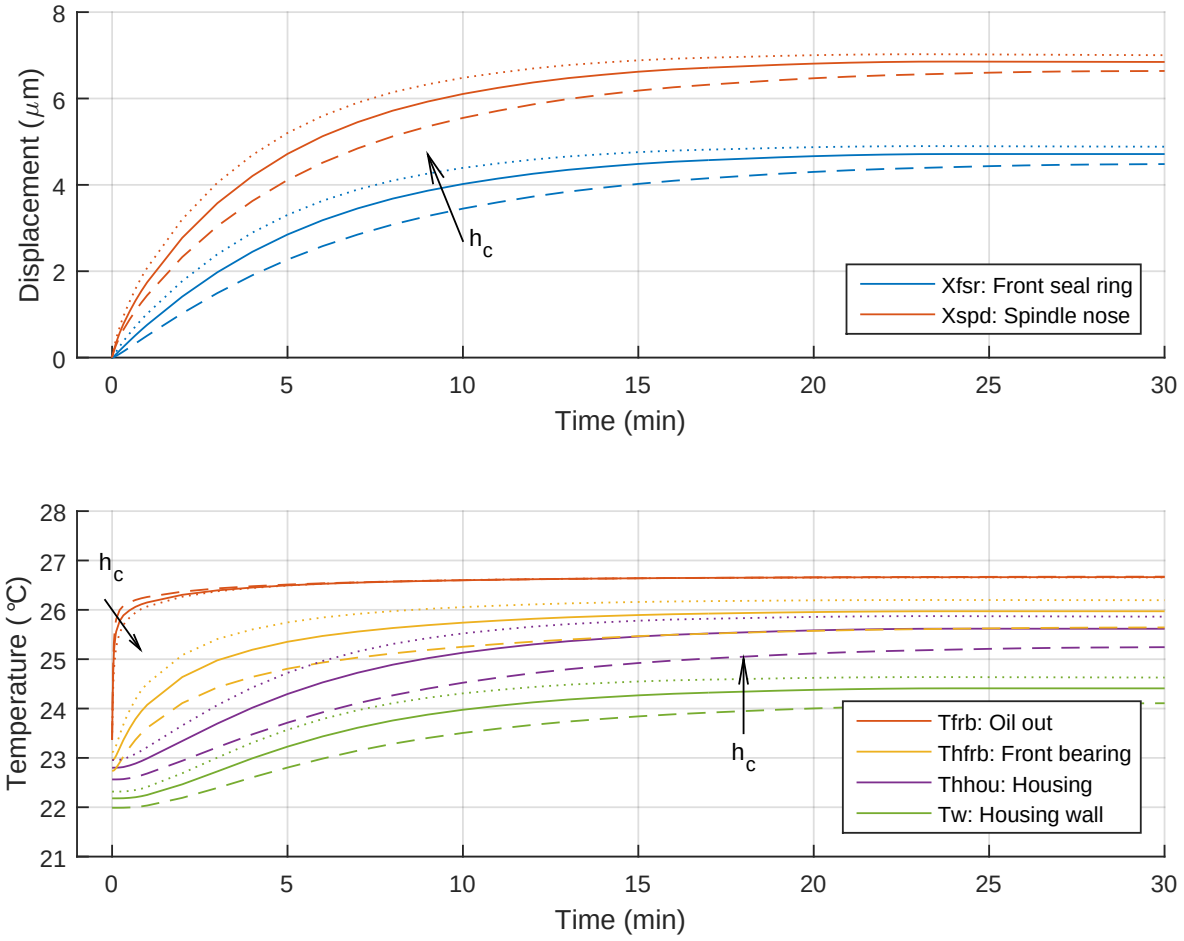

Figure 7.2: Simulated 2000 rpm step with varied outflow domain convection

Ambient air convection

Heat transfer to the ambient air adds a cooling effect to the spindle nose and housing. This is a relatively small effect compared to the fluid domains. However, for the spindle nose this is the only heat sink. Order of magnitude estimates of the heat transfer coefficients are found in literature [25] and used as an upper and lower limit. The variations are listed in Table 7.1. The lower limit for the housing wall is approximately the computed value.

Parameter	Reference	Lower limit	Upper limit
Housing wall	2.5	3	25
Axial spindle nose wall	38	25	200
Radial spindle nose wall	55	25	200

Table 7.1: Ambient air convection coefficient variations (in $W/(m^2\ K)$)

The results of the three simulations are displayed in Figure 7.3. These parameters mainly influence the steady state value, especially of the components that directly interact with the ambient air. Changing the amount of convective heat transfer to air has almost no influence on the speed of the response.

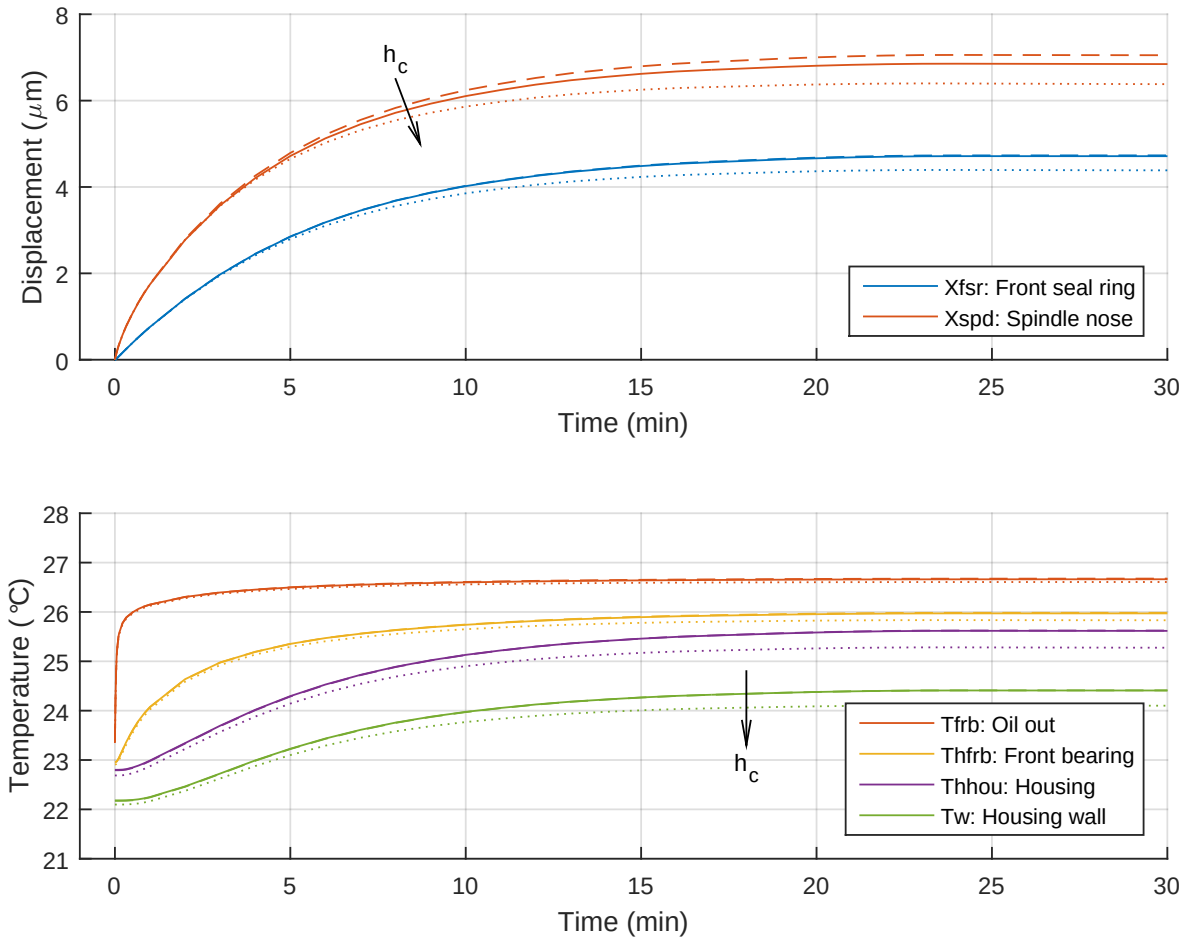

Figure 7.3: Simulated 2000 rpm step with varied ambient air convection

Thermal contact

Definition of the thermal resistance of the interfaces depends on many parameters, one of which is the surface roughness. This specific property is briefly investigated. The nominal asperity roughness is 1 μm, which is based on a roughness measurement of the contact surface of the front bearing. Studies with no thermal contact (equivalent to flat surface, 0]mum) and with 10 μm roughness are computed for comparison. The latter value is well above the standard production roughness.

The modified thermal contact parameter mostly influences the temperature of the housing. The temperature of the housing decreases with increasing roughness. This leads to a temporarily increased front bearing temperature (Thfrb) in the transient part of the step to satisfy the balance of energy. The oil and bearing temperature are unaffected in steady state. The additional resistance in the thermal system causes a drop in temperature over the interface, which can be seen in the lower steady state value of the housing.

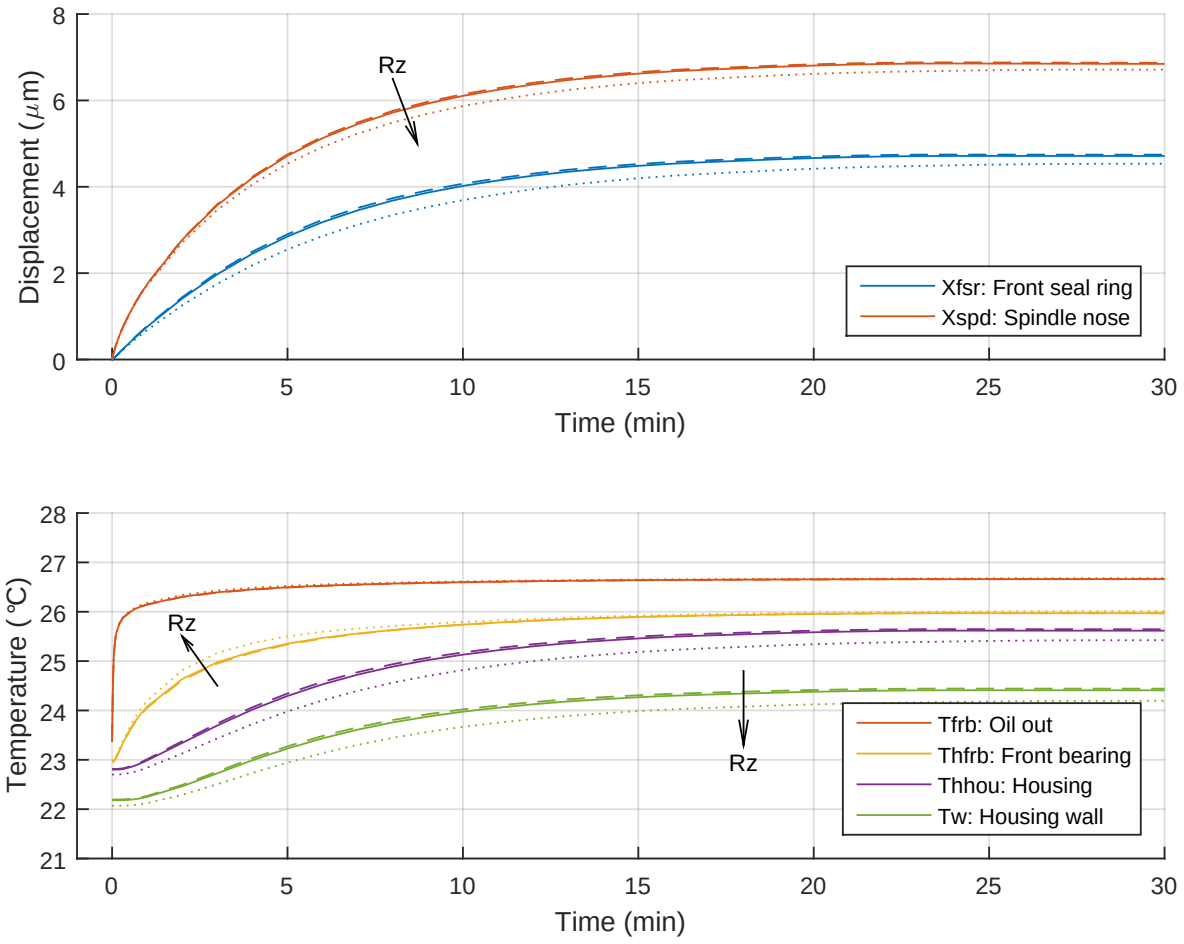

Figure 7.4: Simulated 2000 rpm step with varied thermal contact

The variation of the surface roughness gives a first indication of the influence of a thermal contact resistance in this system. Judging the entire influence of this phenomenon requires more extensive research. Parametric sweeps of the contact characteristics is relatively simple in Comsol. The flexible model definition also allows structured testing of other aspects, such as different contact models.

Stator radiation

Finally, simulations are performed to assess the influence of stator radiation on the total model response. In the analytical calculations of Section 4.6 it was concluded that the stator radiation is not a dominant source of heat transfer. Evaluation of the simulated results is therefore limited to the model with and without this feature.

The results in Figure 7.5 show how the stator radiation feature, although low in power, influences the transient behaviour of the model. Omitting radiation from the model results in a slightly flattened response (dashed graphs) when the temperatures converge to their respective steady state values. However, neither the initial transient response or steady state value are affected.

It must be noted that the model solves significantly quicker without the radiation feature. The solution time for the transient study is only 45 seconds without radiation, versus 322 seconds including this additional heat transfer mode. From the graphs it also appears that the solver takes less steps and performs linear interpolation to obtain the requested time samples, since the response with radiation is much smoother. The observed difference could well be a strictly numerical issue.

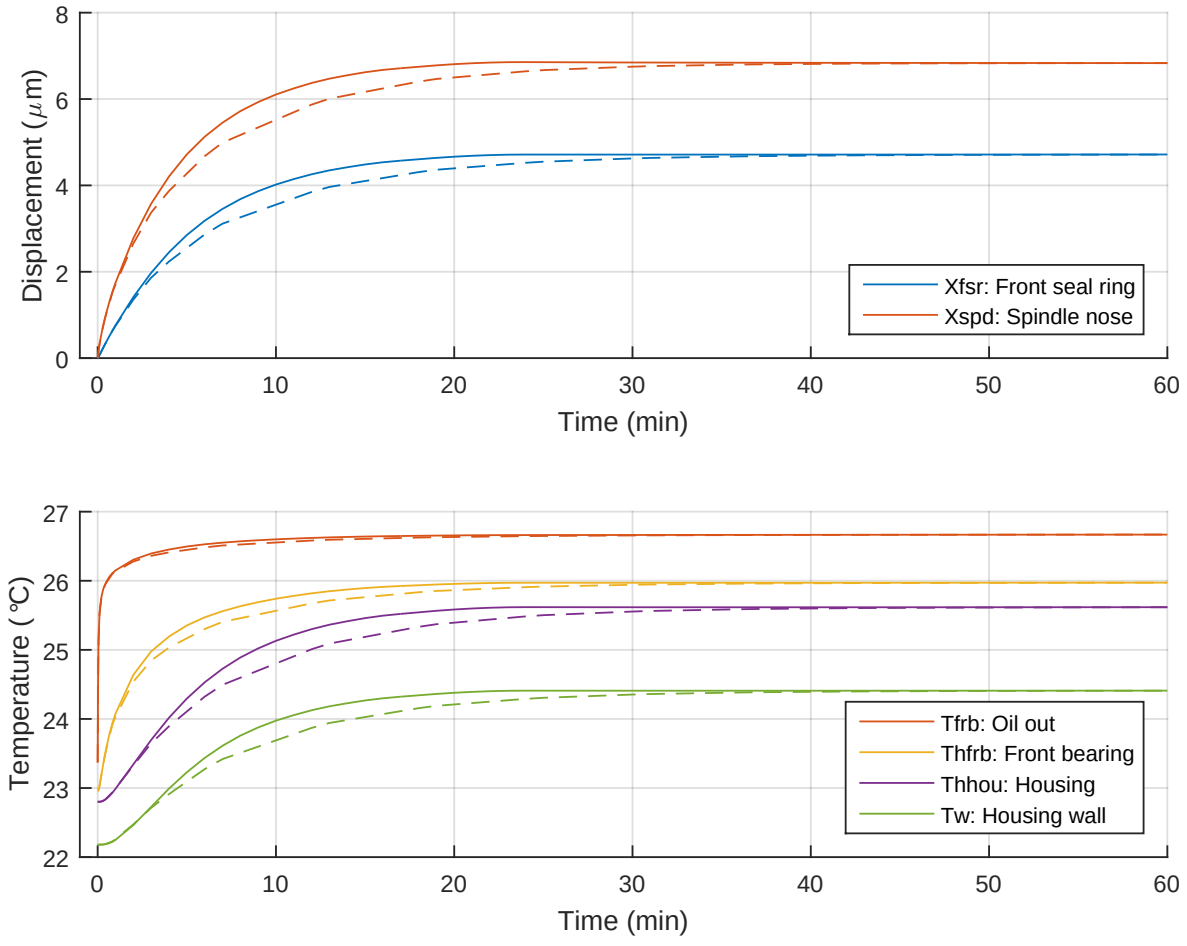

Figure 7.5: Simulated 2000 rpm step with varied stator radiation

7.2 Modelling assumptions

In the course of the model development many assumptions had to be made to determine the characteristics of the thermomechanical behaviour. The most important assumptions are discussed in this section.

The calculation of the flow resistance and viscous dissipation in the bearing fluid domains is based on the Reynolds equation. The use of this approach is only valid if the variation of pressure and viscosity across the film height in the bearing gap is negligible. Further simplifications that are made in Rowe [27] also build on the assumption that the viscosity of the bearing oil is independent of temperature.

An additional model of a radial bearing with a discretised fluid domain is built to investigate the pressure and temperature field in the bearing gap (Appendix F). The results show that the oil pressure is uniform across the gap height, variations are in the order of the numerical accuracy (in this case 10^{-12} Pa). It also shows that the oil only requires a short length to develop a steady profile (approximately 1-1.5x h_g).

The fluid flow velocity in the gap has a parabolic profile, which leads to the highest amount of viscous shear near the walls and no shear at the centerline. Figure 7.6 shows the temperature and viscosity across the gap height. Four cross-sections are evaluated along the length of the gap, indicated by fractions of the total length L_w.

The results from the fluid model show that there is a certain variation of the temperature across the gap height. This effect is the largest at the gap entry (L=0) at a total difference of 5.8 °C. At the end of the gap (L=Lw) this difference is reduced to 3.0 °C. The variation of temperature across the gap height also influences the viscosity of the bearing oil. At the gap entry the variation is approximately 15% of the specified value.

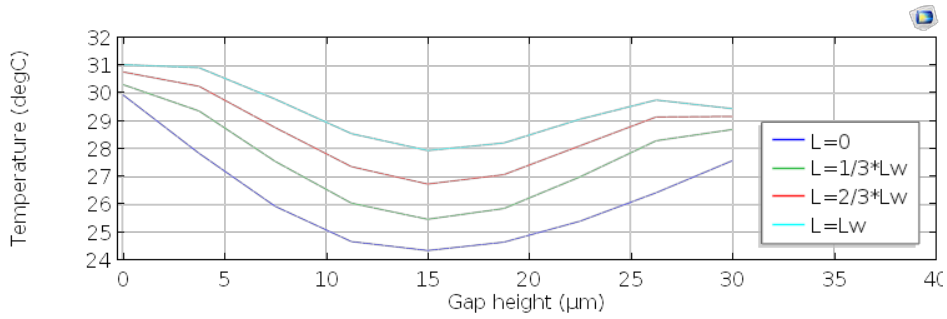

(a) Oil temperature

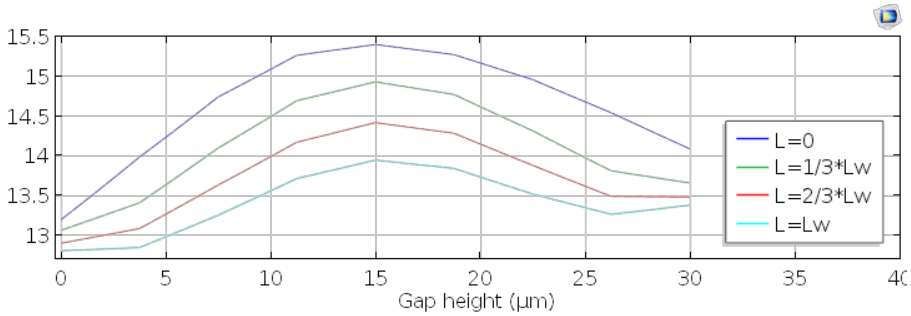

(b) Oil viscosity

Figure 7.6: Fluid properties across gap height at 4 cross-sections

Using a limited number of bulk elements also simplifies the temperature field. In practice there is an increase in the fluid temperature as the oil if forced through the outflow gap. This leads to a certain degree of temperature increase of the wall along its length, whereas

the heat transfer coefficient calculation is based on a wall with uniform temperature.

The fluid model is also used to evaluate the wall temperature increase. When the spindle is stationary the increase along the wall is 1.2 °C, at 2000 rpm this increases to 1.6 °C. In the model of the spindle assembly there is a smaller increase of the wall temperature. Along the outflow wall of the radial bearing there is only a 0.03 °C increase. The inner and outer wall of the radial bearing have respectively a 0.11 and 0.12 °C. The results suggest that it can be useful to refine the bulk elements along the gap length.

Finally, an assessment of the change in gap height is made. The spindle model only describes the coupling from the temperature field to the displacements. If the deformations lead to significant changes in the gap height it is also necessary to continuously update the outflow resistance and viscous dissipation.

The deformation state of the reference model is analysed to determine the change in gap size. For the axial bearing the displacements are such that all gaps are reduced in height by approximately 2 μm. The radial bearing has a slightly widened gap at the rear wall (by 0.7 μm) and a reduction in gap height of 3.5 μm at the front wall.

The influence of the gap height on the viscous dissipation is an inverse proportional effect. However, the volumetric flow rate has a cubic dependency on the gap height. As the gap closes the flow rate drops and viscous dissipation rises. In an insulated stationary case the relation between temperature rise and gap height is a fourth degree effect. The 10% change in gap height would then lead to a 46% increase in the temperature difference. However, the convective heat transfer also removes a part of the increased dissipated power. The temperature related drop in viscosity might also reduce the actual dissipation.

7.3 Experimental validation

Finally, the results of the simulations are compared to the experimental step response measurements. The evaluation is performed with both the machine error and spindle subassembly measurements. It is based on the nominal model that has been used as the reference in Section 7.1.

Comparison with machine error measurement

The temperature difference in the front bearing oil is displayed in Figure 7.7. Both the simulated and experimental data have been set to zero with respect to the temperature at the start of the step response. The difference between the simulated and measured temperature is shown in the bottom graph. The comparison shows that there is an additional transient effect that is not incorporated in the model. It also shows that the simulated oil temperature has a faster response to the step input than the actual oil temperature.

Next, the temperature of the housing sensors is compared to the simulated temperature at the equivalent location (Figure 7.8). Here it is clear that the response of the model is slower than the measured values. This might be caused by the oil drain channels. The warm bearing oil is drained from the assembly by channels in the housing. These create an additional heat transfer at multiple locations around the circumference. It can also be an indication that the convective heat transfer coefficient in the outflow domains is too low.

The match between the modelled and measured displacements shows a mostly linear deviation in Figure 7.9. From these graphs it can also be derived that the response of the model is slower than the actual spindle. The differences strongly related to the deviation in the housing temperature. However, the linear trend that is visible after 5 minutes indicates that there might also be an external effect that causes the displacement sensors to drift. Note that the measurement takes place in a fully assembled machine. The thermal state of

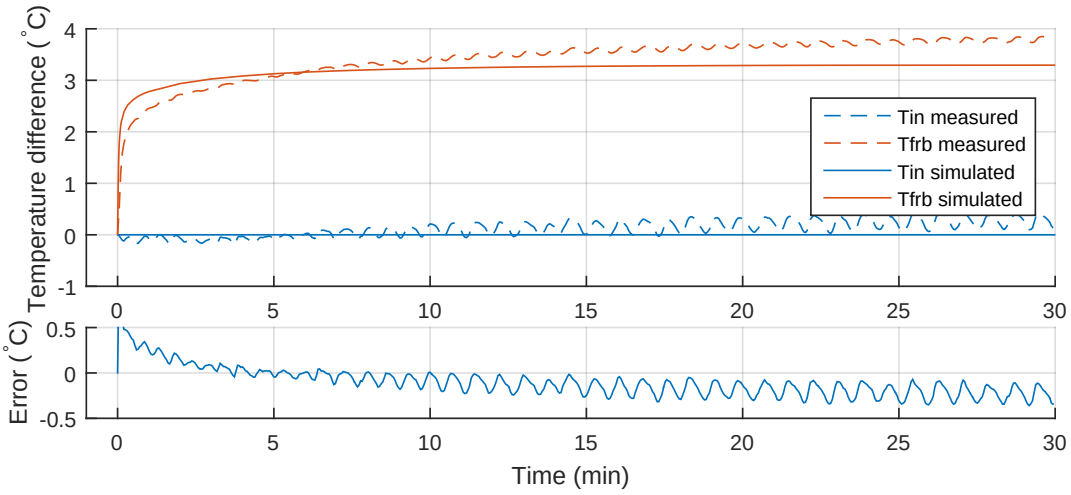

Figure 7.7: Configuration 1: simulation versus measurement (oil temperature)

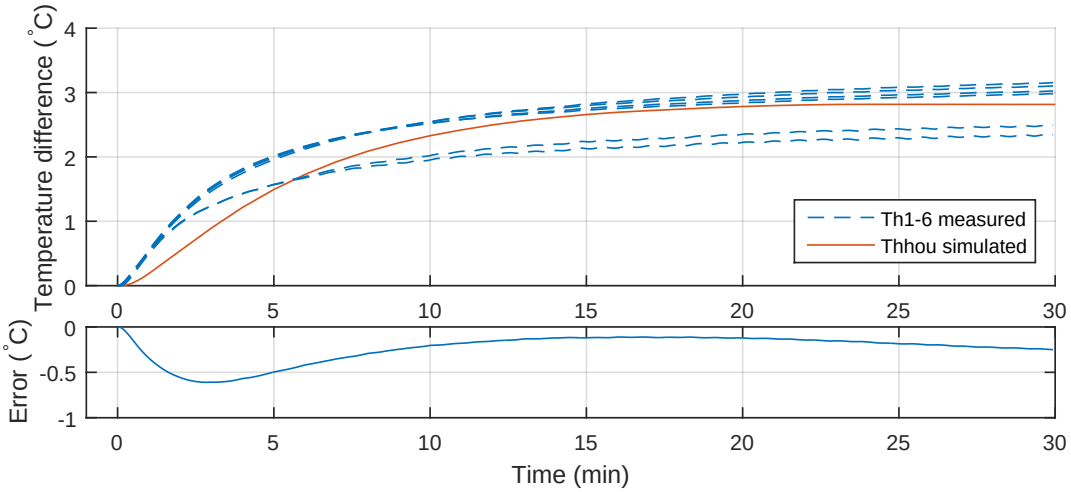

Figure 7.8: Configuration 1: simulation versus measurement (housing temperature)

the tool changer that holds the displacement sensors could change during the measurement.

Comparison with spindle sub-assembly measurement

The comparison of the simulations and spindle sub-assembly measurements is performed based on the second measurement described in Section 6.2. This series showed the least disturbance from external effects.

Figure 7.10 shows the simulated and experimental bearing oil temperature. There is no drift in the measured temperature, as opposed to the comparison in Figure 7.7. However, there is a stationary difference of 0.7 °C. From the error in the bottom graph it can be concluded that there is an additional slow transient effect in the measurement.

The new set-up of the internal sensors, with three temperature probes in the bearing body, shows promising results. The difference between the simulated and measured bearing temperature is less than 0.3 °C for the duration of the step. From the results it is also clear that the simulated housing temperature responds too slowly to the step input. The peak difference during the transient phase is approximately −0.6 °C. Nevertheless, the overall correspondence of the measurement and simulation appears quite promising.

The comparison of the displacement values also shows a much better fit than in the first

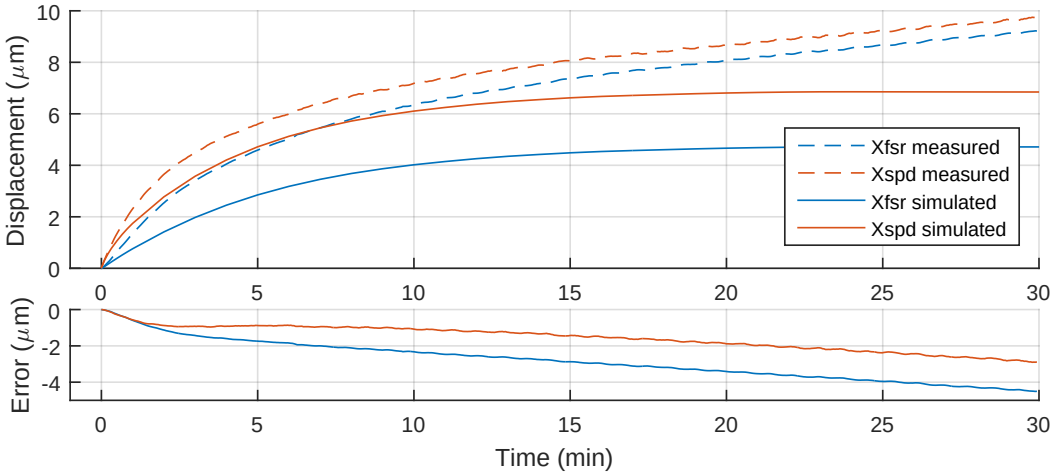

Figure 7.9: Configuration 1: simulation versus measurement (displacement)

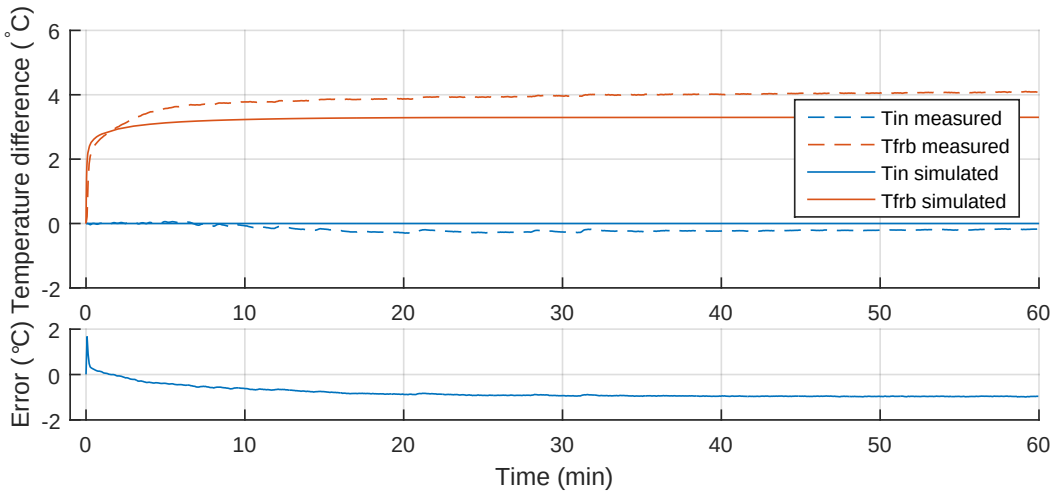

Figure 7.10: Configuration 2: simulation versus measurement (oil temperature)

measurement series. Especially the response speed and final value of the spindle displacement (Xspd) is quite accurate, considering the negative trend in the measured signal. This is not the case for the front seal ring displacement (Xfsr). The simulated displacement is approximately 2.5 μm too small.

For these results it has to be noted that the displacement sensor on the front seal ring was placed at the lowest point of the component. The simulation is based on the assumption of axial symmetry. However, the warm outflow oil is drained at the lowest point of the spindle. This results in a non-uniform temperature load around the circumference. The placement of the sensor shows that the housing and seal ring can expand more than the spindle nose.

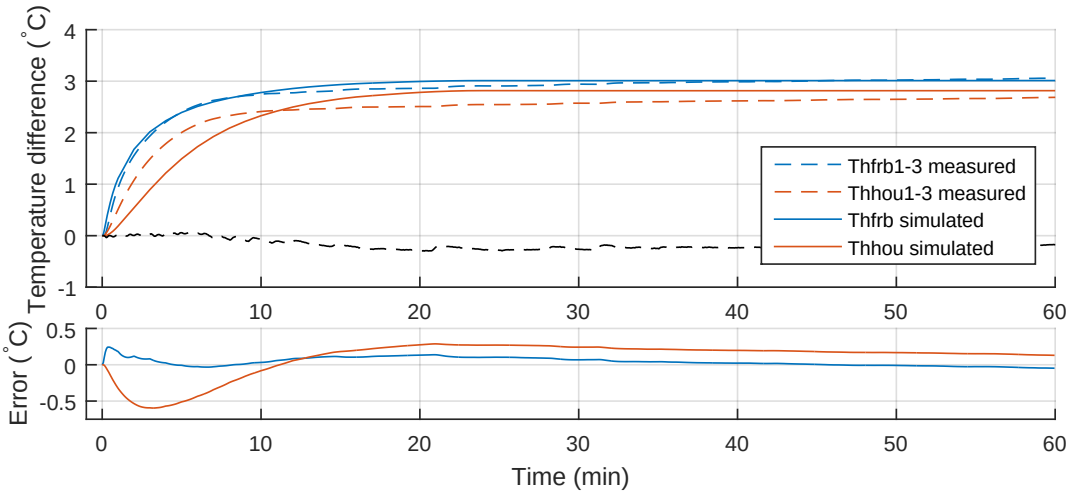

Figure 7.11: Configuration 2: simulation versus measurement (housing temperature)

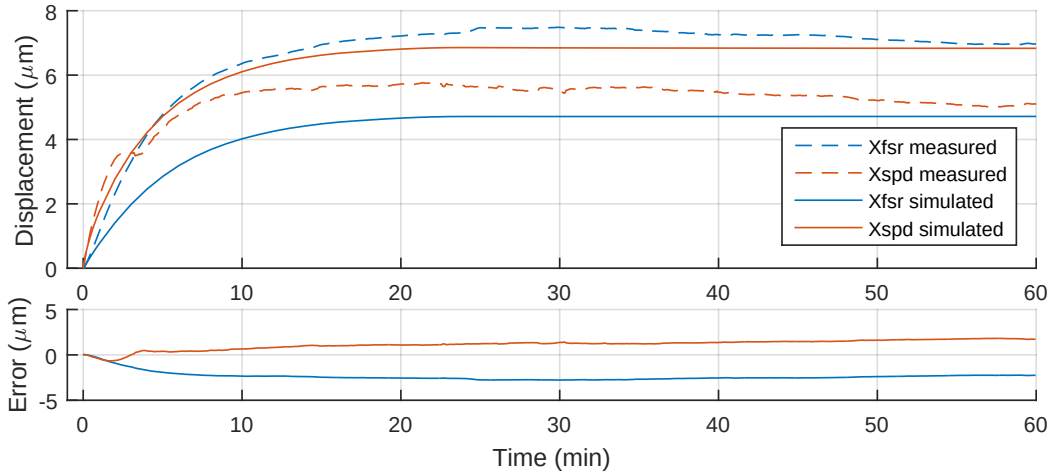

Figure 7.12: Configuration 2: simulation versus measurement (displacement)

Chapter 8

Conclusion

In the course of this research a parametric finite element model of a hydrostatic machine tool spindle has been developed. The model describes the thermomechanical behaviour of the spindle in stationary and transient conditions.

A new method for generating finite element models in Comsol has been proposed to enable the definition of the spindle model. The method is based on a generalised structure of the interaction between Matlab and Comsol in the LiveLink^{TM} *for* Matlab interface. One of the main advantages of this approach is ability to flexibly define and manage complex models.

A structured set of model definitions contains all information to define and parametrise the finite element model. This gives the unique opportunity to store all analytical calculations, definitions and model results in a single Matlab variable. Rebuilding an entire model is achieved with a single function call. This eliminates possible artefacts from modified settings and also reduces the need to store the Comsol model file, which is often much larger than the counterpart in Matlab.

Parameter variations have been investigated to give a first impression of the sensitivity of the results to analytical inaccuracies. The values of the parameters have only been investigated briefly in the sensitivity analysis. However, the first iteration of the model already shows promising results in terms of the match with the experimental data.

Two sets of experiments have been performed to investigate the transient thermal error of an industrial spindle. Modifications to the design were proposed and implemented to assess the internal temperature of the assembly. These internal variables provide an important foothold for model evaluation.

The most important purpose of the model is to investigate design variations. This research has resulted in many opportunities to investigate properties of the spindle assembly with the proposed approach. Being able to give an order of magnitude assessment of the influence of design variations on the final thermal performance is an important step forward.

Chapter 9

Recommendations

This research was focussed on setting up a parametric model of a machine tool spindle. The demand for a fully parametric structure had a defining influence on the development time. Now that the model is fully functional it is time to use it for investigation of the thermal error phenomenon. One of the first tasks is to elaborate the model variations to get a better understanding of the dynamics of the system.

Model refinement

The results of the simulations have brought a number of possible improvements into focus. The convective heat transfer of the outflow area is the most influential parameters that was investigated with the parameter studies. Modelling the outflow domains with a turbulent fluid dynamics model could improve the insight in the heat transfer in these areas.

A refinement of the fluid elements in the bearing gaps is also an interesting option. Increasing the number of bulk elements is one of the possibilities. However, this does add to the accounting complexity. Alternatively it would be interesting to assign laminar fluid dynamics domains to replace the single gap elements. This greatly increases the discretisation of the gap domains while keeping the accounting manageable.

At the moment there is only a unidirectional coupling between the thermal and mechanical equations. If the analytical bearing calculations are transferred to the Comsol environment it is possible to evaluate the actual bearing gap and use this to update the fluid flow. It also enables the implementation of a temperature dependent viscosity. Switching to bi-directional coupling does add significantly to the computing time.

Finally, it would be useful to expand the study variations. The current model only has a stationary study and a transient analysis with a constant spindle speed. Programming delayed steps or load cycles would create a closer match between the model and actual operating conditions.

Continued development of the generalised structure

The Matlab model structure also offers opportunities for further development. In the current state it is possible to create, modify and store model entities. It would be very useful to develop a tool for model comparison that efficiently highlights the differences.

Building and rebuilding models is performed with external functions. The approach with function based definition of features is very helpful in reducing the amount of actions that have to be taken by the end user. Separating information from function calls is one of the important achievements of this research. The next step in development could be to investigate an object oriented approach. This is possible in Matlab by creating a custom class that serves as a framework to store one or more model configurations. The critical

difference is that the functions can then be incorporated as internal methods. Changes of parameters can automatically trigger a rebuild or set a notification that the definitions and stored output are no longer synchronised.

Thermal error measurement

Many of the experiments showed some form of disturbance during the step response or recovery. The research took place in a production environment, which inevitably includes unexpected influences on the measurements. One of the advantages of the measurements in the fully assembled machine was that the spindle assembly is protected from the environment. The dedicated oil conditioning circuit also proved more reliable than a large capacity chiller for multiple sub-assemblies.

Further measurements will be performed on similar spindles to assess the variations due to production tolerances. The next step is to investigate other spindle designs with the same topology. The final purpose of the flexible model set-up is to provide reliable information about new spindle designs that have yet to be built.

Appendix A

Model geometry

Confidential

Appendix B

Material properties

Several materials are used in the model of the spindle assembly. A list of the solid materials is presented in Table B.1. Steel is used for most of the structural components. Only the bearings are a bronze alloy and the cooling jacket is made of aluminium.

Material	E (GPa)	ν (-)	ρ (kg/m^3)	α (1/K)	c_p (J/(kg K))	k (W/(m K))
Steel	210	0.28	7800	$11 \cdot 10^{-6}$	440	14
Bronze	95	0.30	8750	$17 \cdot 10^{-6}$	376	51
Aluminium	72	0.33	2810	$23 \cdot 10^{-6}$	960	180
Copper	110	0.35	8700	$17 \cdot 10^{-6}$	385	400

Table B.1: Material properties of solids

Table B.2 shows the required material properties of the bearing oil and motor coolant. The latter is a mixture of water and ethylene-glycol (anti-freeze), which is commonly used to prevent corrosion in water-based cooling systems. Air is also included in the model to incorporate the heat transfer to the surroundings. These properties are derived from the built-in material model of Comsol and evaluated at 20 °C.

Material	ρ (kg/m^3)	μ (Pa s)	c_p (J/(kg K))	k (W/(m K))
Bearing oil	881	0.015	188	0.15
Ethylene-glycol	1040	0.0015	3856	0.258
Air	1.205	$1.81 \cdot 10^{-5}$	1.005	0.0257

Table B.2: Material properties of fluids

Appendix C

Electric motor specification

Figure C.1 shows both the efficiency and dissipated power of the stator. The motor is not very efficient at stationary conditions below 1000 rpm due to the low friction of the hydrostatic bearings. This results in an increased dissipation below this speed.

Confidential

Figure C.1: Electric motor dissipation at stationary load

Note that the inertia effects of accelerating the spindle and the added mass of the bearing oil is neglected at this point. Comsol can automatically compute the mass, volume and rotational inertia of a (axisymmetric) component. This feature can be used to compute the additional mechanical power for a change in speed. Instead of the direct speed-dissipation interpolation a 2d table will have to be created for the efficiency. Based on the total mechanical power and current speed the efficiency and power dissipation can be evaluated. The added mass of the tangentially moving oil and air are still neglected in this refined approach.

Appendix D

Generalised model definition

Adding features

```
%% ME2490: Add feature to Comsol model
function Model = addFeature(Model,feat)
%% Basic feature definitions
% Create or call feature
if feat.create
    try
        Feat = createFeature;
    catch
        Feat = openFeature;
    end
else
    Feat = openFeature;
end

% Add label
if ~isempty(feat.label)
    Feat.label(feat.label);
elseif ~isempty(feat.tag)
    Feat.label(feat.tag);
end

% Select geometry/model
if strcmp(feat.model,'geom1')
    if strcmp(feat.feature,'cpl')
        Feat.selection.geom('geom1',feat.dimension);
    else
        if ~strcmp(feat.feature,'physics')
            Feat.geom(feat.model,feat.dimension);
        end
    end
elseif strcmp(feat.model,'comp1')
    Feat.model(feat.model);
end

% Select relevant geometry
if ~isempty(feat.selection)
    Feat.selection.named(feat.selection);
end

%% Add features properties (set, indexed and/or named)
% Add set features
```

```
for n1 = 1:size(feat.value,1)
    switch size(feat.value,2)
        case 1
            Feat.set(feat.value{n1,1});
        case 2
            Feat.set(feat.value{n1,1},feat.value{n1,2});
        case 3
            Feat.set(feat.value{n1,1},feat.value{n1,2},feat.value{n1,3});
    end
end

% Add indexed features
if ~isempty(feat.index)
    for n1 = 1:size(feat.index,1)
        % Extract values
        tag         = feat.index{n1,1};
        values      = feat.index{n1,2};
        [nrow,ncol] = size(values);

        for n2 = 1:nrow % Add all values
            for n3 = 1:ncol
                Feat.setIndex(tag,values(n2,n3),n2-1,n3-1);
            end
        end
    end
end

% Add named features
if ~isempty(feat.named)
    for n1 = 1:size(feat.named,1)
        switch size(feat.named,2) % Check for number of arguments
            case 1
                Feat.(feat.named{n1});
            case 2
                if isempty(feat.named{n1,2})
                    Feat.(feat.named{n1});
                else
                    Feat.(feat.named{n1,1})(feat.named{n1,2});
                end
        end
    end
end

%% Nested functions
```

Building a model object

Creating a model object is performed by the code in line 9. The code starting at line 19 is to automatically define all features described in the fields of the previously discussed Matlab structure *model.features*.

```
1  %% ME2490: Automatic generation of Comsol model from Matlab
2  function Model = buildModel(model)
3  %% Create model
4  % Import COMSOL objects
5  import com.comsol.model.*
6  import com.comsol.model.util.*
7
8  % Create default model
9  Model = ModelUtil.create('Model');              % Create Model object
10 try
11     Model.modelPath(model.general.path);            % Set path
12 catch
13     fprintf('Path not specified, using working directory\n')
14     Model.modelPath(pwd)
15 end
16 Model.modelNode.create('comp1');                % Create component
17 Model.hist.disable;                             % Disable history
18
19 %% Add features
20 % Find feature types
21 try
22     types = fields(model.features);
23 catch
24     fprintf('No feature types found, return\n')
25     return
26 end
27
28 % Add features
29 MElist = [];                              % Error message variable
30 for n1 = 1:length(types)
31     fprintf('- %s\n',types{n1})
32     for n2 = 1:size(model.features.(types{n1}),1);
33         feat = model.features.(types{n1})(n2);
34         if feat.enabled
35             try
36                 Model = addFeature(Model,feat);
37             catch ME
38                 if ~isempty(feat.label)
39                     ermsg = feat.label;
40                 elseif ~isempty(feat.tag)
41                     ermsg = feat.tag;
42                 else
43                     ermsg = feat.feature;
44                 end
45                 warning('Add %s feature failed\n',ermsg)
46                 MElist = [ME; MElist]; %#ok<NASGU,AGROW>
47                 return
48             end
49         end
50     end
51 end
52 assignin('base','ME',MElist)
```

Appendix E

Experimental results

Confidential

Appendix F

Radial bearing fluid domain model

A simple numerical model with a fluid and thermal description is set up to assess the flow profile and thermal characteristics along the gap length. The model describes one half of a radial bearing with the same dimensions and properties as the spindle assembly model. The geometry and fluid velocity are shown in Figure F.1.

The fluid flow is described by a fixed inlet pressure at the top left line wall segment and a free outflow condition at the end of the bearing gap on the right. The red lines indicate the fluid flow streamlines. The detailed picture of the gap entrance shows the distribution of the flow velocity at the inlet of the gap. The domain describing the bearing gap is separated in three segments. This creates four lines across the gap height at which the variation of properties can be assessed.

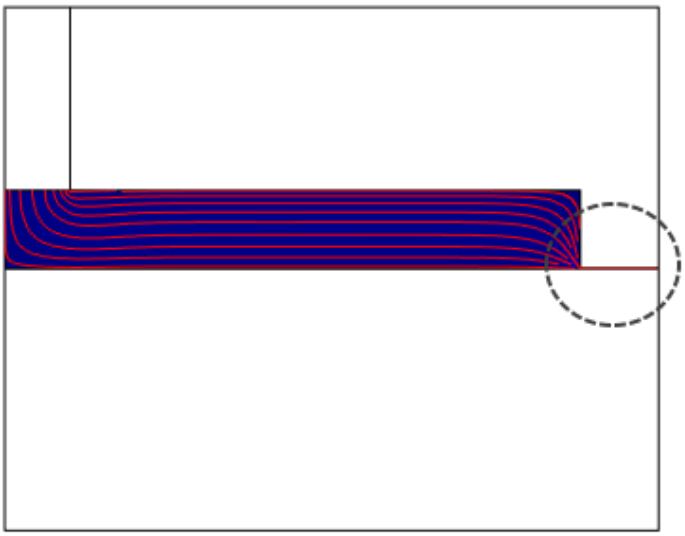

Figure F.1: Fluid domain model geometry and flow streamlines

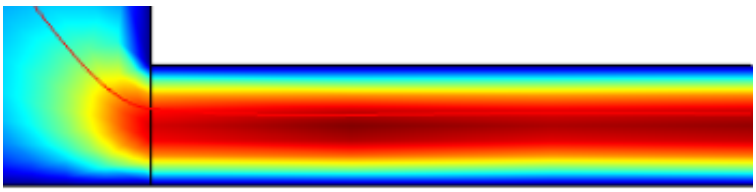

Figure F.2: Fluid velocity at the inlet of the radial bearing gap

Bibliography

[1] E. Abele, Y. Altintas, and C. Brecher. "Machine tool spindle units". In: *CIRP Annals-Manufacturing Technology* 59.2 (2010), pp. 781–802.

[2] M.H. Attia and L. Kops. "Computer simulation of nonlinear thermoelastic behavior of a joint in machine tool structure and its effect on thermal deformation". In: *Journal of Manufacturing Science and Engineering* 101.3 (1979), pp. 355–361.

[3] M.H. Attia and L. Kops. "Nonlinear thermoelastic behavior of structural joints-solution to a missing link for prediction of thermal deformation of machine tools". In: *Journal of Manufacturing Science and Engineering* 101.3 (1979), pp. 348–354.

[4] B. Bossmanns and J.F. Tu. "A power flow model for high speed motorized spindles - heat generation characterization". In: *Journal of Manufacturing Science and Engineering* 123.3 (2001), pp. 494–505.

[5] M. Broussely, Y. Bertin, and P. Lagonotte. "Reduction and optimisation of thermal models using Kirchhoff network theory". In: *International Journal of Thermal Sciences* 42.8 (2003), pp. 795–804.

[6] J. Bryan. "International status of thermal error research (1990)". In: *CIRP Annals-Manufacturing Technology* 39.2 (1990), pp. 645–656.

[7] A. Chatterjee. "An introduction to the proper orthogonal decomposition". In: *Current science* 78.7 (2000), pp. 808–817.

[8] D. Chen et al. "Thermal error of a hydrostatic spindle". In: *Precision Engineering* 35.3 (2011), pp. 512–520.

[9] J.-S. Chen and W.-Y. Hsu. "Characterizations and models for the thermal growth of a motorized high speed spindle". In: *International Journal of Machine Tools and Manufacture* 43.11 (2003), pp. 1163–1170.

[10] K.S. Cherukuri. "Thermal network theory for switchgear under continuous current". PhD thesis. National Institute of Technology Rourkela, 2007.

[11] C.H. Chien and J.-Y. Jang. "3-D numerical and experimental analysis of a built-in motorized high-speed spindle with helical water cooling channel". In: *Applied Thermal Engineering* 28.17 (2008), pp. 2327–2336.

[12] *Comsol Heat Transfer Module User's Guide*. 2015.

[13] *Comsol Programming Reference Manual*. 2015.

[14] *Comsol Reference Manual*. 2015.

[15] J. Driesen, R.J.M. Belmans, and K. Hameyer. "Finite-element modeling of thermal contact resistances and insulation layers in electrical machines". In: *Industry Applications, IEEE Transactions on* 37.1 (2001), pp. 15–20.

[16] T. Holkup et al. "Thermomechanical model of spindles". In: *CIRP Annals-Manufacturing Technology* 59.1 (2010), pp. 365–368.

[17] *IBS Spindle Analyzer*. URL: http://www.ibspe.com/category/machine-tool-inspection-and-analyzer-solutions/spindle-analyzer.htm.

[18] J. Jędrzejewski et al. "High-speed precise machine tools spindle units improving". In: *Journal of Materials Processing Technology* 162 (2005), pp. 615–621.

[19] A.H. Koevoets et al. "Optimal sensor configuring techniques for the compensation of thermo-elastic deformations in high-precision systems". In: *Thermal Investigation of ICs and Systems, 2007. THERMINIC 2007. 13th International Workshop on*. IEEE. 2007, pp. 208–213.

[20] D. Li et al. "Calculation method of convective heat transfer coefficients for thermal simulation of a spindle system based on RBF neural network". In: *The International Journal of Advanced Manufacturing Technology* 70.5-8 (2014), pp. 1445–1454.

[21] Z. Liu et al. "Thermal characteristic analysis of high-speed motorized spindle system based on thermal contact resistance and thermal-conduction resistance". English. In: *The International Journal of Advanced Manufacturing Technology* (2014), pp. 1–14.

[22] *LiveLink for Matlab User's Guide*. 2015.

[23] J. Mayr, S. Weikert, and K. Wegener. "Comparing the Thermo-mechanical Behaviour of machine Tool Frame Designs Using a FDM–FEM Simulation Approach". In: *Proceedings ASPE annual meeting*. 2007, pp. 17–20.

[24] J. Mayr et al. "Thermal issues in machine tools". In: *CIRP Annals-Manufacturing Technology* 61.2 (2012), pp. 771–791.

[25] A.F. Mills. *Basic heat and mass transfer*. Vol. 2. Prentice Hall Upper Saddler River, NJ, 1999.

[26] R. Ramesh, M.A. Mannan, and A.N. Poo. "Error compensation in machine tools, a review. Part II: Thermal errors". In: *International Journal of Machine Tools and Manufacture* 40.9 (2000), pp. 1257–1284.

[27] W.B. Rowe. *Hydrostatic, aerostatic and hybrid bearing design*. Butterworth-Heinemann, 2012.

[28] T.A.M. Ruijl. *Ultra precision coordinate measuring machine. Design, calibration and error compensation*. Delft University of Technology, 2001.

[29] T.A.M. Ruijl. "Thermal effects in precision systems: Design considerations, modelling, compensation and validation techniques". In: *Diamond Light Source Proceedings* 1.MEDSI-6 (2011), e60.

[30] P. Shore. "Thermal issues: past and present".

[31] *Special interest group meeting: Thermal Issues*. URL: http://www.euspen.eu/OurEvents/ThermalIssues2016.aspx.

[32] *Sumitomo turning tool*. URL: http://www.sumitomotool.com/index.php?id=65&L=0.

[33] N. Urasaki, T. Senjyu, and K. Uezato. "Influence of all losses on permanent magnet synchronous motor drives". In: *26th Annual Conference of the IEEE*. Vol. 2. IEEE. 2000, pp. 1371–1376.

[34] A. Van Beek. *Advanced engineering design: lifetime performance and reliability*. Vol. 1. 2006.

[35] M. Weck et al. "Reduction and compensation of thermal errors in machine tools". In: *CIRP Annals-Manufacturing Technology* 44.2 (1995), pp. 589–598.

[36] H.Y. Wong. *Heat transfer for engineers*. 1977.